COSMIC X-RAY SURVEYS

VOLUME 2   -

by

R.J. FRANCEY, B.Sc.(Hons.)

CONTENTS

CHAPTER FIVE

PAYLOAD DESCRIPTION AND PERFORMANCE

5.1 INTRODUCTION

This chapter includes the basic experimental aims,
specification, peculiarities, and where applicable,
performance and preliminary data analysis for each of the
six UAT flights. Flights I and II were practically
identical and are treated together. In discussion of the
integrated but unlaunched V, VI payloads, emphasis is
placed on accurate presentation of laboratory calibrations
of the new counter types. These give insight into the
counter operation and will be necessary for data analysis.

5.2 FLIGHTS I AND II

Two identical ancillary payloads, sited in multi-
purpose rings were prepared for Skylarks SL426 (I) and
SL425 (II). Four LND counters in each rocket were mounted
in pairs to form two independent detection systems, A and B,
each having an effective area of 22 cm² and facing in
diametrically opposite directions in a plane normal to the

spin axis (i.e. along the $\pm$ OZ rocket axes). Identical
normal, vertical, rectangular fields of view (see 3.6.1)
were used for all systems. The quoted experimental aims
were "to survey the southern sky, in particular the
Magellanic clouds and the galactic disc south of the galactic
centre, for sources of X-rays in the energy range 2-8keV".

The detection system and flight parameters are
summarized in table (5.1).

5.2.1 Discussion of the Detection Systems

The LND proportional counters have been described in
Appendix C.   Counter lifetimes, involving a gradual
decrease in gain and worsening of energy resolution, had
time-scales ranging from months to many years. Some of the
worst examples were refilled with a 90% Xe, 10% CH_4 gas
mixture two to three weeks prior to launch by Dr. A.G.
Fenton. In all cases the deterioration in a time scale
comparable with the flight duration, even in vacuum, were
negligible. Pre-flight calibrations enabled amplifier gains
and bias levels to be set within days of launch, and after
this time, gains measured 15 minutes before launch were used
to calculate the effective energy discrimination levels for
each system. Systems A on both flights showed no gain
deterioration after final adjustment; small correction was
necessary for I, B and a much larger correction (corresponding

TABLE 5.1

Detector Summary	Flight I (A,B)	Flight II (A,B)	Comment
collimator (FWHM)	10.5^O x 35°	as in I	Vertical (3.6.1)
effective area (cm²)	22 (x 2)	"	
window (mg cm⁻²)	14 (Be)	"	
gas (mg cm⁻²)	29 (Xe - 10%CH₄)	"	2" depth at N.T.P.
nominal bias levels (keV)	2, 5, 8	"	(5.2.1)
energy resolution] A	52, 81	34, 28	individual counters
FWHM (5.9keV),%] B	100, 25	130, 20	(2 per system)
veto efficiency	$V_{cr} \simeq$ .75 (p.h.a.)	as in I	(3.5.5)

Flight Summary			
launch time (U.T.)	0032hr, 4 April, 1967	2236hr, 20 April, 1967	
local time (C.S.T.)	1002am, " " "	0806am, 21 " "	
apogee (km)	219.9	218.6	
time above 80km (sec)	350	350	approx.
spin rate (deg.sec⁻¹)	33.6	-28.2	(5.2.2)
precession rate (deg.sec⁻¹)	0.87	0.65	
half cone angle (deg.)	66	66.3	
co-ords.precession axis (RA, dec)	23hr, -79°	17.6hr, 22.8^O	

to a 27% gain change) for II, B.

Samples of the beryllium windows were broken out of each of the damaged counters after recovery and measured as discussed in Section 3.3. The measured thicknesses with a mean of about .0033 inches (15 mg cm^{-2}) were used in the data analysis.

Four full and two subswitched telemetry channels were available. The subswitched channels were halved and used to monitor the temperature of four thermistors mounted in the payload. These results are discussed in 2.7.3, and coupled with pre-flight calibrations of the electronics packages, implied that the overall gain of a detection system varied less than $\pm$ 5% due to temperature changes in flight. The electronics for each detection system differed from that described in section 4.3 (figure 4.2) in having only two channel pulse height analysis, 16 step staircases (n=4), and no anticoincidence rejection. Four sets of 16 step staircases, corresponding to the 2-5keV and 5-8keV count rates from A and B, were each sampled by one full telemetry channel (at 80 samples per second).

An instrumental difficulty, relating to a shift in one of the three bias levels in flight I after final adjustment, is discussed in section 5.2.3; apart from this everything functioned in the desired manner.

5.2.2 Discussion of the Attitude Solutions

UAT attitude solutions were obtained in the manner described in section 2.4.6. On both flights the diagonal and vertical sun slits continuously scanned the sun for two periods of about 100-150 seconds, one at the beginning and the other late in flight. For these periods the position of the + OX axis in space was determined by triangulation from the sun and magnetic field positions, the two sections of precession cone so obtained were fitted to a circle on the celestial globe, and a constant precession rate assumed. British Aircraft Corporation (BAC) attitude solutions were also provided. A test of a particular solution was its ability to predict the times of sighting X-ray sources whose positions are accurately known (in these flights, Sco XR-1 and the sun). An additional criterion for flight I was the ability to give a consistent position for the new strong X-ray source, Cen XR-2, observed both at the beginning and end of flight.

In <u>flight I</u>, the sun and magnetic field positions were separated by only 33 degrees, and early in the flight the +OX axis moved almost along the line passing through these positions. Thus small errors in determining the angles $S\hat{O}X$ and $M\hat{O}X$ produced large errors in the triangulated OX position. The two sections of precession cone obtained in this manner did not lie on a circle, and the UAT solution,

based on a circle of best fit, did not give consistent

positions for Cen XR-2, although the agreement for Sco XR-1

was within 1^O. Three BAC solutions were provided, each an

improvement on the one before. The third solution gave good

agreement for the sun and consistent positions for Cen XR-2,

but gave a Sco XR-1 position some 4° from the measured one.

A program was written to rotate the BAC solution about the

sun position to give better agreement with Sco XR-1. A

rotation of 5° in a co-ordinate system with the sun at

zenith gave an agreement of better than 1^O for Sco XR-1.

For example, such a rotation could be associated with an error

in magnetic field position of about $2\frac{1}{2}^O$, and since uncertainties

larger than this existed in UAT solutions, it was decided to

use the rotated BAC solution with parameters listed in

table (5.1).

Figure (5.1) shows the scan path over the sky of the

0Z rocket axis (detection system A). The galactic longitude

(1^{II}) and latitude (b^{II}) are plotted for each instant

(0.1 sec) of flight, and the position at each second after

launch is labelled immediately to the right of the trace. The

collimator field is shown relative to the scan direction; it

becomes distorted away from the centre of the Hammer "equal

area" projection. The ground level horizon is shown at the

time of launch; the rocket horizon at 80 Km is almost 10°

below, and at apogee 15° below this. Source positions and
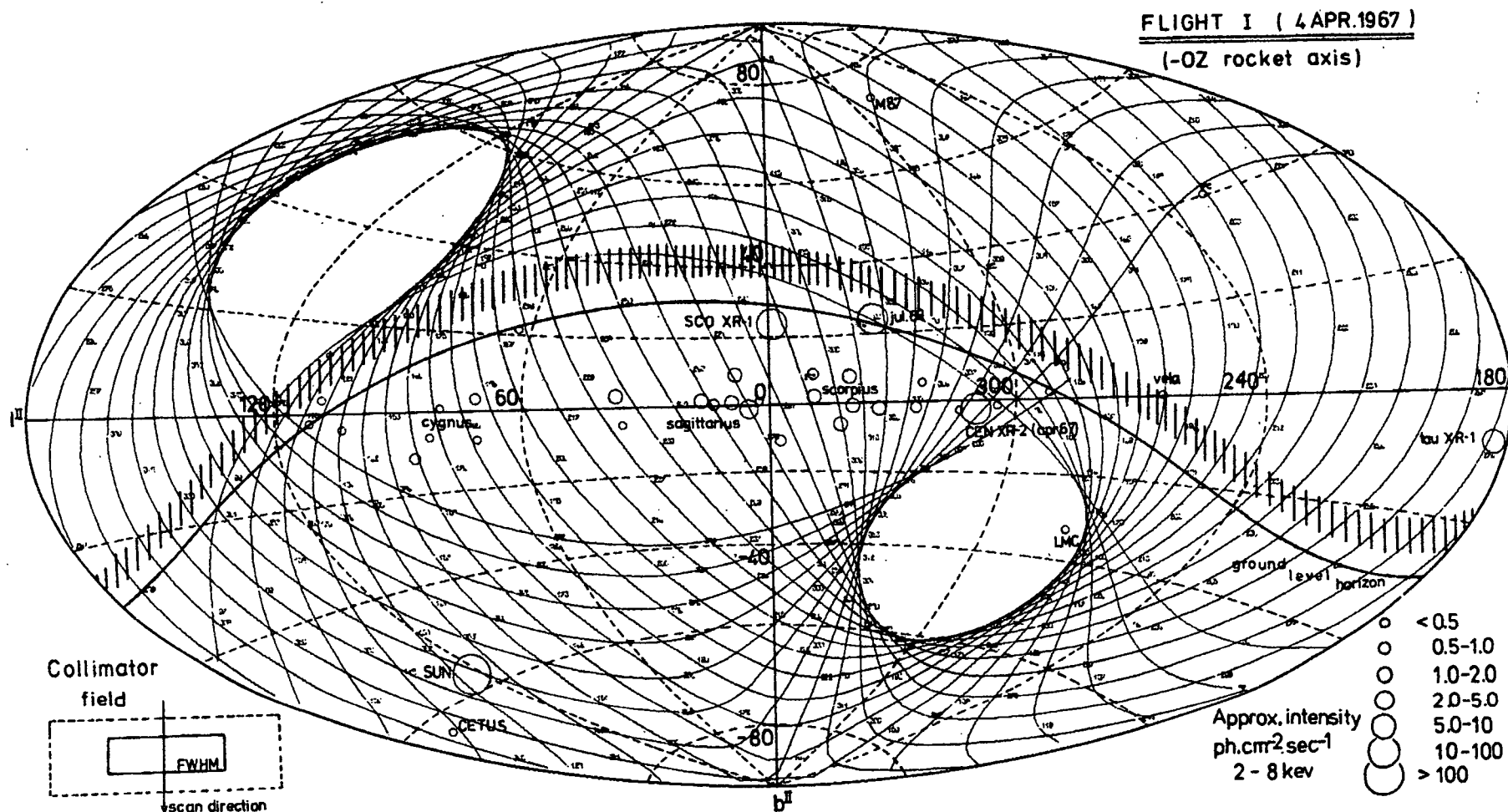
FIGURE 5.1: Flight I Attitude Solution

rough relative intensities (2-8keV) are taken from Mayer et
al (1970) for the Sagittarius-Scorpius region, Giacconi et
al (1967) for the Cygnus region, Chodil et al (1967b) for the
Vela, Centaurus regions, Thomas et al (1969) for the July,
1969, source, this thesis for the Cetus and Cen XR-2 (Apr.
1967) positions and Friedman et al (1967) for other sources.
Caution must be excercised in accepting the position or even
the existence of sources shown with intensities < 0.5 photons
$cm^{-2} sec^{-1}$ and other such sources may exist in some of the
above regions.

Flight II was launched at a time of much larger sun-
magnetic field vector separation (65°). A well defined
circular precession cone was evidenced by an excellent fit
to the two sections obtained by triangulation. This circle
passed very close to the anti-solar direction at +238
seconds (indicated by a complete loss of vertical sun slit
data), and in order to interpolate the spin rate accurately
over the period of no sun sightings, the times of "sighting"
the centre of the precession cone were calculated for the
periods for which sun slit data existed —— the differences
between successive "sightings" should have been constant
throughout the flight. In fact the time differences indicated
a gradual decrease from 13 seconds to 12.5 seconds and the
interpolation was made allowing for a 4% despin between +100
and +400 seconds. A program, using the cone half angle, the

attitude of precession axis and the precession period determined the rocket OYZ plane. The direction of look of the counters in this plane were phased to the precession axis "sightings". This solution predicted the Sco XR-1 position to within 2^O (and, of necessity an accurate sun position) and has no apparent inconsistencies. On the other hand the BAC solution erred some 8° from the Sco XR-1 position and contained a similar discrepancy for the sun position late in flight. The UAT solution with parameters listed in table (5.1), was used for data analysis, and figure (5.2) shows the sky area scanned by detection system A. Ground level horizon and source positions are included.

The co-ordinate transformations employed in both attitude solutions are generally applicable to rocket surveys and are reproduced in Appendix A.

5.2.3 Data Reduction

Photographic records of each staircase output were manually digitalized to give the number of counts (or steps) per 0.1 seconds throughout each flight. The first steps in determining source positions and intensities are described in sub-section 3.6.1 on collimators, for the case of slowly spinning rockets. In both I and II, $\alpha_s = 10.5^O$ and a detector response to a single scan across a point source is a triangle of base $2\alpha_s/\omega_s \simeq 0.7$ seconds. A least squares
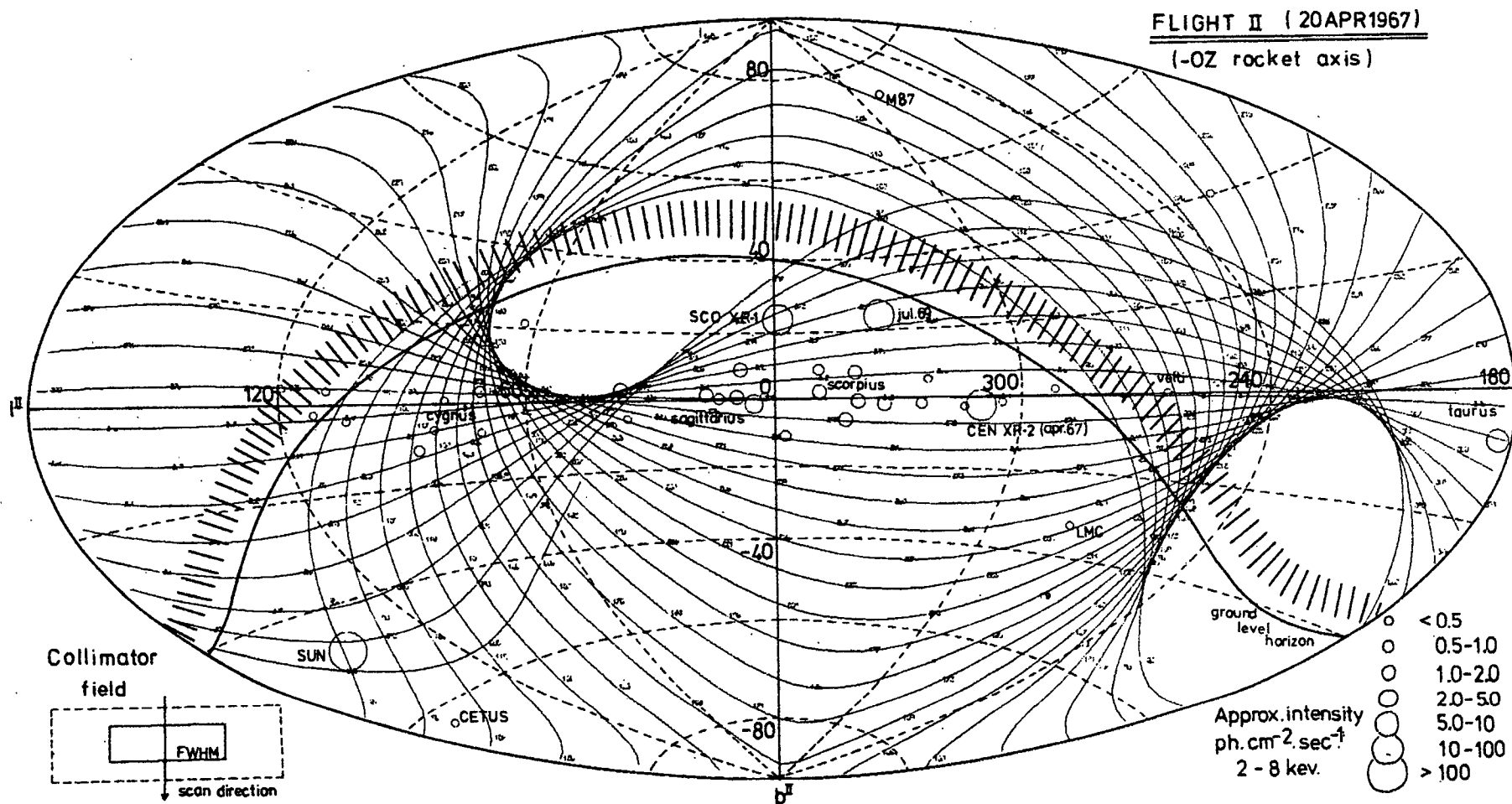
FIGURE 5.2: Flight II Attitude Solution

fitting technique (Appendix B) was programmed to fit the correct triangular response to each set of 6 to 8 "digitalized" data points obviously representing a source. The program output comprised a maximum count rate A_s, its variance $V(A_s)$, time of peak t_s, and its variance $V(t_s)$, for the triangle of best fit. A_s was interpreted as the number of source photons per second, modified only by the collimator response normal to the spin direction and the counter efficiency and energy resolution.

With a separation of successive scans ≤ about 10° (figures 5.1, 5.2) and collimator full width of 70° <u>normal to the spin direction,</u> an accessible and sufficiently strong source yielded a set of at least six successive sets of A_s, t_s values for each detector system. The collimator response normal to the spin direction was assumed to be triangular with FWHM, $\alpha_p = 35^o$ (a good approximation, see table 3.7). Then by using the attitude solutions to obtain the angular separation between successive scan paths at times of maximum source count rate, i.e. at each t_s, a "theoretical" response function of A_s against t_s was determined. For the Sco XR-1 response on I and the Cen XR-2 response on II, this response was triangular and symmetric and the least squares fitting technique used above was immediately applicable. However for the Cen XR-2 on I and Sco XR-1 on II, the relative phasing of spin and precession

resulted in a theoretical response function noticeably

asymmetric, and non linear after the peak. In these cases

an approximate response function was employed, and consisted

of an asymmetric triangle, characterized by different "widths"

before and after the peak.

The time of peak (t_p) resulting from these fits, was

used to interpolate linearly between the positions representing

neighbouring values of t_s, so yielding an actual source

position and its statistical variance. The ordinate A_p at t_p

of the fitted response then gives the source intensity

modified only by the energy dependent response of the counter.

The method of correcting for counter <u>efficiency</u> and

energy <u>resolution</u> are described in section 3.4. As has been

already mentioned, the energy resolution of the LND counters

was poor. In flight I, where the counters had field

forming electrodes to correct for end effects, the response

to Fe^{55} X-rays was symmetrical but "smeared" out with FWHM

(5.9keV) ranging from 30% to 100%. Thus the analysis of I

data, employed a gaussian response with

$$\sigma = 0.18(h\nu)^{\frac{1}{2}} + \{FWHM(5.9keV) - 18\} (h\nu)$$

in equation (3.22). The term in curly brackets is a constant

percentage added to bring the resolution up to that observed

at 5.9keV. For flight II counters, the large end effects

were incorporated by considering a gaussian component with σ

similar to above for two thirds of the counts, and a

rectangular response from zero energy to $h\nu$ for one third of
the counts, in accord with observed Fe^{55} pulse distributions.
The convolution of source intensity, counter efficiency and
gaussian (plus rectangular) response was numerically
integrated for a wide range of source parameters, and for
0.1keV energy intervals (from 1 to 10keV) in a program
written by Dr. Harries.

There remains the possibility that measurements of
source spectra were influenced by a gain hysteresis effect
due to the sun sightings. A possible effect is mentioned in
4.3.3. The maximum electronic charge collected at the anode
on one scan of the sun ($\sim 1/3$ sec) is 10^{-6} -10^{-7}coulomb.
At least initially this is neutralized by charge from the
last filter capacitor in a time of the order of 10^{-3} seconds,
so that the electronic charge on the anode is smaller than,
but a noticeable fraction of, the static anode charge
$q = CV \simeq 10^{-8}$ coulombs. Space charge acts on the gas gain
to prevent the electronic charge from becoming comparable to
the stored charge. The corresponding decrease in anode
voltage is therefore small, say up to 1-10%, but this gives
much larger changes in gas gain (see table 3.1). On the other
hand the recovery time, after passing the sun, for a small
voltage deviation is dominated by the last stages of the
filter and in this case will be of the order 0.5 - 1 secs
at the most. As can be seen from figures (5.1), (5.2), both

Sco XR-1 and Cen XR-2 are several seconds from the sun. In
fact in flight II, when Cen XR-2 shows a decrease in
intensity from I, Cen XR-2 is observed and measured on scans
occurring some 150 seconds after the last sun sighting.

For Sco XR-1 an exponential spectrum similar to
equation (1.5) was used, i.e.

$$\frac{dN}{d(h\nu)} = K(h\nu)^{-1} \exp(-h\nu/k) \text{ photons keV}^{-1}\text{cm}^{-2}\text{sec}^{-1} \quad (5.1)$$

here $k(\text{keV})$ represents the "temperature" of the source. The
total 2-8 keV count rates obtained from the analysis were in
good agreement between the two flights, and the ratio of
(2-5 keV)/(5-8 keV) counts in flight II indicated a source
temperature in good agreement with those obtained on April
10 (Cooke et al, 1967) and May 18 (Chodil et al, 1967b)
However, the ratios obtained for Sco XR-1 (and also Cen XR-2)
on flight I implied an unreasonably flat spectrum.
Measurements on the recovered electronics indicated that
(only) the middle bias level for flight I had changed since
final calibration (presumably in the locking process) and
that the I bias levels were in fact from 2-4.5 keV and
4.5-8 keV. Using these limits the ratio of low to high
energy counts gave excellent agreement with the flight II
Sco XR-1 temperature. (The slight dependence of this
argument on the requirement for the two sightings of Sco XR-1,
with equal 2-8 keV intensities, to record the same

temperature, is justified in spite of the now obvious

variability of this source. This is evident from a study of

all available Sco XR-1 measurements discussed in section 8).

5.2.4 Summary of Results

Between launch and about <u>40 to 50 Km</u> on both I and II,

all detector outputs gave a saturated response ($\ll 16 \times 80$

counts per second), with the effect commencing first and

persisting longest in the lower energy channels. This was

most likely due to microphonic action in the detectors,

associated with the thrust phase of the flight, as slight

sensitivity to vibration was observed in preflight tests.

Above these altitudes and <u>below 70 Km</u> the count rate

was approximately constant in time and from flight to

flight, with equal counts in both energy intervals. This

was attributed to primary cosmic rays and secondary charged

particles and photons discussed in subsections (3.5.1), (3.5.2),

and was assumed to be a constant contribution to the count-

rate at higher altitudes.

Between <u>70 and 90 Km</u> a marked increase in count was

observed. The effect was most marked when detectors looked

up out of the atmosphere and was strongest in the low energy

(2-5 keV) channels. The possibility of the increase being

due to low energy charged particles unable to penetrate below

70 Km was considered and thought unlikely, mainly because of

the insensitivity of the LND counter to such particles,
discussed in section (3.5.3), and the magnetically quiet
conditions during both flights. Also a search for a pitch
angle distribution in the increased flux was unsuccessful,
however as mentioned in (3.5.3), a small contribution from
electrons is extremely difficult to separate from X-ray
events. The difference in count rate when detectors looked
up (but not at known point sources), and the count rate below
70 Km was taken to represent a <u>diffuse X-ray</u> flux. The
large field of view and small area made it difficult to
obtain sufficient data uncontaminated by point sources or
horizon etc. to make a detailed study of the diffuse X-rays
—— no statistically significant flux variations (>20% - 30%)
were found with galactic latitude. The combined data of
both flights gave results compatible with a power law of the
form

$$\frac{dN}{d(h\nu)} = (19 \pm 3) \, h\nu^{-\left(1.75 \pm \substack{1.7 \\ 0.3}\right)} \text{photons keV}^{-1} \text{cm}^{-2} \text{sec}^{-1} \text{ster}^{-1}$$

$$(5.2)$$

which is not significantly different from the result of
Seward et al (1967), taken in a similar region of the
galaxy. All available diffuse X-ray measurements are
discussed in more detail in section 7.2.

The increase between 70 and 90 Km in detectors looking
down into the atmosphere was only significant in the low
energy channels, and varied with the sun direction. This

effect was explained in a very satisfactory manner by Dr.

Harries, in terms of an albedo of scattered solar X-rays and

solar-excited fluorescent X-rays from the atmosphere, and is

discussed in detail elsewhere (e.g. Harries and Francey, 1968).

Above 90 Km, X-rays from point sources, unattenuated

by the atmosphere, were observed above the background of

cosmic ray induced events and the diffuse X-rays. Sco XR-1

and Cen XR-2 were detected on at least seven consecutive scans

by each detection system on both flights and so were subjected

to detailed analysis.

The published UAT position for Cen XR-2

13.9hr. RA, -64° dec

310° 1^{II}, -2.3^{O} b^{II}

is the mean position of the independent determinations from

each flight. These, with statistical and estimated

systematic errors are shown in figure 1 of Harries and

Francey (1968), and result in approximately a 4° error

circle. No attempt was made to combine statistical errors

in the direction parallel to the scan, from neighbouring

scans. As will be seen in Chapter 6, flight II offers a

unique opportunity to obtain the Cen XR-2 galactic longitude

to much greater accuracy, as a result both of combining

statistical errors in the manner suggested and of scan

directions allowing accurate determination of the position

relative to Sco XR-1. The second factor markedly reduces

the dependence of the positional determination on the

accuracy of the attitude solution. The resulting position has

great significance in view of more recent X-ray surveys of the

region.

The most outstanding results from these flights were

(1)   the discovery of Cen XR-2 in a region of sky for which

a flux upper limit of approximately 1/100 th. that observed

on flight I was claimed (Chodil et al, 1967b), and

(2)   the unique information on the Cen XR-2 spectrum variation

on a time scale of three weeks, the first such information

obtained for an X-ray source.

Examination of even the raw count rate totals indicated that

whereas the Sco XR-1 flux was similar on both flights, the

Cen XR-2 flux exhibited a marked decrease from I to II.

Since the two channel pulse height analyser was unable to

distinguish the actual shape of the spectrum (e.g. whether

exponential, power law or blackbody), the results were first

published in an exponential form, similar to equation (5.1),

showing clearly the statistical significance of the

measurements (Francey et al, 1967). Subsequent and more

detailed spectral information on Cen XR-2 (Chodil et al, 1968b)

is more compatible with a power law shape, (as are recent

data by Rao et al, 1969a, for an object which has "reappeared"

near the Cen XR-2 position). Assuming simple power law

source spectra the UAT Cen XR-2 spectral data are given by

Apr 4 : $\dfrac{dN}{d(h\nu)}$ (2-8 keV) = (79 ± 4) $h\nu^{-(2.12\pm.15)}$

ph. $\text{keV}^{-1}\,\text{cm}^{-2}\,\text{sec}^{-1}$ (5.3)

Apr 20 : $\dfrac{dN}{d(h\nu)}$ (2-8 keV) = (114 ± 6) $h\nu^{-(2.75\pm.25)}$

ph. $\text{keV}^{-1}\,\text{cm}^{-2}\,\text{sec}^{-1}$ (5.3a)

Figure (5.3) shows the lines of best fit and included are

the May 18 (1967) data of Chodil et al (dashed line).

The dotted line shows the exponential Sco XR-1 spectrum at

intensities representing both flights I and II. Also

included are upper limits of LRL (28Sept67) and flight III

(1Dec67, section 5.3) assuming a spectral index the same as

the last sighting ($\simeq$ -2.75).

The Sco XR-1 data are represented by

Apr 4 : $\dfrac{dN}{d(h\nu)}$ (2-8 keV) $\simeq$ (56 ± 5) $h\nu^{-1}$ $\exp(-h\nu/4.5\pm.5)$

ph. $\text{keV}^{-1}\,\text{cm}^{-2}\,\text{sec}^{-1}$ (5.4)

Apr 20: $\dfrac{dN}{d(h\nu)}$ (2-8 keV) $\simeq$ (50 ± 5) $h\nu^{-1}$ $\exp(-h\nu/4.5\pm.5)$

ph. $\text{keV}^{-1}\,\text{cm}^{-2}\,\text{sec}^{-1}$ (5.4a)

A search for X-rays from the Magellanic clouds was one

of the stated aims of these flights, and figure (5.1) shows

a large number of scans close to the LMC position on flight I.

Times of "sighting" the LMC were read from the attitude

solution for 26 scans past the position (13 of which were by

detector A and are shown in figure 5.1). Count rate data

were arranged about these times and superposed. No

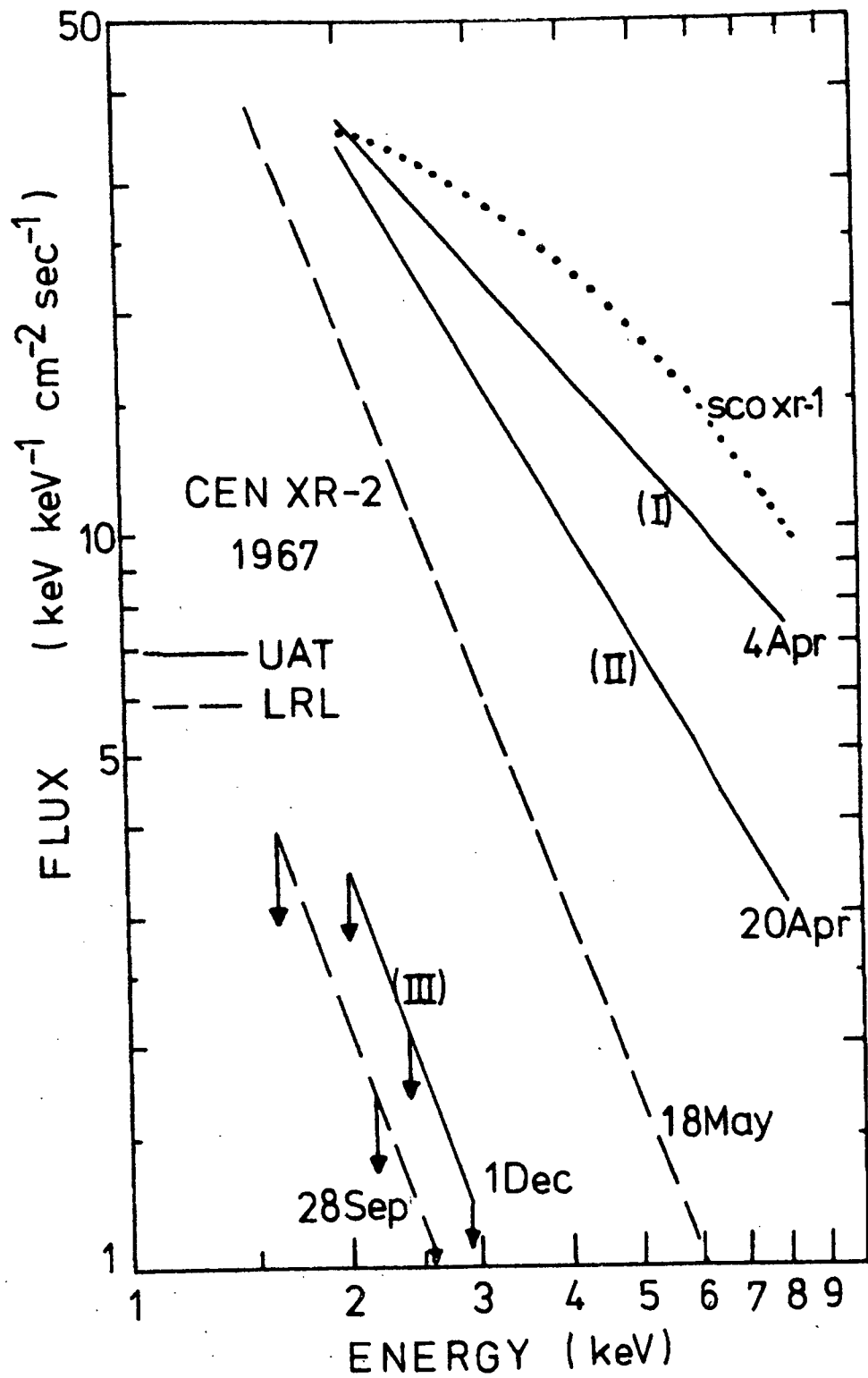significant count rate increase was observed implying a point

FIGURE 5.3: Variability of Cen XR-2 Spectrum (c.f. table 6.1).
(Mean Apr-May Sco XR-1 spectrum included for comparison)

source flux upper limit (correcting for collimator

transmission) of

$$I_{LMC} \; < \; 0.2 \; \text{counts} \; cm^{-2} sec^{-1} \; (2-8 \; keV) \qquad (5.5)$$

Recent evidence for an extended LMC X-ray source of 12°

width and flux 0.2 photons $cm^{-2} sec^{-1}$ over a significantly

wider energy interval (1.5 - 10.5 keV), (Mark et al, 1969),

would be undetectable on either of these flights.

X-rays were detected from the <u>galactic centre</u> region

but were not resolved into point sources. The total fluxes

observed were consistent with the results of Friedman et al

(1967) and more recently those of Mayer et al (1970). Both

rockets scanned the <u>Cygnus</u> region; the large number of

flight II scans over the region permits sufficient super-

position to get significant responses, which in the light of

more recent data are quite meaningful and are discussed in

Chapter 6. Finally the <u>sun</u> was scanned and on every

occasion saturated the relevant telemetry output. This

placed a lower limit of 2000 counts sec^{-1} between 2-8 keV on

the solar flux; the analysis of atmospheric albedo yielded a

solar flux of about 10^{5} photons $cm^{-2} sec^{-1}$.

5.3   FLIGHT III

A third ancillary experiment was accepted for inclusion

on an engineering round, SL 422A. Limited finance and

preparation time influenced design and major considerations were

(1)   the existence of a complete set of unused I and II hardware, and

(2)   the immediate availability of a ring not requiring milling for apertures, i.e. the standard base ring.

Three independent detection systems A, B and C were employed with UAT BR counters in A and B, and two refurbished flight II LND counters in C. The engineering tests included a new parachute for head recovery, plus a rocket "spin up" system to reduce impact dispersion. It was anticipated that the initial imparted spin would damp out after 5 seconds and not affect the motion of the rocket above the atmosphere. However both this factor plus a greater likelihood of inertial asymmetries than in a newly designed rocket, meant there was no guarantee of the ideal survey motion experienced on flights I and II.

The UAT purpose was again a survey one, as well as an inflight test of the new counters. Although UAT had no influence on launch time, it was hoped to once more scan the Cen XR-2 and Sco XR-1 positions. Table (5.2) summarizes the detection system and flight parameters, which are discussed below.

TABLE 5.2

FLIGHT III

Detector Summary	System A	System B *	System C
collimator (FWHM)	4.2° x 36.85° (vert.)	4.5° (hexagonal)	$\begin{cases} 4.1^{\circ} \text{ x } 35^{\circ} \text{ (vert.)} \\ 4.1^{\circ} \text{ x } 35^{\circ} \text{ (45}^{\circ} \text{ diag.)} \end{cases}$
effective area (cm^2)	43.9	87.0	2 x 11.7
window (mg cm^{-2})	23 (Be)	1.77, $(C_{10} H_6 O_4)_n$	23 (Be)
gas (mg cm^{-2})	4.8 (P-10)	4.82 (P-10)	29 (Xe $-10\%CH_4$)
bias settings (keV)	2,3.2,4.5,6,8	2,3.2,4.5,6,8	2, 8
energy resolution FWHM (5.9keV),%	25	17.5	100, 35
veto efficiency	$V_{cr} \simeq .76$ (a/c)	$V_{cr} \simeq .76$ (a/c)	$V_{cr} \simeq .75$ (p.h.a.)

Flight Summary

launch time (U.T.)	0638 hr., 1 December, 1967	
local time (C.S.T.)	0338 p.m. " " "	
apogee (km)	181	
time above 80 km (sec)	260	
spin rate (deg.sec^{-1})	15.9	
precession rate (deg.sec^{-1})	0.24	
half cone angle (deg.)	~90	(* in-flight calibration)
co-ords of prec. axis.	2 hr., $- 61^{\circ}$	

5.3.1 Discussion of Detection Systems

To give flexibility in the event of an unexpected
rocket motion and to enable better source resolution, and flux
and position estimates, a wide range of collimator types was
employed. The A collimator was similar to the type on
flights I and II. System B used a honeycomb collimator
giving good resolution normal to the spin direction, useful
in a cluttered star field or with a rocket motion implying
a large number of scans over a restricted region. Separate
and identically constructed collimators were placed over the
two counters of system C {one vertically and the other
diagonally (at 45°), see 3.6.1} and the counter outputs
monitored separately.

System A electronics comprised 4 channel pulse height
analysis, and anticoincidence rejection and differed from
that shown in figure (4.2) only in the number scalers, (n).
The 2-3.2 keV and 3.2-4.5 keV outputs were on 32 step stair-
cases (n=5), each sampled by a full telemetry (TM) channel).
The 4.5-6 keV and 6-8 keV outputs used 16 step staircases on
half TM channels, (i.e. the total system A X-ray output was
monitored on 3 TM channels). A further half TM channel
carried an 8 step (n=3) guard count rate.

System B incorporated inflight calibration in the form
of a small {~400 counts sec^{-1}) Fe^{55} source permanently
irradiating the guard counter. Since only guard pulses

occurring in coincidence with, or less than 8 µsec after an

X-ray pulse were vetoed, the number of random rejections was

about 0.3% of the X-count rate. A shielded "Ledex" switch

at the counter allowed the X and G outputs to be reversed on

command, i.e. the G output was analysed in the 4 channel pha

for the duration of the command, permitting location of the

Fe^{55} peak. The Ledex calibrations occurred only for times

when the rocket was below 70 Km (e.g. see section 2.8). In

all other respects the B electronics were identical to those

in system A. An unusual feature in the B counter was the

0.5 mil Melinex window exposure during launch. The excellent

support and heat shielding provided by the honeycomb

collimator in laboratory tests indicated that the use of

exposed plastic windows might be feasible, and in view of the

high cost of beryllium, was incorporated, with future flights

in mind.

The separate outputs from the C1 and C2 counters were

monitored in single 2-8 keV energy channels, in each case a

half TM channel sampling an 8 step staircase. A combined

C1 and C2 output was prescaled by 2^5 before being sampled as

an eight step staircase with half a TM channel. With a total

scaling factor of 2^8 it was hoped to obtain an approximate

measure of the sun X-ray flux as a further check on the X-ray

albedo theory mentioned in 5.2.4.

Although all three systems yielded some information, there were some disappointing aspects of this flight. The gain of the B counter decreased rapidly after the final flush (at launch -20 min.). The gas valve on plumbing was immediately suspect, but because of the ancillary status of the experiment it was not possible to interrupt the count down sequence to allow rectification. The counter still responded, with reduced gain, to the calibration source at 70 Km on descent. However a leak which tended to decrease gain at ground level may well have implied an increase in gain above the atmosphere if the counter pressure decreased, so that considerable uncertainty exists in the detailed behaviour of system B. The effectiveness of system A was also reduced, this time by an abnormally high guard count rate which saturated the TM ($>$ 320 cts/sec) and appeared to reduce the efficiency of the X counter due to random rejections. This has been a most puzzling feature since this system functioned normally on recovery; it is possible that physical movement of electronics or foreign matter during launch initiated EHT discharge which cured itself on impact.

Interpretation of the data from both A and B might have been vastly simplified by an inflight cross reference between these and the C detector (which functioned normally), as would have been provided by a sighting of the sun, Sco XR-1

or other relatively strong X-ray sources. The unusual rocket
motion, described below, prevented the detectors from
scanning any strong source.

5.3.2 Discussion of Attitude Solutions

The rocket motion above the atmosphere was such that at
no time did the diagonal sunslits sight the sun, although the
vertical slits gave a response throughout most of the flight.
This information plus the slow spin rate implied large
precession cone angle and slow precession rate. In addition
to this, the Z magnetometer functioned incorrectly and
prevented an inflight magnetometer calibration which would
have given information on the cone angle. Finally since the
X-ray detectors at no stage scanned the position of a strong
source, no additional aids or accuracy criteria existed.

Mr. Barnden obtained an approximate attitude
solution using the remaining magnetometer data plus vertical
sunslits, and this was used for data analysis. The solution
was in substantial agreement with a recent, more detailed BAC
solution whose authors make the following comments. "The
solution ...... fits the sun cell data to a r.m.s. error of
0.72 degs. suggesting an overall accuracy of ± 1.5 degrees.
.....we have assumed a cone angle of 90° although we have no
means of proving this because of the small movement in
precession .... checked as far as possible and feel

reasonably sure that it is a valid solution". The parameters of this solution are listed in table (5.2) and the path of the $(+0Z -\pi/6)$ rocket axis, corresponding to system C, is shown against galactic longitude and latitude in figure (5.4). The ground level horizon and source positions are indicated.

5.3.3 Data Reduction and Results

Although no obvious sources were apparent on flight records, as might be expected from figure (5.4), the high scan density over previously poorly scanned regions near the South galactic pole was sufficient reason to digitalize all data into 0.1 second count rates, as for flights I, II. The most obvious method of analysis, in view of the rocket motion was to superpose successive scans, and using this procedure Mr. Barnden isolated a noticeable deviation above the background for the C vertical collimator counter, using 5 scans. The C diagonal collimator data were then searched keeping in mind the relative peak phasing for an off axis source, and the most significant count rate deviation was obtained adding three of the above scans. Summing all the data from system C a peak 3.6 standard deviations above the mean background level was obtained, where the total counts due to peak and background over a time representing the FWHM of the collimator response have been compared with the established background level as in 5.2.4. Using the separation of peak
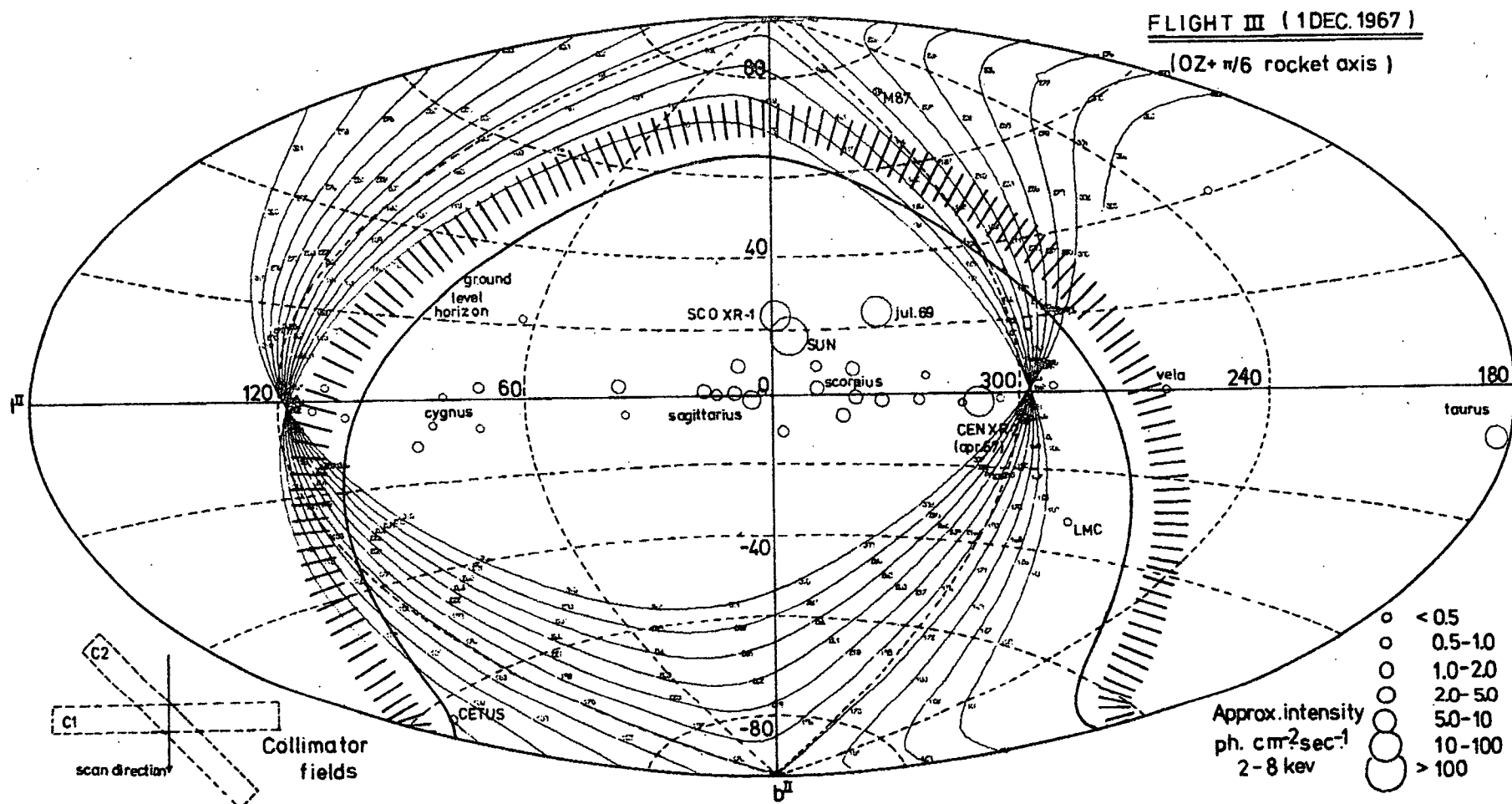
FIGURE 5.4: Flight III Attitude Solution

times between vertical and diagonal collimators for this
situation gives a likely source position of 2.0hrs RA, -6° DEC
($1^{II} = 164^\circ$ $b^{II} = -62^\circ$), in the constellation <u>Cetus</u>.

This means that the B detector, with honeycomb
collimator, would have seen the source only on the first scan,
if at all, and no confirmatory information was obtained from
it. The A detector with vertical collimator viewed the source
on at least 5 scans, hampered however by an unknown reduction
in sensitivity due to the high guard rate. Adding A detector
scans about the "source" position yields a peak 2.0σ above the
mean background level.

Since this position was scanned on previous UAT flights,
both the I and II records were re-examined. As seen in
figure (5.1) the source and sun positions are unresolved by
the 10.5° FWHM collimators of I. In II, figure (5.2), four
scans were added about the source position and over the
FWHM of the response function a peak 2.7σ above the mean
background level obtained.

Both the III-C and II peaks imply a Cetus source with
intensity about <u>1.5 photon cm^{-2} sec^{-1} over 2-8 keV</u>. Adding
the peak rates, normal errors according to the relation

$$\sigma = \left(\sigma_1{}^2 + \sigma_2{}^2 + \sigma_3{}^2\right)^{\frac{1}{2}},$$

and mean background levels for the three sightings, the
significance of the peak increases to <u>4.6σ</u> above the mean
background. Since the response on any one scan is ill-

defined, an error circle of 15° radius about the above
position is quoted, incorporating the collimator full width
and attitude uncertainties. A search of the literature to
1969 yielded no flight with comparable sensitivity in this
region, with the majority of spin stabilized and attitude
controlled rockets concentrating on the more prolific source
regions in the galactic disc.

A second important result from flight III comes from
the large number of scans close to the Cen XR-2 position,
whose angular separation from the scan paths implies a mean
vertical collimator transmission 55% that for a scan right
over the source. Using the detector C results and assuming
a spectrum of similar shape to that observed on 18 May, $6\frac{1}{2}$
months earlier (see figure 5.3), an upper limit of

$$I_{\text{Cen XR-2}} \leqslant 1 \quad \text{photon cm}^{-2}\text{sec}^{-1} (2\text{-8 keV}) \tag{5.7}$$

is obtained. This upper limit is greater than one obtained
by Chodil et al (1968) September 28, 1967, of 0.5 photons
$\text{cm}^{-2}\text{sec}^{-1}$ (2-10 keV), however in view of the variability of
this source, discussed in the next chapter, it retains
significance.

5.4   FLIGHT IV

In January, 1969, the flight IV payload was totally
destroyed 40 seconds after launch due to a vehicle

malfunction (portrayed in a spectacular fashion in Appendix C). The rocket, SL 781, was primarily launched to flight test the new, powerful Goldfinch boost motor and from the UAT view this implied greater acceleration and vibration, but a heavier payload for the same apogee.

UAT were given a primary status on this rocket and weight, space, power and telemetry allowances vastly exceeded anything available before or since. The detector details are summarized in table (5.3). The use of a large number of independent detection systems, all calibrated throughout flight (below 70 Km and for 5 seconds at apogee), and with variations in window type, area, collimator shapes etc. from one to the other, is obviously a good way to avoid systematic errors. Unhampered by normal payload restrictions, this experiment would have provided a unique opportunity to obtain absolute X-ray measurements of a large number of sources (for a well behaved flight I, II type motion) plus information on possible systematic errors.

A point source survey was the principal UAT objective, and the great advantages of 7-9 independent point source sightings per scan, with the detector variety listed, can be inferred from discussions of the following flights. Also, as an aid in determining accurate attitude, an additional sun cell, aligned with the collimators and covering the +OX rocket direction, plus cameras to photograph the horizon

TABLE 5.3

FLIGHT IV

Detection System	Collimator FWHM (deg.)	Eff. area (cm²)	Window (mg cm⁻²)	Gas (20°C) (mg cm⁻²)	Bias Levels (keV)	Energy Res. FWHM(5.9keV)	Background Rej. Efficiency
NC- A1*	4.5 (hexag.)	570	$0.9(C_{10}H_8O_4)_n$	7.6,P-10	1,2,3,4,5,6,	17%	$V_{cr}= .84$ (guard)
A2*	"	"	$1.45,(CH_2)_n$		7,8,12		
NC- B1*	2.7x33 (vert.)	220	$0.9,(C_{10}H_8O_4)_n$	6.0,P-10	1,2.5,4,6,10	"	$V_{cr}= .78$ "
B2*	"	"	$1.45,(CH_2)_n$				
NC- C1*	5 x 36 (vert.)	60	$0.89(CH_2)_n$	3.8,P-10	.25,.30,1.50,	"	$V_{cr}= .75$ "
C2*	"	"	"		3.0.		
BR- A*	4 x 37 (vert.)	65	12.5, Be	as in flight III			
BR- B*	4.5 (hexag.)	87.0	$1.77,(C_{10}H_8O_4)_n$				
BR- C1*	3 x 35 (vert.)	30	23, Be	4.0,P-10	2, 8	20%	$V_{cr} \simeq .75$ "
C2	3 x 35 (diag.)	29.5	"				
EL- A	35 x 35	1.5	9, Be	14,Xe-CH₄	>2 (electrons>85keV)	30%	$V_{cr}= 1.0$ "
B	" (gap of 1500gauss magnet)	1.5	"		>2 (electrons>250keV)		

(* in-flight calibration)

were included in the UAT payload.

Secondary aims of the flight were more unusual and deserve special mention.

(1)   Though these collimator shapes were better suited to a point source rather than diffuse X-ray survey, the comparison of results from counters with similar collimators and different areas and vice versa, provides valuable information on the diffuse radiation. The exact composition of the diffuse count rate was to be probed firstly using a prescaled BR-C output (as in flight III) to measure the sun flux and obtain more information on the atmospheric albedo, discovered in flights I and II. (This is important if the diffuse flux is obtained by an "up-down" difference, a method frequently employed by other authors). Secondly, the possibility of low energy electron contamination (discussed in 3.5.3), was to be investigated using a technique similar to O'Brien, i.e. a magnetic "broom" was included over one of two identical counters (in this case proportional counters with a common gas volume). Electrons $<$ 250keV were prevented from entering the counter with the magnet, otherwise sensitive to $<$ 80keV electrons. In addition the comparison of "diffuse" counts from each side of the NC-A or NC-B counters would have provided information on electron contamination —— the transmission of the two windows by low energy X-rays are similar, e.g. at 2keV, $(I/I_0)_{Melinex} \simeq 0.73$

and (I/I_0) Propafilm $\simeq 0.70$, however the electron transmission

depends mainly on the mass of the windows, and electrons with

energy $E \gtrsim 23$keV penetrate the Melinex and with $E \gtrsim 30$keV,

the Propafilm. The pulse height analyser permits only a

narrow "slice" of the electron spectrum above these limits to

be sampled (~ 5keV, and slightly narrower for the Propafilm),

thus a difference in count rate would have resulted from the

presence of a steep electron spectrum.

(2)   The NC-C counters were to probe a relatively new area

of investigation, the cosmic X-ray fluxes below 0.28keV. The

40G Propafilm, employed for the first time in a cosmic X-ray

detector to the author's knowledge, provided reasonable

efficiencies below 0.28keV (Francey et al, 1969, also figure

3.5), without resort to special window supporting meshes etc.

The solar induced fluorescence of the atmosphere which

saturated the low energy detectors of Grader et al (1969)

would have been far less serious, in this case, since the

Propafilm transmission efficiencies for 0.50keV oxygen and

0.38keV nitrogen $K\alpha$ X-rays are less than $10^{-2}\%$. The

detector gain was to be monitored in flight. As in all other

calibrated detectors a "fail-safe" calibration method was

employed in which an Fe^{55} source was permanently mounted

over a small beryllium window in the wall surrounding each

gas volume. X-rays were prevented from entering the window

by an intervening, spring loaded, aluminium shutter which

could be held open only in the presence of a +28v pulse from

the rocket bus.   In this case the NC-C amplifier gains were

simultaneously divided by a fixed factor (~2.5) to bring the

amplifier output into the pulse height analyser range (0.25keV

to 3keV).

The only information salvaged from the flight was

obtained from telemetry records during free fall of the head

from about 2 Km.   These showed that all counters were

functioning normally and in particular that large areas of

thin plastic windows and long thin anodes in the new counters

had withstood accelerations, vibration, and buffeting (due

to premature nose cone ejection) in excess of that expected

on a normal flight.

5.5   FLIGHTS V AND VI

Flights V and VI are the first of a program of UAT

"X-patrol" experiments.   With the cessation of engineering

rounds prepared and launched in Australia by WRE, a major

consideration in the X-patrol proposal was minimization of

costs of U.K. integration for ancillary UAT payloads.   A

continuation of a survey program was proposed with enough

payload flexibility to cover the general aims of

(1)   a study of point source variability, or

(2)   an investigation of possible anisotropies in the

diffuse X-ray background, at short notice, depending on launch time and rocket motion. Motivation for these studies is discussed generally in **Chapter 1**.

The development of large thin window counters with markedly improved background rejection efficiency and adaptation of electronics to handle despun or spun up rockets are the only significant changes from earlier payloads. Ease of changing collimators on the detectors allows emphasis to be placed on a particular source, or a background survey.

Both V and VI rockets (SL728, SL 727 respectively) have spin rates about 3 revs. $\sec^{-1}$ and UAT have no control of launch time. The detector details are summarized in tables (5.4), (5.5) with flight V incorporating one new T8 detector, plus NC counters similar to those on IV. Flight VI has two T8 detectors.

5.5.1 Corrections for Collimators

The fast spin rate implies small precession cone angles (table 2.1) and thus a large number of scans around a narrow band of the sky. Both rockets carry combination vertical-diagonal collimators to assist in source location (section 3.6). One side of the V-NC counter has a vertical collimator tilted 20° towards the rocket +OX axis to allow greater sky coverage. Response functions have been measured as described

TABLE 5.4

FLIGHTS V, VI COLLIMATOR PROPERTIES

Detector	Collimator Type(3.6.3)	Spin Direction			Perp. Spin Dirn.	
		$\alpha_s(^o)$	$T_s(\%)$	$\delta_s(\%)$	$\alpha_p(^o)$	$\delta_p(\%)$
V - NC A1	vertical	4.20	83.0	-3.7	33.0	+5.3
- NC A2	tilted (20°)	3.60	77.0	+0.9	20.3 + 15.6	0
- T8	diagonal(33.5^o)	4.50	84.5	-2.6	(6.2)*	
VI- T8 A	vertical	3.40	80.6	-2.8	34.8	+4.0
- T8 B	diagonal(33.5^o)	4.50	84.5	-2.6	(6.2)*	

(* see 5.5.1)

TABLE 5.5

FLIGHTS V, VI DETECTION SYSTEMS

Detection System	Eff. area (cm^2)	Window ($mg\ cm^{-2}$)	Gas ($20^{\circ}C$) ($mg\ cm^{-2}$)	Bias Levels keV	Energy Res. FWHM(5.9keV)	Backg. Rej. Eff. V_{cr}	$V(Co^{60})$
V- NC A1	442	0.91 $(CH_2)_n$	7.6,(P-10)	1.2,3.5,4,6,9	17.5%	.84	negligible
- NC A2	442	"	"	"	"	.84	"
- NC B	(Pulsar detector prepared by University of Adelaide)						
- T8	349	0.91 $(CH_2)_n$	7.6,(P-10) / + guard 11.7	1.2,2.5,4,6,9 / 1.2,4,6,9	17.5% / 20%	0.75*	0.75*
VI-T8 A	338	"	as for V-T8	as for V-T8	as for V-T8	.93*	0.9*
-T8 B	349	"	"	"	"	"	"

(* see 5.5.4)

in 4.4.6, table (5.4) summarizes the parameters of best fit
triangles to the measured results. The maximum transmission
T_s and differences from the true response δ_s are incorporated
into the effective window areas quoted in table (5.5). (In
actual data analysis the spin direction triangle will be
convolved with the telemetry sampling time as described in
section 3.6). The data for best fit triangles in the
direction perpendicular to the spin may not be required for
these spun up rockets, with direct reference to the measured
collimator response giving the desired information. This is
given for the T8 vertical collimator in figure (4.8) and is
shown for the two NC collimators in figure (5.5). As
indicated in table (5.4) the tilted collimator is asymmetric
about the peak which is 70° from +OX. (The change in slope
of measured points for angles $> 40^{o}$ is due to the light beam
intersecting the collimator outside wall and is not a real
effect.)

The response of the diagonal collimators is given by
equation (3.32a), and has been measured only in the spin
direction. The collimator cell size is similar to that for
the T8 vertical collimator, i.e. w = 0.17 ins; l = 1.735 ins;
d = 2.50 ins and the measurement is in good agreement with
(3.32a). The response along the collimator long axis, which
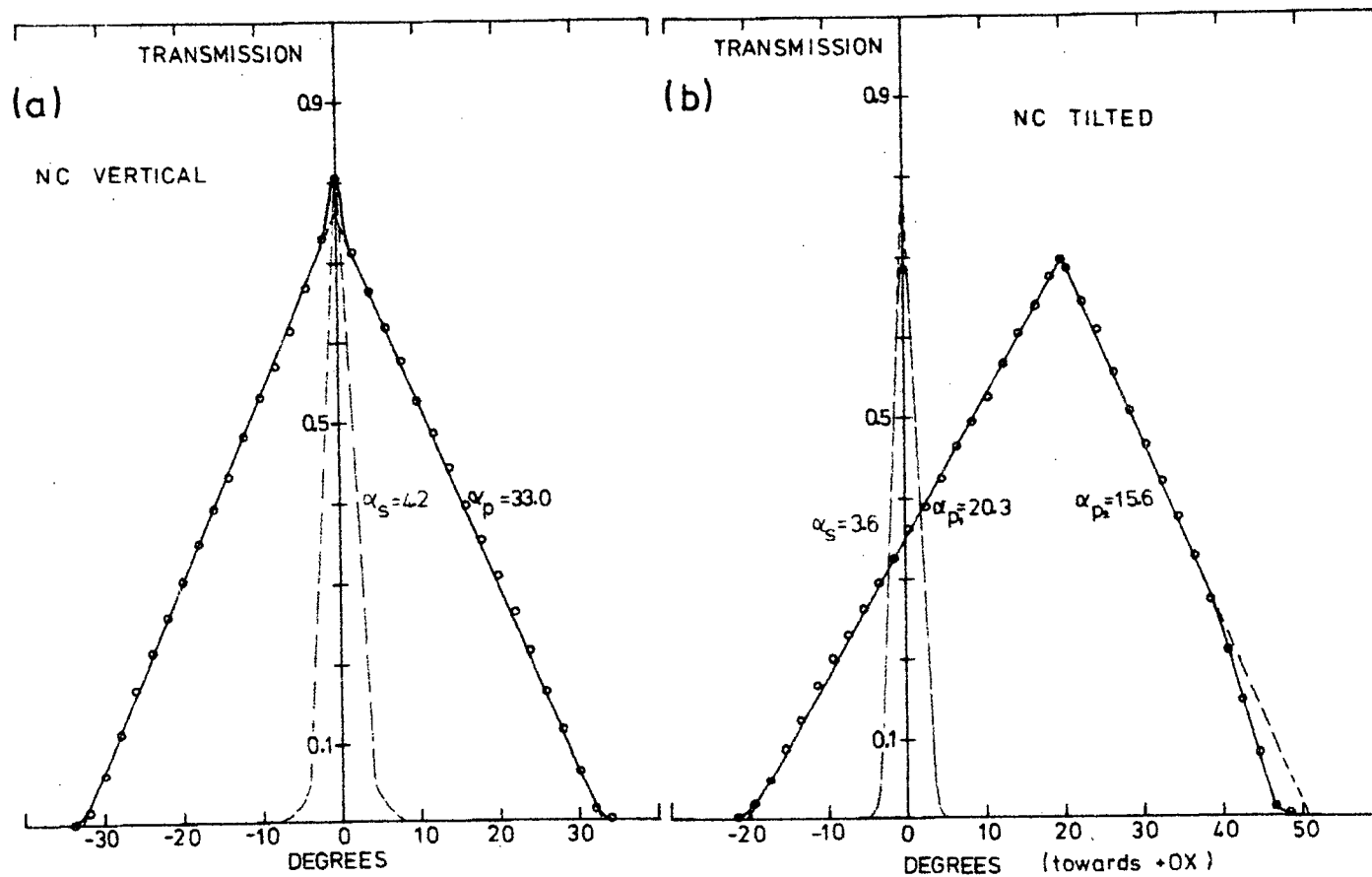is of interest here, is similar to that shown for the T8
vertical.

FIGURE 5.5: Calibration of NC Collimators. (a) NC Vertical response in Spin and Perpendicular directions. (b) ditto, NC Tilted (20° toward +OX).

5.5.2 Effective Area

The effective areas of table (5.5) have been obtained from the total window areas by subtracting

(1)   the area blocked by the collimator housing (mainly in the region of end effects, 4.4.3)

(2)   the area blocked by reinforcing collimator plates and cross bars (assumed circular and close to the window)

(3)   the edge area of counter baffles if they do not coincide with collimator plates or bars.

The remainder is multiplied by T_s, the maximum transmission of the best fit triangle to the spin direction collimator response, and adjusted by the small percentage δ_s to account for the difference in area between the triangle and measured response. Note that a negative δ_s implies an underestimation of source intensity, and to account for this requires division of the measured rate by a smaller area. Correction for window obscuration by the T8 bay aperture and NC mounting rods must be included in the table (5.5) values, prior to use.

5.5.3 Calibration

The NC counters are calibrated, on command, with a "fail safe" ledex arrangement as described for the IV-NC detectors. In the T8 counters the guards are permanently irradiated with a small Fe^{55} source ($\sim$400 cts.sec^{-1}), as with the III-BR counters. In this case each guard output is pulse height

analysed and continuously monitored on four low speed telemetry channels (four quarter channels) giving continuous inflight calibration of the counter. The guard bias levels are included in table (5.5).

5.5.4 Background Rejection

The $V_{c r}$ efficiencies are calculated using equation (3.29), with the exception that the flight V T8 counter $V_{c r}$ is adjusted to account for measured dead regions in the guard (see section 4.5). For the flight VI T8 counters the full $V_{c r}$ values are listed in anticipation of remedial measures presently being applied and tested in these counters.

As an indication of the effectiveness of rejection of nuclear collision induced background, the mean rejection efficiencies when counters are subjected to Co^{60} gamma rays are included (see 4.4.7). Anticipated improvement in the T8 rejection efficiency is again included for the flight VI counters.

5.5.5 Launch

Flight V was successfully launched 09.07 hrs. UT, 16 Apr 1970. All counters, except NC-B appeared to have functioned normally except for a gain decrease caused by the detectors scanning over the sun (see 4.3.3). Data analysis is proceeding.

Flight VI was successfully launched 00.30 hrs. UT, 10 July 1970. Preliminary data indicates that both T8 counters functioned in the desired manner.

CHAPTER SIX

DISCUSSION OF ROCKET RESULTS

6.1 INTRODUCTION

While the nature of X-ray sources remains obscure, continuous re-appraisal of early results in the light of more recent (and sometimes more sophisticated) observations can place restrictions on interpretations arising from the latter, as is the case here.

6.2 LOCATION OF CENTAURUS XR-2

A history of the reported observations of Cen XR-2 is given by Harries (1968). This is extended in table (6.1), and the positional information emphasized. The different intensity measurements are compared and discussed more fully in section 8.4.3. There is a general overall tendency to decrease at both rocket (see also figure 5.3) and balloon energies strongly suggesting a common origin. A "reappearance" at rocket energies in Nov. 68 and an apparent conflict in the Jan-Feb. 1968 results of UCSD and Buselli may indicate a more complicated variation. (The

Date	Group	Vehicle	Energy keV	Flux ergs cm^{-2} s^{-1}	Power Law Index	Collimator FWHM "Azimuth" "Zenith"	Celestial Coord. ra	dec	Galactic Coord. l^{II}	b^{II}*
28Oct65	LRL(G)	RS	2-10	$<2_{10}-9$	-					
13Dec66	Bowyer	RD	1.5-8	"strong"	-		"within 10° of UAT"			
4Apr67	UAT	RD	2-8	$1.5_{10}-7$	1.15	10.5 x 35	208±6	63±3	310.1	-1.3
10Apr67	LEIC	RD	2-5	$1.6_{10}-7$	-	30 x 30	200±4	-60±2	306.9	2.4
20Apr67	UAT	RD	2-8	$1.0_{10}-7$	1.75	10.5 x 35	210±6	-64.5±3	310.6**	-2.9
18May67	LRL(C)	RS	2-8	$2.6_{10}-8$	2.8	10 x 30 (vert & diag)	201±5	-62±2.5	307.1	0.3
28Sep67	LRL(C)	RS	2-5	$<3_{10}-9$	-		-	-		
15Oct67	MIT	B	20-52	$<4_{10}-9$	1.2	13° circular	196.5±3	-64±2	304.9	-1.5
24Oct67	MIT	B	20-52	$2.6_{10}-9$	-	17.5^{o} "	197±6	-64.5±3	305.0	-2.0
17Nov67	UCSD	S)	10-30	$5.2_{10}-9$	1.44	23° "	-	-		
21Nov67	UCSD	S)								
1Dec67	UAT	RD	2-8	$<5_{10}-9$	-					
Jan-Feb68	UCSD	S	10-30	$<$ thresh	-					
29Feb68	Buselli	B	30-40	$<7_{10}-10$	-	10 x 30	-	-		
12Jun68	LEIC	RD	2-5	$<1_{10}-9$	-					
3Nov68	PRL	RS	2-20	$1.5_{10}-8$	1.2	8.7 x 17.2)	201±2	-62.5±2	307	-0.2
7Nov68	PRL	RS	2-20	$2.3_{10}-8$	0.9	8.7 x 17.2)				

IDENTIFICATION				
Cen B	202.95	-60.30	309.74	1.58
NGC 5189	202.50	-65.80	307.19	-3.53
WX Cen	197.25	-63.12	305.26	-0.61
Kes 17	195.8	-62.4		

sighting by Bowyer et al on 13 Dec.1966, has been reported
without evidence and, because of grave difficulties
experienced by these authors in producing an attitude
solution, also for reasons discussed below and in Chapter 8,
is not accepted).

There is a very disturbing lack of agreement in the
reported location of Cen XR-2, indicating either large
systematic errors in attitude solutions or source confusion.
(The possibility of a 10° change of position in 6 months is
not considered seriously because of the velocity and
distance of a source, implied by such a large change of
position). A re-analysis of UAT flight II data yields an
accurate determination of galactic longitude, relatively
insensitive to the attitude solution once its gross features
are established. The process is described below but first
it is enlightening to discuss known details of the various
attitude solutions.

6.2.1 Rocket Observations

The first four rocket sightings of Cen XR-2 in 1967
almost certainly refer to one and the same predominant
object despite the scatter in reported locations. This is
because no source of comparable intensity has been observed
from this region (within $\sim 30^{o}$), before or since, and the
time scale of the intensity decrease is in excellent agreement

with that of the only similar variable, Cen XR-4 (July 1969),

(see figure 6.3). The alternative is that there are two or

more normally unobservable but strongly flaring X-ray stars

in the region with flare time scales≪month, an unlikely one

in view of the relatively stable behaviour of the majority

of sources. Accepting that there is a single point source,

the scatter in reported positions 4 Apr, 10 Apr, 20 Apr,

18 May, 1967, must represent systematic attitude errors

greatly exceeding the quoted ones and the method of estimating

errors must be questioned.

The UAT solutions are discussed in 5.2.2. A number of

points relevant to the present discussion are worth

reiterating:

(1)   the gross features of the rocket motions, shown in

figures (5.1,5.2), are in agreement with BAC least squares

solutions using data from standard three-axes magnetometers

and four sets of sunslits, and quite independent UAT

determinations from the same data.

(2)   Confirmation of attitude solutions during portions of

the flights come from X-ray sightings of the sun and Sco

XR-1. For Sco XR-1 this requires that the statistical

significance of the source count rate allows accurate

determination in the scan direction and the rocket motion

allows the determination "perpendicular" to the scan direction.

TABLE 6.1

OBSERVATIONS OF CENTAURUS XR-2

LRL(G)   -   Grader et al (1966)

Bowyer   -   Bowyer et al (1968)

UAT   -   this thesis, sections 5.2.4, 5.3.3

LEIC   -   Cooke et al (1967), (1969)

LRL(C)   -   Chodil et al (1968b)

MIT   -   Lewin et al (1968b),

UCSD   -   Peterson (1969)

Buselli   -   Buselli (1968)

FRL   -   Rao et al (1969a)

RS   -   spun up rocket

RD   -   despun rocket (see 2.4.6)

B   -   balloon

S   -   satellite

*b^{II} error is similar to dec. error, and l^{II} error is approximately half the r.a. error in this region.

** for more accurate position see below.

Date	Group	Vehicle	Energy keV	Flux ergs cm^{-2} s^{-1}	Power Law Index	Collimator FWHM "Azimuth" "Zenith"	Celestial Coord. ra	dec	Galactic Coord.* l^{II}	b^{II}
28Oct65	LRL(G)	RS	2-10	$< 2_{10}-9$	-		"within 10° of UAT"			
13Dec66	Bowyer	RD	1.5-8	"strong"	-					
4Apr67	UAT	RD	2-8	$1.5_{10}-7$	1.15	10.5 x 35	208±6	63±3	310.1	-1.3
10Apr67	LEIC	RD	2-5	$1.6_{10}-7$	-	30 x 30	200±4	-60±2	306.9	2.4
20Apr67	UAT	RD	2-8	$1.0_{10}-7$	1.75	10.5 x 35	210±6	-64.5±3	310.6**	-2.9
18May67	LRL(C)	RS	2-8	$2.6_{10}-8$	2.8	10 x 30 (vert & diag)	201±5	-62±2.5	307.1	0.3
28Sep67	LRL(C)	RS	2-5	$< 3_{10}-9$	-		-	-		
15Oct67	MIT	B	20-52	$< 4_{10}-9$	1.2	13° circular	196.5±3	-64±2	304.9	-1.5
24Oct67	MIT	B	20-52	$2.6_{10}-9$	-	17.5° "	197±6	-64.5±3	305.0	-2.0
17Nov67	UCSD	S)	10-30	$5.2_{10}-9$	1.44	23° "	-	-		
21Nov67	UCSD	S)								
1Dec67	UAT	RD	2-8	$< 5_{10}-9$	-					
Jan-Feb68	UCSD	S	10-30	$<$ thresh	-					
29Feb68	Buselli	B	30-40	$< 7_{10}-10$	-	10 x 30	-	-		
12Jun68	LEIC	RD	2-5	$< 1_{10}-9$	-					
3Nov68	PRL	RS	2-20	$1.5_{10}-8$	1.2	8.7 x 17.2)	201±2	-62.5±2	307	-0.2
7Nov68	PRL	RS	2-20	$2.3_{10}-8$	0.9	8.7 x 17.2)				
				IDENTIFICATION		Cen B	202.95	-60.30	309.74	1.58
						NGC 5189	202.50	-65.80	307.19	-3.53
						WX Cen	197.25	-63.12	305.26	-0.61
						Kes 17	195.8	-62.4		

sighting by Bowyer et al on 13 Dec.1966, has been reported

without evidence and, because of grave difficulties

experienced by these authors in producing an attitude

solution, also for reasons discussed below and in Chapter 8,

is not accepted).

There is a very disturbing lack of agreement in the

reported location of Cen XR-2, indicating either large

systematic errors in attitude solutions or source confusion.

(The possibility of a 10° change of position in 6 months is

not considered seriously because of the velocity and

distance of a source, implied by such a large change of

position). A re-analysis of UAT flight II data yields an

accurate determination of galactic longitude, relatively

insensitive to the attitude solution once its gross features

are established. The process is described below but first

it is enlightening to discuss known details of the various

attitude solutions.

6.2.1   Rocket Observations

The first four rocket sightings of Cen XR-2 in 1967

almost certainly refer to one and the same predominant

object despite the scatter in reported locations. This is

because no source of comparable intensity has been observed

from this region (within $\sim 30^{\circ}$), before or since, and the

time scale of the intensity decrease is in excellent agreement

with that of the only similar variable, Cen XR-4 (July 1969),
(see figure 6.3). The alternative is that there are two or
more normally unobservable but strongly flaring X-ray stars
in the region with flare time scales$\ll$month, an unlikely one
in view of the relatively stable behaviour of the majority
of sources. Accepting that there is a single point source,
the scatter in reported positions 4 Apr, 10 Apr, 20 Apr,
18 May, 1967, must represent systematic attitude errors
greatly exceeding the quoted ones and the method of estimating
errors must be questioned.

The UAT solutions are discussed in 5.2.2. A number of
points relevant to the present discussion are worth
reiterating:

(1)   the gross features of the rocket motions, shown in
figures (5.1, 5.2), are in agreement with BAC least squares
solutions using data from standard three-axes magnetometers
and four sets of sunslits, and quite independent UAT
determinations from the same data.

(2)   Confirmation of attitude solutions during portions of
the flights come from X-ray sightings of the sun and Sco
XR-1. For Sco XR-1 this requires that the statistical
significance of the source count rate allows accurate
determination in the scan direction and the rocket motion
allows the determination "perpendicular" to the scan direction.

(3)   For both Sco XR-1 and Cen XR-2, the high count rates and precessing motion on both flights permitted location to within $1-3^{o}$ relative to the rocket axes.

(4)   The final attitude solutions gave good agreement in the independent assessments of the Cen XR-2 position, and of course were forced to fit the sun and Sco XR-1 X-ray positions.   Fortunately the Cen XR-2 sightings occurred at times close to either a Sco XR-1 or sun sighting on all occasions.

(In addition flight II gives excellent agreement with reported positions of other galactic X-ray sources, see section 6.3, below).

The April 10, data of <u>Leicester</u> University were also obtained from a despun Skylark rocket launched from Woomera, and the following comments can be made:

(1)   The rocket was launched at night and attitude was determined with reference to only the magnetometers of the standard instrumentation, plus an horizon sensor in an accompanying experiment (B. Cooke, private communication).

(2)   The 30° x 30° collimator is far from ideal for a positional determination, and while a strong source such as Cen XR-2 (10 Apr, 1967) would allow a reasonably accurate statistical fit to the collimator response function in the scan direction, in general it is very difficult to eliminate contamination from other sources.   A large count rate

discontinuity at the horizon, a result of the large

sensitivity to diffuse X-rays with this collimator, is also

capable of confusing results.

(3) Sco XR-1, which along with the sun provided an accurate

inflight attitude calibration on the UAT flights, was on the

horizon. Its position could be gauged accurately only if

there were scans parallel to the horizon (and thus only in

galactic latitude). Although Tau XR-1 was sighted on three

separate occasions it was also near the horizon and in any

case the statistical accuracy of peak response location (with

this weaker source) would be considerably worse than for

Sco XR-1 or Cen XR-2.

The <u>LRL</u> data of May 18, represent a markedly different

situation with respect to attitude solution. The rocket had

negligible precession and high spin rate, ~ 5 rev sec^{-1}.

The X-ray detectors made a large number of scans around the

horizon during which time the galactic disc from Scorpius -

Centaurus, through Vela to Taurus arced above the horizon

(forming an angle of about $20°$ with the horizon). Aspect

determination is considerably simplified from the despun

case. It can be determined from a magnetometer giving the

spin rate, and phased relative to the sightings of known

strong X-ray sources. The solution is assisted by crossed

X-ray collimators, giving a measure of the elevation of the

stronger sources off the (rocket) horizon.

Points relevant to the present discussion are:

(1)   In order to obtain a significant number of counts from weaker sources all scans are superposed giving a single count rate profile per detector for the whole flight. For this flight **peaks** due to both Sco XR-1 and Tau XR-1 provided phasing information.

(2)   The Cen XR-2 peak obtained from the superposition is unresolved from nearby sources, despite a similar collimator FWHM to UAT. This is a result both of the angle of the scans to the galactic disc (giving poorer resolution to sources distributed in galactic longitude than scans along the disc) and the very much reduced Cen XR-2 intensity relative to contaminating sources. Some subjective judgment is required on the relative intensities and positions of sources near Cen XR-2, particularly since one of them Cen XR-3, has only been reported on this flight.

In all four cases it appears as if there are ambiguities and uncertainties capable of explaining the scatter in observed location. The discussion tends to favour the UAT results on the grounds of good statistical location of the Cen XR-2 count rate peak with a minimum of confusion due to known sources, a check of the attitude solutions in the periods of interest, and the good agreement between the two independent solutions. Possibly the greater access to UAT

data contributes to this bias, but in any case the more
accurate assessment of Cen XR-2 galactic longitude, described
below does not depend on a choice between these alternate
positions or attitude solutions.

The other rocket flights mentioned in table (6.1) were
made by PRL, 3 Nov, 7 Nov, 68. Both represent situations
practically the same as LRL in regards rocket motion and
altitude determination, with the exception that there were
no crossed collimators (and in which case the small
declination errors are surprising). The requirement for the
observed count rate deviation to be due to the same source
as the Apr. 67 one is far less demanding.

6.2.2 Balloon and Satellite Observations

The MIT balloon flight on 15 Oct, 1967, represents the
best positional determination for the source observed at
energies above 10keV. This flight has both a smaller field
of view and better counting statistics than later ones (the
latter being partly due to maximum observed source intensity
on this date). The attitude determination, done with
reference to a magnetometer and sun sensor is claimed to give
the direction of telescope axes to within 1° throughout the
flight for the 15 Oct. case, and presumably Sco XR-1 X-rays
provided an inflight attitude check. These factors plus the
agreement with position determined on the 24 Oct 67, MIT

balloon flight give considerable weight to the location

reported by MIT for the high energy object.

The statistics for the Buselli sighting do not allow

an accurate positional determination (G. Buselli, private

communication) and this is possibly also the case for the UCSD

results, (OSO III) which quote the MIT position but give no

discussion or errors.

6.2.3   Identification

Identification with optical or radio objects is greatly

hampered by the proximity of the source or sources to the

galactic plane.   Nevertheless table (6.1) includes the

positions of four prominent objects in the region.   Cen B

is a strong radio source regarded by Shklovsky as a supernova

remnant 185 (Poveda and Woltjer, 1968); Kes 17 is a non thermal

radio source, a possible supernova remnant, Milne (1970).   The

optical objects in planetary nebula NGC 5189, and WX Cen were

suggested as identifications of Cen XR-2 by Feast (1967),

Blanco et al (1968), and Eggen et al (1968) respectively.

6.2.4   Cen XR-2 (Apr.67) Galactic Longitude

Flight II offers a unique opportunity of determining

the galactic longitude of Cen XR-2.   Accepting figure (5.2)

as a reasonable representation of a rocket motion it can be

seen that there are several scans essentially parallel to

the galactic disc in this region, and many of these also pass

Sco XR-1 a small part of a spin period earlier.

The approach employed here is to use the approximate attitude solution to predict the single scan count rate profiles expected from Sco XR-1 plus a single point Cen XR-2 source at the various positions quoted in table (6.1). These are compared directly with the observed "raw" count rates. Second order effects due to the incorrect attitude solution and contamination by known weak sources are allowed for in the interpretation of the compared results.

Figure (6.1) shows a series of 11 consecutive scans by detection system A over the region of interest. These have been obtained from the attitude solution as follows; the galactic co-ordinates of the directions in the rocket XZ plane (remembering that OX is the spin axis and $\pm$ OZ the detector axes), at 0°, $\pm 15^{\circ}$, $\pm 30^{\circ}$ from the $-OZ(A)$axis have been evaluated and plotted every 0.1 seconds of the scan. (With a mean spin period of 12.55 seconds during this part of the flight, this corresponds approximately to every 2.87° of galactic longitude). The time of maximum response to a given source within the 70° full width of the collimator long field of view can then be predicted to an accuracy of about .01 seconds. This is illustrated in figure (6.1) for only two short periods of scan 21, where the dashed lines were obtained by joining the 0°, $\pm 15^{\circ}$, $\pm 30^{\circ}$ points by a smooth curve. Open circles show the various Cen XR-2 positions (the
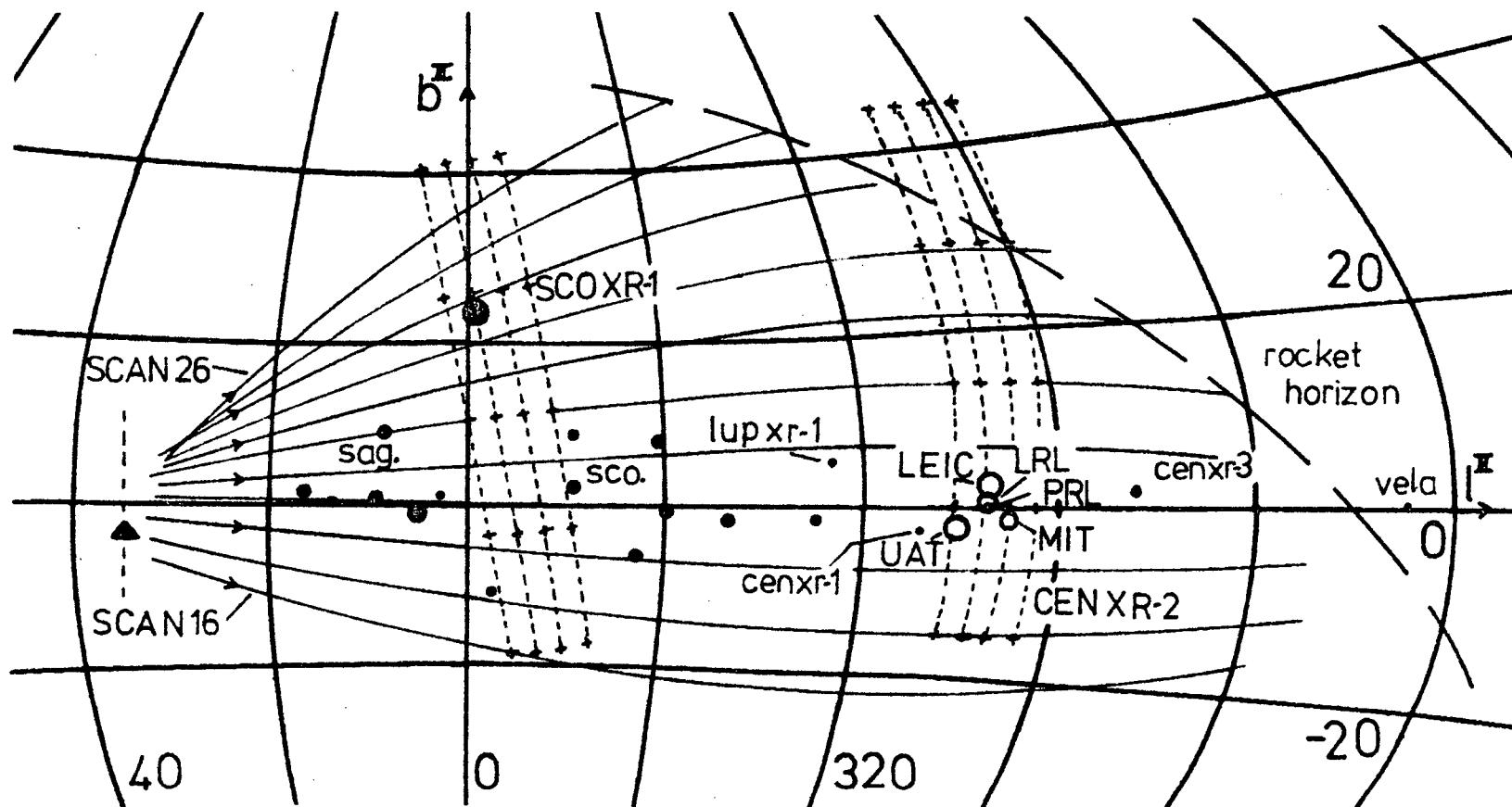
FIGURE 6.1: Positions of Cen XR-2. Eleven scans of Flight II detector A giving accurate position of Cen XR-2 relative to Sco XR-1. Dashes are collimator long axis each 0.1 seconds of scan 21.

UAT mean position, section 5.2.4, is used). Closed circles
indicate other sources. As in figure (5.2), the circle size
is a rough indication of source intensity.

Columns (3)-(5) of table 6.2(a) list the predicted
times of sightings of Sco XR-1, and the Cen XR-2 positions
of UAT and MIT (the extremes in galactic longitude). Also
included in brackets are the angular separations of the
source positions from the predicted scan paths at the time
of sighting.

The times of occurrence of count rate peaks, obtained
from the least squares fitting technique of Appendix B, are
given in columns (6), (7) of table 6.2(a). Note that the
fitting of the triangular collimator response has been
restricted to scans for which the source position lies within
the FWHM ($\alpha_p = 35^{\circ}$) of the collimator long axis, and that for
reasons discussed in 5.2.1 the statistical significance of
detector B results are generally inferior to those collected
with A.

The differences between the count rate peak times and
predicted peak times are collected into table 6.2(b). The
errors combine the standard deviations in the count rate peak
position and the estimated $\pm$ .01 second predicted response.
Apart from a tendency to increase near the end of the flight
(perhaps associated with gradual re-entry) the differences
indicate no obvious systematic trends and the consistency of

TABLE 6.2(a)

FLIGHT II TIMES OF SOURCE MAXIMUM RESPONSE

Scan	Detector	Predicted from Attitude Solution Pk time ± .01 secs: (Angle from scan)			Count Rate Peak Time(± σ)	
		Sco XR-1	Cen XR-2: UAT	MIT	Sco XR-1	Cen XR-2
16	A		273.20 (−20°)	273.41		
	B		279.40 (−17°)	279.68		279.440 ± .019
17	A		285.76 (−13°)	285.97		285.750 ± .016
	B		292.04 (− 9°)	292.24		292.010 ± .017
18	A		298.32 (− 5°)	298.51		298.330 ± .015
	B		304.60 (− 1°)	304.78		304.540 ± .017
19	A		310.86 (2°)	311.05		310.810 ± .014
	B		317.13 (6°)	317.32		317.110 ± .016
20	A	321.74 (−18°)	323.40 (10°)	323.60		313.350 ± .016
	B	328.01 (−15°)	329.67 (14°)	329.87		329.700 ± .017
21	A	334.30 (−13°)	335.90 (17°)	336.10	334.240 ± .013	335.880 ± .016
	B	340.57 (−10°)	342.16 (20°)	342.35	340.510 ± .013	
22	A	346.84 (− 7°)	348.41 (24°)	348.62	346.790 ± .013	
	B	353.10 (− 5°)			RF	
23	A	359.36 (− 3°)			359.310 ± .012	
	B	365.62 (− 1°)			365.610 ± .012	
24	A	371.85 (2°)			371.820 ± .011	
	B	378.09 (3°)			378.000 ± .014	
25	A	384.33 (5°)			384.260 ± .013	
	B	390.57 (7°)			390.500 ± .013	
26	A	396.81 (10°)			396.720 ± .013	
	B	403.05 (12°)				

RF − Recording Failure

TABLE 6.2(b)

PREDICTED TIME MINUS COUNT RATE PEAK TIME

Scan	Detector	Time Difference $\pm \sigma$ secs.		
		Sco XR-1	Cen XR-2 (UAT)	Cen XR-2 (MIT)
17	A		-.04 ± .02 +.01 "	+.24 ± .02 +.22 "
	B		+.03 "	+.23 "
18	A		-.01 "	+.18 "
	B		+.06 "	+.24 "
19	A		+.05 "	+.24 "
	B		+.03 "	+.21 "
20	A		+.05 "	+.25 "
	B	(Gal.Centre)	-.03 "	+.17 "
21	A	+.06 ± .02	+.02 "	+.22 "
	B	+.06 ± .02	(outside FWHM)	
22	A	+.05 ± .02		
	B	R.F.		
23	A	+.05 ± .01		
	B	+.01 ± .01		
24	A	+.03 ± .01		
	B	+.09 ± .02		
25	A	+.07 ± .02		
	B	+.07 ± .02		
26	A	+.09 ± .02		
	B			
weighted mean		.044 ± .004	+.017 ± .006	+.220 ± .006

the values is emphasized in figure (6.2). This shows the detector A raw count rate histograms along with the collimator response best fits to the Sco XR-1, Cen XR-2 peaks. The times of predicted response are clearly indicated. For each source position the weighted mean of the differences of table 6.2(b) have been obtained and are included in the table.

In the case of Sco XR-1, the mean difference is +.044 seconds. This is not entirely due to the errors in attitude solution. For example using the source positions and intensities for the galactic centre region given by Mayer et al (1970), then for scan 21A the contribution of the Sagittarius and Scorpius sources to the anticipated Sco XR-1 peak results in a slight broadening and a shift in mean position -.015 seconds. Inspection of figure (6.1) shows how this shift towards the Sagittarius sources tends to persist even as the relative Sco XR-1 intensity increases, since the contribution by the other Scorpius sources quickly diminishes. Accepting a -.015 ± .007 second shift as encompassing this "second order" source contamination effect, leaves an attitude solution error along the scan direction of

$$+.029 \pm .008 \text{ seconds.}$$

This implies that the UT Cen XR-2 position used in the analysis, i.e. with $l^{II} = 310.3^{\circ}$, is in error by the angle swept out by the rocket in (.029 - .017) = .012 ± .010 secs.
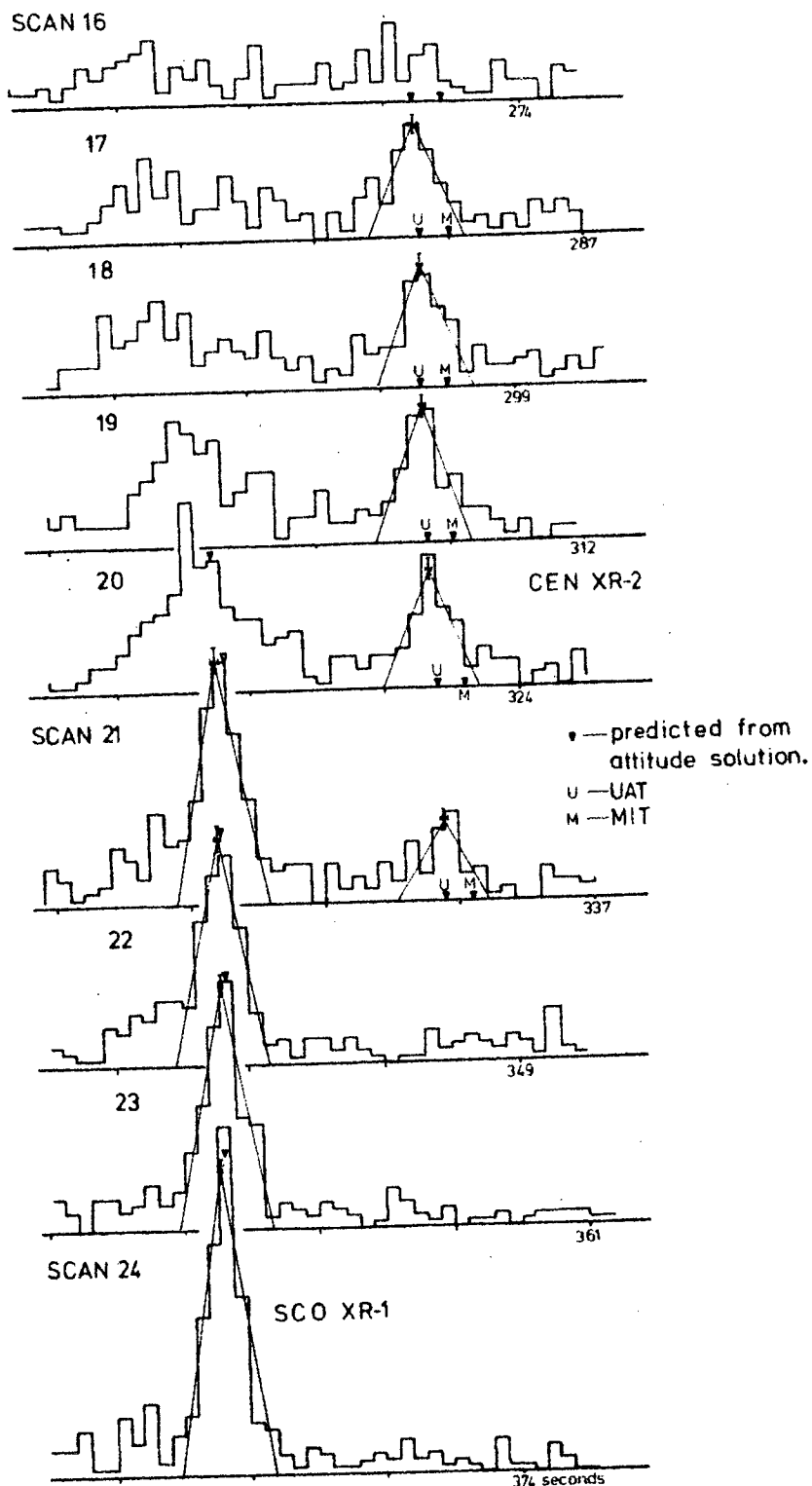
FIGURE 6.2: Count Rate profiles corresponding to Scans 16-24 of Figure (6.1). Least squares fits to Sco XR-1, Cen XR-2 peaks are compared to peak positions predicted from both UAT, MIT source positons.

Since the scan paths are very nearly parallel to the galactic

disc in the region and (certainly for scan 19) move at

$360/12.55 = 28.7^{\circ}$ of galactic longitude sec^{-1} in the

direction of decreasing longitude, this implies a Cen XR-2

(Apr.67) position of

$$1^{II}_{\text{Cen XR-2(Apr.67)}} = 310.0 \pm 0.3^{\circ} \qquad (6.1)$$

The MIT position with $1^{II} = 304.9 \pm 1.5^{\circ}$ is clearly

excluded, as was obvious from the raw count rate data of

figure (6.2). Accepting the MIT position for the object

detected in hard X-rays, presumably the same object as that

seen by UCSD (Nov.67) and Buselli (Feb.68), implies that

these hard X-rays come from a quite different region of

space than Cen XR-2 (Apr.67), i.e. Cen XR-2 (Apr.67) and

Cen XR-2 (Oct.67) are _different objects_ despite similarities

in behaviour with respect to variability.

Error bars on the LRL postion very nearly overlap

those in equation (6.1). The direction of LRL scans does not

permit good resolution of their Cen XR-2 position and the

UAT one, and a small error in their determination of the

source separation from the scan plane would reduce the

differences in galactic longitude. The position of the

Cen XR-3 source, reported by LRL and unresolved from their

Cen XR-2 peak, was scanned and resolved on flight II. The

published intensity of 0.7 x counter efficiency (2.1-9.5 keV)

can be meaningfully applied to the UAT counters which have practically identical window-gas combination. Count rate data within a FWHM of the predicted peak time for Cen XR-3 were added for six scans 18 A,B, 19 A,B, 20 A,B giving a total of 70 counts compared with the expected background rate of 59.2 $\pm$ 2 counts (derived from $\sim$ 20 seconds of data away from known X-ray sources). In the observation time, the measured rate exceeds the mean background rate by just over 1σ, which is not considered significant. Using the LRL intensity a total of $\sim$ 100 counts would have been expected, i.e. a significant 3σ response. These data indicate that Cen XR-3, if it exists, is weaker (or was weaker on 20 April, 1967) than reported by LRL. Cooke et al (1969) report the suggestion of a source at this longitude but $b^{II} \simeq -15^{\circ}$, not incompatible with UAT results, but still implying an incorrect extraction of LRL Cen XR-2 data.

The Leicester position error bars do not overlap the flight II longitude, even though there is no doubt that both flights saw the same strong source. As already mentioned, it is not difficult to imagine systematic errors in attitude solution within the limits of published information which could explain the difference. A similar uncertainty can be considered in the case of the PRL data, though it is equally likely that Cen XR-2 (Nov.68) is associated with the MIT object.

The identification of Cen XR-2 (Apr.67) can be definitely excluded in the cases of Kes 17, WX Cen and NGC 5189, but not in the case of Cen B. Cen B is at the limit of the UAT error bars in the b^{II} direction ($\sim 3^{\circ}$). There are no data on the variability of radio emission, though observations over more than 10 years at a variety of frequencies have seen the source as strong. Hamilton and Haynes (1968) by comparing the 10MHz intensity with earlier high frequency measurements conclude that Cen B is $<$ 2.3 kpc from the solar system. Note that the identification of MIT's Cen XR-2 (Oct.1967) with WX Cen is still a possibility.

6.3   MODELS OF CEN XR-2

6.3.1   Cen XR-4 (Jul 69)

Interest in Cen XR-2 has been revived not only by the unexpected MIT and PRL reports but also by the observations from Vela satellites 5A, 5B of the sudden appearance and gradual disappearance of Cen XR-4. Figure (6.3) is reproduced from Evans et al (1970) showing the behaviour of Cen XR-4 as monitored by the 3-12 keV scintillators, each with two channel pulse height analysis. The times of two independent observations of Cen XR-4, discussed below, are included. The intensity variation of Cen XR-2 is directly compared with the Cen XR-4 count rate data by Evans et al by normalizing to the
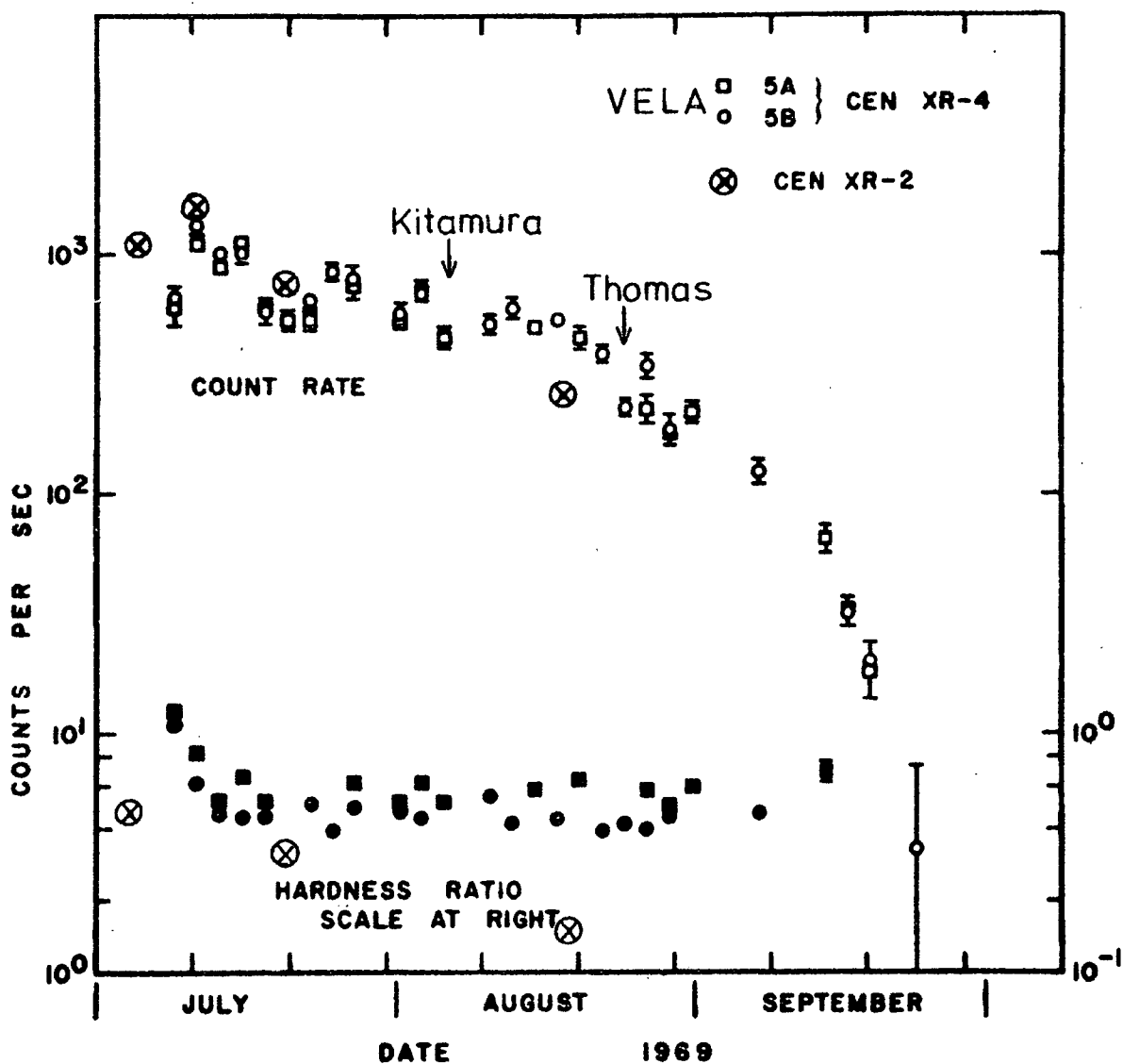
FIGURE 6.3: Variability of Cen XR-4, Cen XR-2 from Evans et al (1970).
Count rates are normalized, Hardness ratios are not.
Times of two independent sightings of Cen XR-4 are
indicated.

peak count rate; the resulting crosses show striking

agreement with the Cen XR-4 count rates. Included also is a

measure of the relative behaviour of a hardness ratio for

Cen XR-2, obtained by integrating the best fit spectra

(figure 5.3) between 2-5 and 5-8 keV and plotting the ratio

of high to low energy fluxes. Because of the markedly

different spectral responses of the different detectors, no

attempt is made to normalize to the Vela hardness ratio. It

is tempting to attribute both sources to a common

astrophysical process, but first differences in the reported

behaviour must be discussed.

The spectral information on Cen XR-2 comes from LRL,

18 May,67. Their data, like that of UAT, are fitted by any

of the forms given in equations (1.4), (1.5), (1.8), however

the power law dependence gives the best fit. The MIT and

PRL spectra are also both more compatible with a power law

but as seen above, do not necessarily refer to the same

object. The obvious contamination of the LRL data by other

peaks may have influenced the spectral shape, particularly

if contaminating spectra were markedly different from that of

Cen XR-2. Cen XR-4, on the other hand, was observed by

rocket on 7 Aug.69 by Kitamura et al (1969) who report an

exponential shape practically identical to that of Sco XR-1,

observed on the same flight. If their characteristic

temperature (kT=7keV) was obtained using a simple exponential

without Gaunt factor (see equations 1.5, 1.6) then this is

an unusually high temperature for Sco XR-1 and the data cannot

be simply extrapolated to explain the balloon results of

Thomas et al (1969), taken on 25 Aug.69, a much softer

spectrum being required. The apparent conflict between the

three sets of data is very likely systematic in origin, but

may indicate a high energy cut-off or break in the Cen XR-4

spectrum, or a spectral variability in a time short c.f.

3 days, the interval between successive Vela sightings.

While the April-May 1967 data show that Cen XR-2 is

decidedly "non-isothermal", an isothermal character is

indicated by the Vela data for Cen XR-4 after the first week.

Criticism might be levelled at the comparison of UAT and LRL

temperatures particularly with the possibility of source

contamination affecting the LRL data, and it could be argued

that the temperature of Cen XR-2 changed sharply about

4 Apr.67 and only slowly afterwards. By comparison with

Cen XR-4 this implies a Cen XR-2 age of only a week or so

on 4 Apr.

Evans et al see a similarity between the intensity

decrease in Cen XR-4 and the light output from nova of the

DQ Herculis type. The light intensity decreases a mean of

0.25 - 0.30 magnitudes per day until 80 to 120 days after

onset, when a much sharper decay occurs to a deep minimum.

There is then a second increase to a reduced maximum

followed by a slow decay and Evans et al point to the MIT and PRL observations of a reappearance of Cen XR-2 as evidence of this behaviour. As seen above, this is certainly not the case if these X-rays originate in the MIT, PRL positions. (Also, the intensity decrease of Cen XR-4 appears in fact to be very nearly linear with time, and the implications of this are mentioned below). There is no object similar to the radio source Cen B within 10° of Cen XR-4.

6.3.2   Models of Cen XR-2 (Apr 67), Cen XR-4 (Jul 69)

The model of Cen XR-2 which has received most prominence is a highly idealized one, requiring the expansion and cooling of a thin hot plasma (Manley, 1967, Chodil et al 1968, Edwards 1968, Harries 1968). In brief the spectral and intensity data for 4 Apr, 20 Apr and 18 May, 1967, are used in equation (1.6) to obtain a temperature T, and emission measure $n_e^2 V/d^2$ (assuming a hydrogenic plasma), on each date. Assuming a constant mass plasma ($n_e V$ = const.) at fixed distance from the solar system implies that the measured fluxes depend only on T, and the inverse of the volume, V^{-1}.

Manley assumed an isothermal source so that for a constant expansion velocity (assumed to be the velocity of sound in the plasma, $V \sim 5_{10} 7$ cm sec^{-1}) the measured flux from a spherical plasma is proportional to t^{-3}, t in seconds.

The other authors incorporate the measured temperatures to arrive at essentially the same result, i.e. a plasma radius expanding from $\sim 3_{10} 14$ cm on 4 Apr 67 with t^3 dependence. A doubling of the plasma volume between 4 Apr. and 18 May then implies an age on 4 Apr of about 4 months, the cooling implies a flux change slightly slower than in t^{-3}. By comparing the total radiated bremsstrahlung, from (1.6),

$$dE/dt \simeq 1.43_{10} -27 \ n_e^2 \ T^{\frac{1}{2}} V \quad \text{ergs.sec}^{-1},$$

with the thermal energy content of the plasma

$$E = 3 \ n_e kTV = 4.14_{10} -16 \ n_e TV \text{ ergs.}$$

then gives a measure of n_e. Harries uses the measured values of T, V to obtain γ in the expression $TV^{\gamma-1} = $ const. In an adiabatic expansion of spherically symmetric particles, $\gamma = 1.67$ and the measured 2.1 is taken to indicate 39% of the cooling is due to radiated photons, the rest to expansion. This gives $n_e \sim 9_{10} 7$ cm^{-3}. Using n_e,V in $n_e^2 V/d^2$ implies a distance d = 0.5 kpc.

Edwards comments on the difficulty in maintaining steady gas expansion through gravitational constraint at the high temperatures and goes on to suggest heating of a gas envelope by an adiabatic strong shock moving radially outwards. To fit the C_{en} XR-2 data requires conservation of the quantity $(n_e^2 V/T)$ during expansion, and this is constant for a shock propagating into a non uniform gas density n, varying as (radius)$^{-2}$. The X-radiation is shown to originate in a thin

shell of thickness $\Delta R \sim R/4$, where $R \propto t^{2/3}$ is the radius of the shock front. As above, this model gives $R \sim 3_{,0}14$ cm on 4 Apr but at this time the source is only about two weeks old and the intensity suggests a distance of 0.3 kpc.

Finally Manley (1968) combines the uniform expansion (approximately isothermal) with a shock wave model to explain the cool (Apr - May 67) and delayed hot (Oct 67) Cen XR-2 radiation respectively. Since the evidence above strongly suggests that these two sources are spatially resolved, this elaborate hypothesis does not appear to be required as yet.

A criticism affecting all of these hot plasma models relates to the expected optical luminosity. The Edwards model is based on the behaviour of recurrent nova, and he predicts an optical outburst of 4th magnitude in March-April 1967. The other models are also suggestive of nova and an ejected plasma at the suggested temperatures should be highly luminous. The lack of observation of optical nova in the vicinity of Cen XR-2 has been excused on the basis of possible obscuration by dust since this is in the direction of the local spiral arm. If Cen XR-4 is taken as a second example of the process, the further lack of optical activity (particularly in view of the 20° separation off the galactic disc in this case) throws some doubt on the nova models. (The tacit assumption is that a nova outburst would have been

detected, either directly or by subsequent comparison of optical plates of the respective regions).

A striking feature of the count rate behaviour of C_en XR-4, pointed out by Evans et al, is the marked deviation from a simple t^{-n} dependence, required by the simple models above. For the nova models to survive (and the similarity of the C_en XR-4 variation to date, with the DQ Herculis type novae deserves further investigation), more convincing evidence for the lack of observed optical activity is required. As well, more complicated models for X-ray emission are necessary. For example some self absorption in the source might immediately explain some of the observed features, such as the initial change in hardness ratio of C_en XR-4. (As pointed out by Manley, a plasma with the mass associated with the C_en XR-2 model, when compressed to within a radius $\sim 10^{14}$ cm, can no longer be considered optically thin).

Prompted by the non luminous character of Sco XR-1, Prendergast and Burbidge (1968) develop the model for plasma heating by mass accretion between binary members of an old nova, as discussed in 1.6.2. They suggest that the Cen XR-2 variability might be the result of a large variation in the mass transfer between the members. Despite possible difficulties with optical thickness as pointed out by Manley

and Olbert (1969), mass accretion between members of a binary
pair has some attractive features, for example the count
rate behaviour of Cen XR-4 is very nearly <u>linear</u> with time,
as might be anticipated from the eclipsing of an emitting
region. Temperature variations may occur with a non-isothermal
emitting region (e.g. Cen XR-2). The Cameron (1969)
accretion model, comprising an optically thick ring of matter
about a white dwarf would exhibit similar properties. Such
X-ray sources might be expected to reappear when the system
is suitably oriented and sufficient accretion occurs.

Models in which X-rays are emitted from a cooling
neutron star can be criticized on similar grounds to the nova
models, though more severely. A neutron star is expected to
result from a super nova explosion the optical and radio
evidence for which would almost certainly have been reported.
Also, a neutron star cools principally by neutrino emission
and Wolf (1966) gives the temperature T at time t (secs)
after an initial very high temperature $(> _{,0} 10^{o} K)$ in the form
$T \propto t^{1/6}$ ^{o}K. Harries has shown the Cen XR-2 intensity data
(including the 28 Sept 67 upper limit) to be incompatible with
neutron star cooling and this is even more evident for Cen XR-4.

The spectral shape and time dependence of X-rays
resulting from the injection of a variety of electron spectra
into a magnetic field, impulsively at t = 0 or at some later

time, or continuously, or at variable rate, are considered by

Tucker (1967). Situations encompassing Fermi acceleration of

the electrons and expansion of a tenuous plasma containing

the field are also considered. For example injection of an

electron spectrum $dN_e/dE = kE^{-n}$ electrons $cm^{-2} sec^{-1} keV^{-1}$ at

$t = 0$, gives a photon spectrum

$$\frac{dN}{d(h\nu)} \quad \alpha \begin{cases} (h\nu)^{\frac{1-n}{2}} & , \quad \nu \ll \nu_b \\ \\ t^{\frac{-n+5}{3}} \quad (h\nu)^{-2\frac{n+1}{3}} & , \quad \nu \gg \nu_b \end{cases}$$

where $\nu_b = 1.1_{10} 9 H^{-3} t^{-2}$ (Hz), and electrons lose energy by

synchrotron radiation alone. Here H (gauss) is the mean

magnetic field strength, and t is measured in years. Harries

(using the above equations close to ν_b) obtains good agreement

with the Cen XR-2 data using $H \sim 10^{-3}$ gauss, n = 3.3, and an

age on 4 Apr 67 of $\sim$ 3 weeks. The "temperature" change is a

result of ν_b moving through the observed frequency range

between 4 Apr and 18 May. Obviously a system can be

engineered to fit the Cen XR-4 data, for example the energy

loss rate can be adjusted by an increasing magnetic field

due to a plasma contraction, or by an electron acceleration

process similar to that described by Manley and Olbert (1969),

see 1.6.2. Without more intimate knowledge of the

astrophysical situations which give such conditions, a

detailed analysis is not warranted.

6.4   CYGNUS - SERPENS SOURCES

As mentioned in 1.6.3 some controversy still exists on
the variability of sources in the Cygnus and galactic centre
regions. The flight II scans, used above to obtain an
accurate Cen XR-2 position, also passed along the galactic
plane from Cassiopeia (on the horizon), through Cygnus to the
galactic centre (see figure 5.2). The convergence and
intersection of the scans permits sufficient superposition to
imply significant responses from anticipated weak sources.
The galactic centre sources and a group in Cassiopeia-Cepheus
are unresolved by the 10.5° collimator FWHM, and the discussion
is therefore restricted to galactic longitudes

$$20^{\circ} \leqslant l^{II} < 100^{\circ}$$

The Cygnus sources are also unresolved by the collimator;
however resolution is assisted by early scans which pass over
the Cygnus region in a direction perpendicular to the plane,
and by the fact that Cyg XR-1, Cyg XR-2 are resolved in both
directions and have always been reported to be much more
intense than others nearby. The results for this flight can
be meaningfully compared with _more_ accurate surveys of the
region.

6.4.1 High Resolution Surveys

By far the most accurate and comprehensive survey of
the galactic disc in this longitude range to date, was made

from rocket by American Science and Engineering (ASE) on 11

October 1966. (Giacconi et al 1967, Gorenstein et al 1967,

Gursky et al 1967). Detectors with vertical and tilted

1° x 40° FWHM collimators (3.6.1) were scanned slowly along

the galactic plane from Scorpius to Cygnus, and manoeuvred in

a complex but controlled fashion over the Cygnus region.

Attitude to within ~ 2' arc was provided by 1 sec interval

photographs of the star field. Proportional counters with

beryllium windows of nominally the same thickness as used by

UAT allow comparison of the _relative_ count rates of sources

with those obtained on flight II. Large window area (~800 cm²)

and relatively long observing time imply good counting

statistics.

Only six sources were detected in $20^{\circ} < 1^{II} < 90^{\circ}$ and

within about $\pm$ 15° of the galactic disc, these are given in

table 6.3. Sources not observed but previously reported in

surveys with inferior angular resolution include Cyg A,

Cyg XR-4 and Vul XR-1 (see Giacconi et al 1967). With

intensities at upper limits set by Giacconi et al, these

would not have been observable on flight II and are not

considered further.

TABLE 6.3

POSITION AND INTENSITY OF ASE(11OCT66) CYGNUS-SERPENS SOURCES

Source	l^{II} degrees	b^{II} degrees	Intensity(2-5keV) (counts cm^{-2} sec^{-1})	Comment
GX+36.3	36.3±0.2	9± 8**	0.15	ScoXR-1(Friedman et al, 1967)
GX+48.7	48.7±0.2	0±15	0.19	
Cyg X-1	71.4*	3.1*	0.40	CygXR-1(" ")
Cyg X-3	80.0*	0.7*	0.13	
Cyg X-4	82.9*	-6.4*	0.05	
Cyg X-2	87.4*	-11.3*	0.36	CygXR-2(" ")

(*errors ± 20', see Giacconi et al, 1967)

(** Friedman, gives b^{II} = 3.3 ± 4.0°)

A second rocket flight yielding accurate and reliable X-ray data in the region was launched by Naval Research Laboratories (NRL) on 7 September, 1967 (Meekins et al 1969). A 220 cm² 0.5 mil Mylar windowed proportional counter with 10° FWHM honeycomb collimator was held in each of the Cyg XR-1, Cyg XR-2 directions for ~41 seconds, as part of a series of inflight manoeuvres over the sky. The hold positions excluded any contribution from other known sources. Meekins et al point out the following:

(1)   A fit of ASE spectral shape to NRL Cyg XR-1 data implies a 26% increase in absolute intensity from 11Oct66 to 7Sept67, a slight spectral hardening is also indicated. These changes may be significant.

(2)   Similarly a 50% increase in Cyg X-2 intensity <u>is</u>

indicated. The ratio of Cyg X-1/Cyg X-2 intensities (2-5keV)

are

$$\text{ASE (11Oct66)} \qquad 1.11 \qquad\qquad (6.2a)$$
$$\text{NRL (27Sept67)} \qquad 0.92 \qquad\qquad (6.2b)$$

The measured spectra of Cyg X-1, -2 and -3 (Gorenstein et al)

show Cyg X-2 with a steeper spectral shape than Cyg X-1 which

in turn is steeper than Cyg X-3. Without entering into a

discussion on whether the flattening is due to hot sources or

interstellar absorption or both, it is recorded that

measurement over 2-8 keV will give a 20% and 25% increase in

intensity of Cyg X-1, Cyg X-3 counts respectively relative to

Cyg X-2, when compared to 2-5 keV data. This fact is required

because data on weaker sources of table 6.3 are only

published in 2-5 keV, where as the total 2-8 keV UAT data are

used below, to give good statistics.

6.4.2 Flight II results

Count rate data (per 0.1 sec) for 10 scans by detector

A (figure 5.2) and 9 by detector B, symmetrically located

about the galactic plane, were arranged about the times of

"sighting" GX 36.3 (these times were obtained from the

attitude solution in the manner described in 6.2.4). The

count rates were simply added and the resulting histogram is

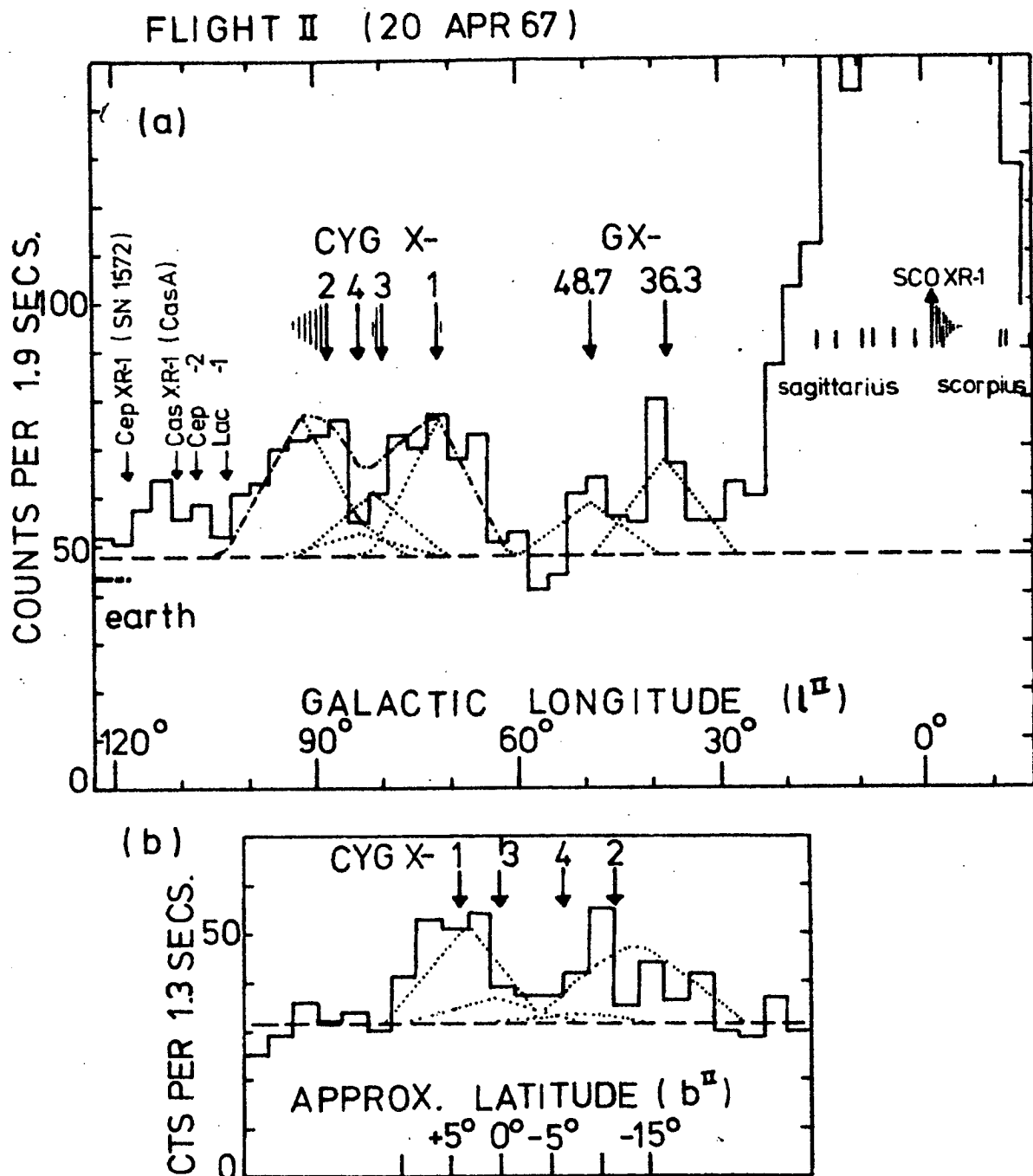plotted against galactic longitude in figure 6.4(a). The

FIGURE 6.4: Cygnus–Serpens Sources: (a) Superposition of scan counts parallel to galactic plane (figure 5.2). (b) Superposition approx. normal to plane. Arrows indicate known source positions.

dashed line represents the mean sky background, obtained

from 20 seconds of data collected for $b^{II} < -30^{\circ}$ and away from

known source positions and the horizon. The galactic longitudes

of the sources listed in table (6.3), and others, are indicated

by arrows, however because of the changing orientation of the

scan lines relative to the galactic plane, only sources close

to $b^{II} = 0^{\circ}$ are expected to give count rate peaks at these

positions.

Two peaks, each of width ~ 0.7 secs (the time

representing the full width of the collimator in the scan

direction) are clearly resolved and correspond roughly to

Cyg X-2, Cyg X-1. The number of counts under each represent

$\sim$ an 8σ increase above the mean background level. That the

majority of counts is indeed compatible with only two strong

source regions near the Cyg X-1, Cyg X-2 positions is shown

in figure 6.4(b). This is the super-position of count rates

from 13 scans (A and B, including scans 3 to 9 of figure 5.2)

roughly perpendicular to the galactic plane and therefore

plotted against galactic latitude. (The dotted lines are

predicted responses from the sources discussed in the

analysis, below). The super-position is arranged about the

predicted times of sighting Cyg X-1 which distorts the response

expected from Cyg X-2. For this reason and because of

possible source contamination with the 70° collimator full

width lying along the plane, these data are not used further

in estimating source intensities.

Proceeding with the analysis of data of figure 6.4(a), the assumption is made that the UAT count rate comprises contributions from only those sources listed in table 6.3 for $25^{\circ} < 1^{II} < 100^{\circ}$. The shapes and positions of responses to sources in the Cyg X-2, Cyg X-1, GX 48.7 and GX 36.3 positions can be predicted using the attitude solution, (because of the convergence of scan paths this can be done for the last two despite uncertainties in their latitude, and Cyg X-2 is the only source for which the collimator triangular shape is seriously distorted). These response functions are shown as dotted "triangles" where in the case of GX 48.7, GX 36.3, they have been normalized to the counts in excess of the mean background within the collimator full widths (counts in the 0.2 sec overlap are equally divided).

For the Cygnus sources, an average angular separation of the scan paths from each source has been obtained from the attitude solution. These are applied to the collimator response function $(\alpha_p = 35^{\circ})$ giving a collimator efficiency for each source, which can be directly applied to the total count rates to obtain source intensity in counts $cm^{-2} sec^{-1}$. Making a further assumption that Cyg X-3, Cyg X-4 have the same intensities relative to Cyg X-2 as reported by ASE, and incorporating the collimator correction then allows the four Cygnus response functions to be normalized to the observed count rates. The sum of the normalized response functions is

shown in figure 6.4(a) to be good representation of the data
(dot-dashed line). Cyg X-2 was chosen as the standard simply
because it is better resolved from Cyg X-3 than is Cyg X-1.
Table 6.4 gives the collimator efficiencies and 2-8 keV
intensities, normalized to the 2-5 keV ASE intensity of
Cyg X-2.

TABLE 6.4

INTENSITY OF FLIGHT II CYGNUS-SERPENS SOURCES

Source	Collimator Efficiency	Normalized Intensity (2-8keV) counts cm^{-2} sec^{-1}	$R = \dfrac{UAT(2-8keV)}{ASE(2-5keV)}$
GX 36.3	0.91	.11 ± .03	0.73 ± .35
GX 48.7	e	(.06 ± .04)/e	0.37±.29<R<.53±47*
Cyg X-1	0.69	.24 ± .06	0.60 ± .21
X-3	0.67	(.13 ± .05	-
X-4	0.60	{ .05 ± .05	-
X-2	0.52	(.36 ± .08	1.00 ± .33

* (see text)

Intensity errors are derived as follows:

If B represents the true average count rate due to background,

bt_b = number of b.g. counts observed in t_b($\sim$ 20 secs);

$(s+b)t_s$ = number of source plus b.g. counts recorded in a time

t_s representing the FWHM of the response function; then the

true average source count rate

$$S = s \pm \sqrt{\frac{s+b}{t_s} + \frac{b}{t_b}} \ .$$

In the case of the ratio R, errors have been obtained by

arbitrarily assuming a $\pm$ 10% error in the ASE Cyg X-1,

Cyg X-2 intensities, and a $\pm$ 20% error for the weaker sources.

The relative Cyg X-1/Cyg X-2 intensity is incompatible

with that obtained by ASE, and by comparison with equations

(6.2a,b) is

$$\text{UAT (20 Apr 67)} \qquad 0.67 \pm 0.31 \qquad\qquad (6.2c)$$

When it is remembered that observations over 2-8keV will

increase the intensities of Cyg X-1, Cyg X-3 by 20%, 25%

respectively, relative to Cyg X-2, the (2-5keV) ratio will be

reduced to less than 0.5, which is also incompatible with the

NRL value.

The GX 36.3 data show an intensity decrease relative to

Cyg X-2 but this is not statistically significant. In any

case the agreement is improved by taking b^{II} closer to the

suggested ASE position than the $b^{II} = 3.3^{o}$ employed above.

The ratio R for GX 48.7 is quoted between limits corresponding

to maximum collimator efficiency of 0.91 and minimum of 0.6

set by the ASE position $b^{II} = 0 \pm 15^{o}$.

6.4.3 Conclusions

Under the assumptions that Cyg X-2 is constant in

intensity from 11Oct66 to 20Apr67 and that source spectral

shapes are relatively invariant, it can be concluded that

(1)   either Cyg X-1 has decreased in intensity (2-8keV) by

~40%, or Cyg X-3 has dramatically decreased in intensity

(2-8keV), (or both);

(2)   GX 48.7 has decreased in intensity (>50%) or its

galactic latitude is $|b^{II}| > 15^o$;

(3)   GX 36.3 is constant in intensity (to within ~ 30%).

If on the other hand a variation in Cyg X-2 alone has caused

the difference in equations (6.2a), (6.2c) then

(1)   Cyg X-2 has increased in intensity ~40% (and would

appear to have decreased again to explain (6.2b);

(2)   for Cyg X-3, Cyg X-4 constant relative to Cyg X-1,

GX 48.7 can be close to the plane and GX 36.3 is still

consistent with a time invariant source.

     If the simplest explanation is the correct one, then a

variation in Cyg X-2 alone is favoured, particularly since its

variability appears to be established between the ASE, NRL

flights while that of Cyg X-1 is not established beyond

doubt by these flights. This type of variation in Cyg X-2

is similar to that observed in Sco XR-1, and strengthens the

case for the identification of Cyg X-2 with an optical object

which is similar to that identified with Sco XR-1 (Giacconi

et al 1967).

     On the other hand Cyg X-1 has long been claimed to vary

at rocket energies, see Chodil (1968c), and is apparently an

established variable at balloon energies, see Bingham and
Clark (1969). It is worth re-emphasizing that the early
rocket surveys were in general incapable of resolving the four
ASE Cygnus sources. All have been analysed allowing for
contributions from minor sources in positions different from
those of Cyg X-3, Cyg X-4 or with no allowance for such sources.
In addition detectors with quite different spectral
sensitivities have been used for intensity comparisons, when
Cyg X-1, Cyg X-2, Cyg X-3 have been shown by ASE to have
markedly different spectral shapes. These criticisms might
also apply to some of the balloon results. There appears to
be no marked correlation between the balloon and rocket
intensity variations for Cyg X-1, indicative of systematic
errors, a variability on a time scale of the order of weeks
or less, or a source in which the 1-10keV and 20-50 keV
emission processes are unconnected.

6.5 CETUS*

Data from flights II, III were used in section 5.3.3
to present strong though not unassailable evidence for an
X-ray source in Cetus. This puts the Cetus source among a
class of other unconfirmed X-ray sources at high galactic
latitude, e.g. Leo XR-1 (Friedman et al 1967), and sources

near 3C273 (Friedman and Byram, 1967) Crater (B. Cooke

private communication), and the Large Magellanic Cloud

(Mark et al 1969b). One object, Vir XR-1, has been observed

on a number of flights and its position suggests identification

with M87 (Bradt et al, 1967). M87, 3C273 and LMC are extra

galactic objects and confirmation of X-radiation from such

objects and the identified other sources at high galactic

latitude will have great bearing on the theories of origin

of the diffuse X-rays, in particular whether or not the

diffuse radiation is the sum of a large number of unresolved

galactic or extra galactic discrete X-ray sources.

*Note in Proof: Dr. B.G. Wilson, University of Calgary,
claims to have observed a strong source in this region in
a recent rocket flight. Further details are not yet
available. (Private Communication, July, 1970).

CHAPTER SEVEN

GALACTIC HALO CONTRIBUTION TO THE DIFFUSE X-RAY BACKGROUND

7.1   INTRODUCTION

Section 1.6.4 summarizes a wide variety of mechanisms suggested as possible origins of the diffuse X-ray flux. No single mechanism explains all the features of the observed spectrum within limits imposed by present knowledge of such things as the cosmic ray spectra, magnetic fields and low energy photon densities, in galactic and extra galactic space. In fact it is not unreasonable to expect appreciable contributions from a number of different processes.

The low frequency radio background and the extra terrestrial electron spectrum are both thought to contain information on galactic processes. Extensive new radio data, and new electron and interstellar magnetic field strength estimates have prompted a reassessment (c.f. Felton and Morrison, 1966) of the possibility of a galactic X-ray contribution. Emphasis has been placed on similarities in the shapes of the electron, radio and X-ray spectra which might be taken as indicating some common origin. The chapter includes and extends work published by Hamilton and Francey (1969).

7.2   X-RAYS

7.2.1   Experimental Data

Observations of the diffuse cosmic X- and gamma ray spectrum are summarized in figure (7.1). There is noticeable steepening of the spectrum below about 1keV and above about 40keV. Between 1keV and 10^3keV, the data are shown fitted by spectra of the form

$$dN/d(h\nu) = \text{const.}(h\nu)^{-(\alpha+1)} \text{ photons}(cm^2 sec \text{ ster } keV)^{-1}$$

$$(7.1)$$

where α is the spectral index of the corresponding <u>energy</u> spectrum, and is given by

$$\left.\begin{array}{ll}\alpha = 0.5, & 1 < h\nu < 40 \quad keV. \\ \alpha = 1.4, & 40 < h\nu < 1000 \text{ keV} \end{array}\right\} \quad (7.1a)$$

The "reasonable" fit above 40keV becomes an excellent one if it is accepted that all the scintillator data (20-100 keV) should be adjusted in a manner suggested by Trombka (1970). (For instance an incident power law photon spectrum with spectral index $(\alpha + 1) = 1.5$ is shown to produce a pulse height spectrum, 60-100 keV, with index 1.7). There is evidence for a spectral feature at 1MeV and/or a spectral break to agree with the tentative 100MeV results. Both require further verification.

Below 40keV, and entering the domain of rocket borne proportional counter measurements ($<$15keV), the scatter in the data is pronounced. There is obviously a marked spectral
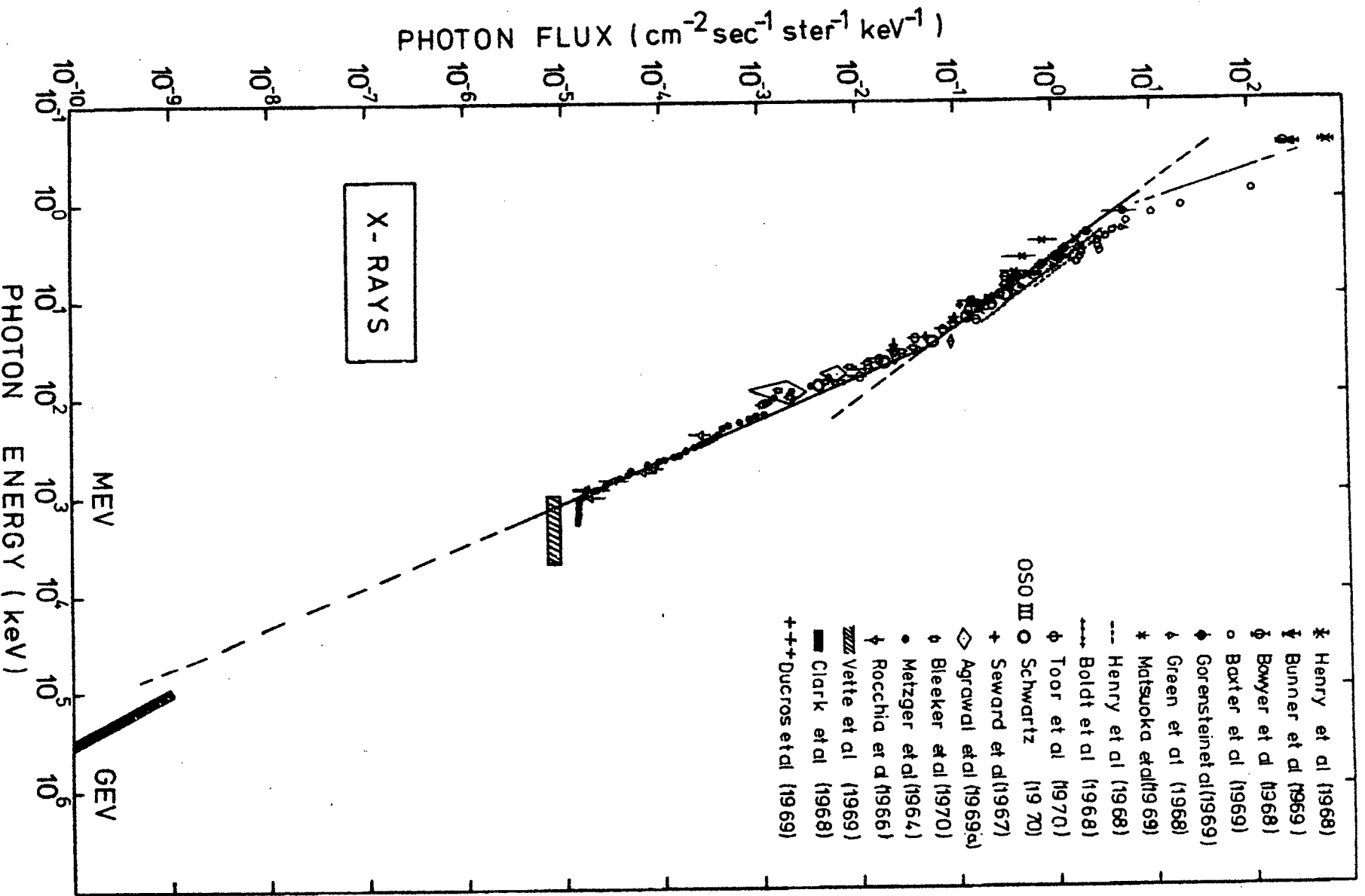
FIGURE 7.1: Summary of Diffuse X-ray Observations

X - RAYS

PHOTON FLUX (cm^{-2} sec^{-1} ster^{-1} keV^{-1})

PHOTON ENERGY (keV)

* Henry et al (1968)
⚡ Bunner et al (1969)
φ Bowyer et al (1968)
o Baxter et al (1969)
◆ Gorenstein et al (1969)
⬥ Green et al (1968)
* Matsuoka et al (1969)
--- Henry et al (1968)
⟷ Boldt et al (1968)
Φ Toor et al (1970)
OSO III o Schwartz (1970)
+ Seward et al (1967)
◇ Agrawal et al (1969a)
⬧ Bleeker et al (1970)
• Metzger et al (1964)
⬦ Rocchia et al (1966)
▨ Vette et al (1969)
■ Clark et al (1968)
+++ Ducros et al (1969)

break below about 1keV. With possible galactic structure in

mind, the 1.5-15 keV observations for which directional and

spectral information are available are summarized in table

(7.1) and figure (7.2).

Problems in comparing data from different experiments

arise from uncertainties in detector efficiency and background

correction. The possibility of electron contamination

(section 3.5.3) is perhaps the most serious and it may be

significant that the observations of Green et al and Baxter

et al, giving among the highest 3.6keV intensities, were

from rockets launched at high geomagnetic latitude. The

observations in regions 1,2,3,4 are considered to be the most

reliable in view of the sophistication of detection systems

and controlled rocket motions which extend the viewing time.

On the other hand the programmed motion often removes the

capability of detecting a pitch angle distribution and thus a

steady electron precipitation; in this respect the thick

beryllium windows of counters employed in regions 3 were the

least sensitive to electrons and also record one of the

lowest intensities. The apparent discrepancy in regions 4 and

7 may come from serious inflight difficulties experienced

during observations in the latter.

Intensity variations (during a single flight) between

the various galactic latitudes in regions 1,3 and 4 were

reported to be less than 5%, 10% and 8% respectively.

TABLE 7.1

ROCKET OBSERVATIONS OF THE DIFFUSE X-RAY BACKGROUND

Region Observed (fig.7.2)	Energy Range (keV)	Spectral Index α	Approx. Intensity at 3.6keV*	Reference
1	2-20	0.35	6.6	Boldt et al (1969b)
2	1.5-8	0.4	7.5	Henry et al (1968)
3a	4-15	0.69	3.9	Seward et al (1967)
3b	4-15	0.73	4.8	Seward et al (1967)
4	1-13	0.70	5.1	Gorenstein et al (1969)
5	2-10	0.68	6.3	Green et al (1968)
6	1.5-4	~0.5	8.6	Baxter et al (1969)
7	2-10	0.3	4.2	Boldt et al (1969a)

* $keV(keV\ cm^2\ sec\ ster)^{-1}$
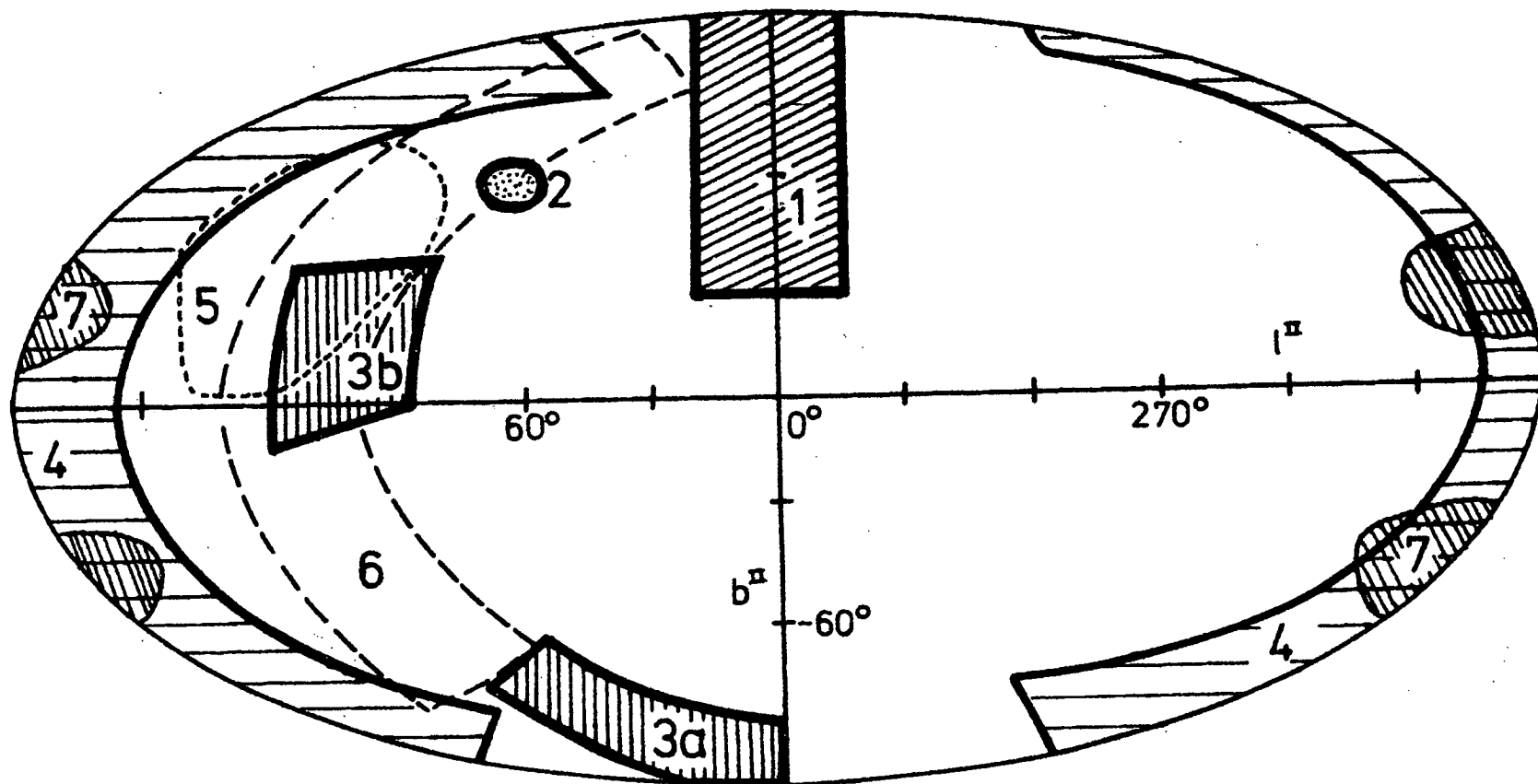
FIGURE 7.2: Areas of Sky covered in Rocket Observations of Diffuse X-rays

Perhaps the most significant background observations to date have recently been reported by Schwartz (1970). Using a single calibrated scintillator on OSO-III, statistically significant 10-50keV count rates were obtained over practically the whole sky in the course of one year. Due consideration was given to electron precipitation, claimed to be widespread. Schwartz arrives at two conclusions important in the present context;

(1) a spectral break occurs at 38 ± 4 keV. This is the first confirmation of a break in a single set of data and the position is in agreement with that used in equation (7.1a). {There is some controversy on the break position however (Gorenstein et al, 1969, Bleeker and Deerenberg, 1970), which possibly might be related to the direction of observation, and requires further investigation.}

(2) there is an upper limit of 3-5% on a halo anisotropy, above 10keV.

Three related factors (already implied from section 3.5.3) cause hesitation in extrapolating this isotropy to 1keV and attributing the scatter in rocket observations to electron precipitation, one being the short time scale (minutes) of the reported strong precipitation events. The second is the relative insensitivity of the proportional count to electrons and finally pitch angle distributions (befitting steady precipitation) have often been considered

but never reported from X-ray astronomy flights. Re-analysis
of the individual rocket data in light of new electron data
might be fruitful.

We can conclude here either that the diffuse X-rays are
isotropic (and therefore most likely extragalactic) and there
are large systematic or background induced errors in the
measurements (with implication of widespread frequent electron
precipitation and steep electron spectra), or that there are
X-ray anisotropies particularly at low energies indicating an
appreciable galactic contribution. From the latter point of
view a difference in spectral index between rocket
observations representing the northern galactic halo

$$(\alpha_N)_{x-ray} \sim 0.4 \tag{7.2a}$$

and those containing a significant contribution from the south

$$(\alpha_S)_{x-ray} \sim 0.7 \tag{7.2b}$$

is most evident from table (7.1), figure (7.2). Since it is
possible to imagine some situations in which a difference in
spectral index will be more obvious than a measured count
rate difference over a selected energy range, equations (7.2)
are noted for comparison with extra-terrestrial electron and
radio spectra. Before doing this the properties of the most
likely galactic X-ray production mechanism, the inverse
Compton effect, are summarized.

7.2.2   The Inverse Compton Effect

An accurate calculation of the spectrum of inverse Compton scattered photons is given by Jones (1967) who shows that the δ-function approximation for scattering by a single electron, employed in the convenient treatment of Felten and Morrison (1966), is a good one. Following the latter, the electron spectrum is expressed in the form

$$n(\gamma) \, d\gamma \; = \; n_0 \gamma^{-m} \, d\gamma \qquad \text{electrons cm}^{-3} \qquad\qquad (7.3)$$

for electrons with

$$\gamma \; = \; (1 - \beta^2)^{-\frac{1}{2}}$$

in the range $d\gamma$. Here β is the ratio of electron velocity to the speed of light. (For electron energy $E = 1\text{GeV}$, $\gamma = 1970$).

For an ambient photon population with mean photon energy $\bar{\epsilon}$ which is isotropic, the mean energy of a scattered photon is

$$\overline{h\nu} \; = \; \frac{4}{3} \, \gamma^2 \, \bar{\epsilon}$$

and for a __black-body__ distribution of ambient photons at temperature T (degK) $\bar{\epsilon} = 2.7 \, k \, T$ so that

$$\overline{h\nu} \; = \; 3.1_{10} -4 \quad \gamma^2 \; T \qquad \text{eV}$$
$$= \; 1.18 \qquad E^2 \; T \qquad \text{keV} \qquad\qquad (7.4)$$

for E in GeV.

If the electrons are also isotropic, the specific intensity received at Earth in a given direction which includes a length R of the electron-photon field region is

$$I(h\nu) \; \simeq \; 10^3 \; (56.9)^{3-m} \; n_0 R \, \rho \; T^{(m-3)/2} \; h\nu^{(1-m)/2}$$
$$\text{eV.} \quad (\text{ eV cm}^2 \text{sec ster})^{-1} \qquad\qquad (7.5)$$

where ρ, the energy density of the ambient photons, is given

by $\rho = \frac{4\sigma T^4}{c}$, σ = Stefan Boltzmann constant,

$3.54_{10} 7$ eV(cm sec deg^4)$^{-1}$, and R is in light years

(= R x $9.46_{10} 17$ cm).

Thus the X-ray spectral index, α, of the last subsection is

related to the electron spectral index m, in equation (7.3) by

$$\alpha_{inv. compt.} = (m - 1)/2 \qquad\qquad (7.6)$$

(Assuming equations 7.2 represent real differences,

attributable to a halo origin, then electron spectra with

m = 1.8, m = 2.4 would be expected in the north and south).

7.3   THE RADIO BACKGROUND

7.3.1 Observations

Hamilton (1969) carried out a critical and comprehensive

review of low resolution radio observations in the directions

of the galactic poles. The results, corresponding to

references 1 to 19 of Hamilton and Francey (1969), are

included in figure (7.3). The brightness B, is derived from

$$B = \frac{2kT}{\lambda^2} \qquad \text{Watts } (m^2 Hz \text{ ster})^{-1} \qquad (7.7)$$

where   k = Boltzman's constant, 1.38_{10} -23 joule deg^{-1}.

        T = temperature, degK.

        λ = wavelength, metres.
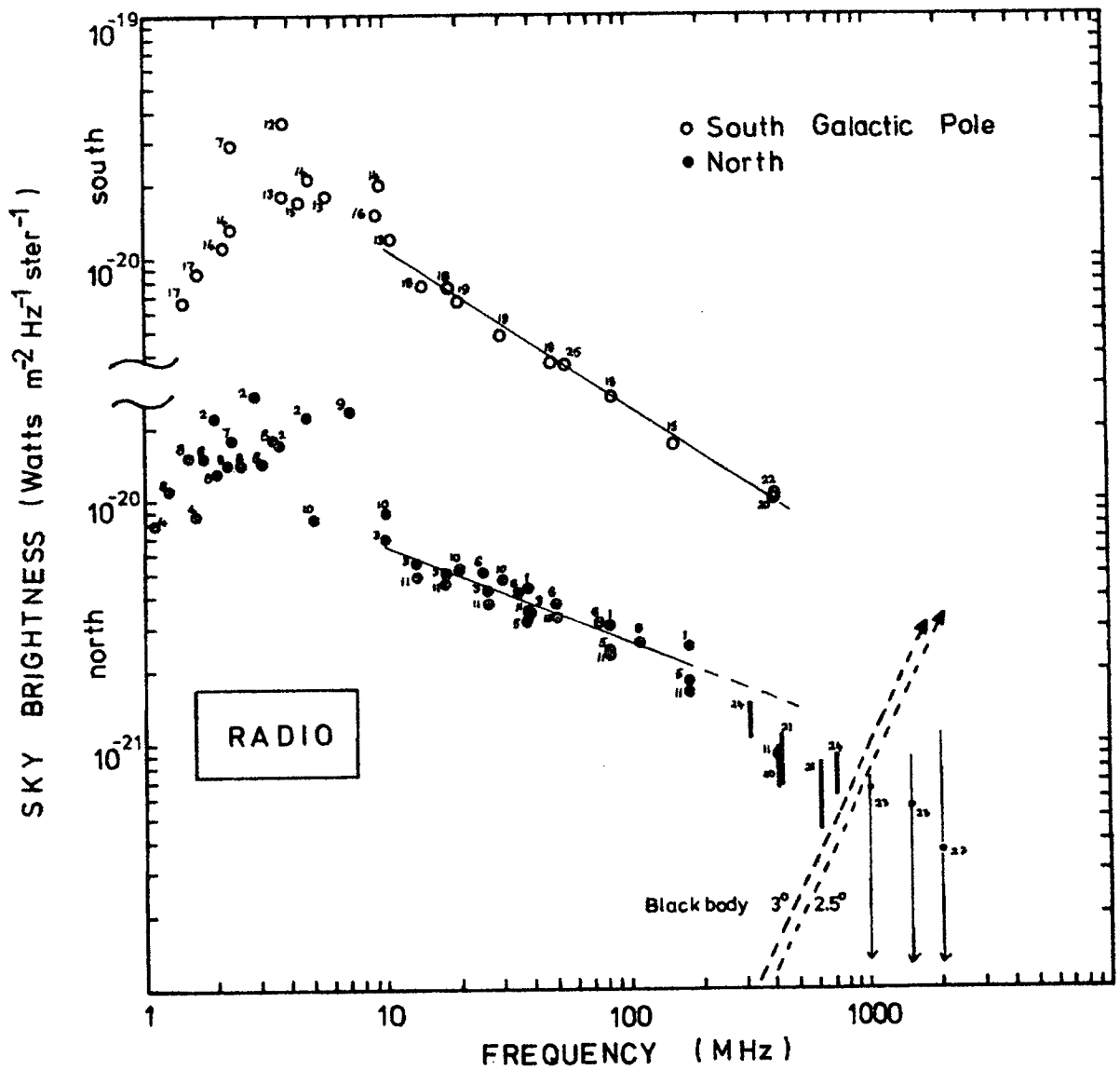
FIGURE 7.3: Summary of Diffuse Radio Observations in the Galactic Pole Directions. Bars indicate extrapolation to Pole Directions using PTS survey (see text).

The brightness scales of the north and south data are displaced

an order of magnitude to aid comparison.

       High frequency data (references 20 to 25) are included

in figure (7.3) taken from:

       20   Pauliny-Toth and Shakeshaft (1962)

       21   Howell and Shakeshaft (1967)

       22   Price (1969)

       23   Pelyushenko and Stankevich (1969)

       24   Wall, Chu and Yen (1970)

       25   Rohan and Soden (1970)

In all these cases (and also the 404 MHz data of reference 11),

a contribution due to a universal microwave black-body

radiation has been subtracted out. Measurements on the

black-body temperature range from the original estimate of

3 degK (Penzias and Wilson, 1966) down to 2.5 degK used by

Pelyushenko and Stankevich (23). The pair of parallel lines

superposed onto the northern halo data of figure (7.3)

represents the microwave background for these two temperature

limits, and apart from the points (23), a 2.7 degK

radiation has been subtracted (see Boynton et al, 1968).

Because of the magnitude of both the atmospheric and cosmic

temperatures relative to the galactic temperatures reported

by Pelyushenko and Stankevich, the points (23) are taken with

considerable reserve (and are indicated with large error bars).

Pauliny-Toth and Shakeshaft (PTS, 20) published 404 MHz temperature contours covering most of the sky, combining their own data about the north pole with measurements by other authors. The upper limit of the plotted point (20) in figure (7.3), north pole, corresponds to the temperature with a base line correction of -4.5 degK as suggested by Price (1969). For each of the plotted points (21) to (24) the upper limit is that published by the respective author (minus 2.7 degK) for regions removed but near the galactic poles (usually the celestial poles). The lower limit is that predicted at the galactic pole (minus 2.7 degK) using the relative brightnesses at 404 MHz taken from the PTS surveys. In all cases the lower limits are probably the more correct estimates of pole brightness.

The differences in 10-200 MHz spectral shape between the north and south are very marked and are shown fitted by a power law, similar to equation (7.1), with

$$(\alpha_N)_{radio} \sim 0.4 \qquad\qquad (7.8a)$$

$$(\alpha_S)_{radio} \sim 0.6 \qquad\qquad (7.8b)$$

(the resemblance to equations 7.2a,b is striking). The north and south brightnesses are similar above 200 MHz, so that at 10 MHz the south is approximately two times brighter than the north. The power law with $\alpha = 0.4$ obviously does not include the very high frequency northern points and the evidence for a

spectral break at about 200 MHz is very good. In contrast,
the data are accurately described by a single power law, with
the scant high frequency data indicating the absence of a
spectral break between 10 and 400 MHz.

Evidence for a galactic halo comes from radio
observations around 80 MHz (Baldwin, 1955, Mills, 1959). A
model for the Southern halo by Hamilton (1969) is unique in
that extensive high resolution surveys at 2.1, 4.7, 10, 30,
85 and 153 MHz have permitted an accurate definition of the
galactic disc component (low frequency absorption in the disc
distinguishing it from more tenuous regions). Unfortunately
similar data at the low frequencies are not available for the
north, a consequence of the non-existence of relatively
"transmitter-free" regions with anomolously low ionospheric
critical frequencies similar to Hobart. (The quality of
present satellite results, apparently plagued by
exospheric emissions, is poor). The Hamilton halo is
presented in figure (7.4) as contours of constant A, for an
integrated extra-disc emission

$$\varepsilon(\nu) \;\; = \;\; A\nu^{-\alpha}$$

normalized to 100 at the south galactic pole. (Northern
points are distorted, most likely due to presence of Cen A).
Dotted lines show a model ellipsoid of revolution with
uniform emissivity throughout, and with dimensions chosen to
fit the high latitude measurements. The relative dimensions
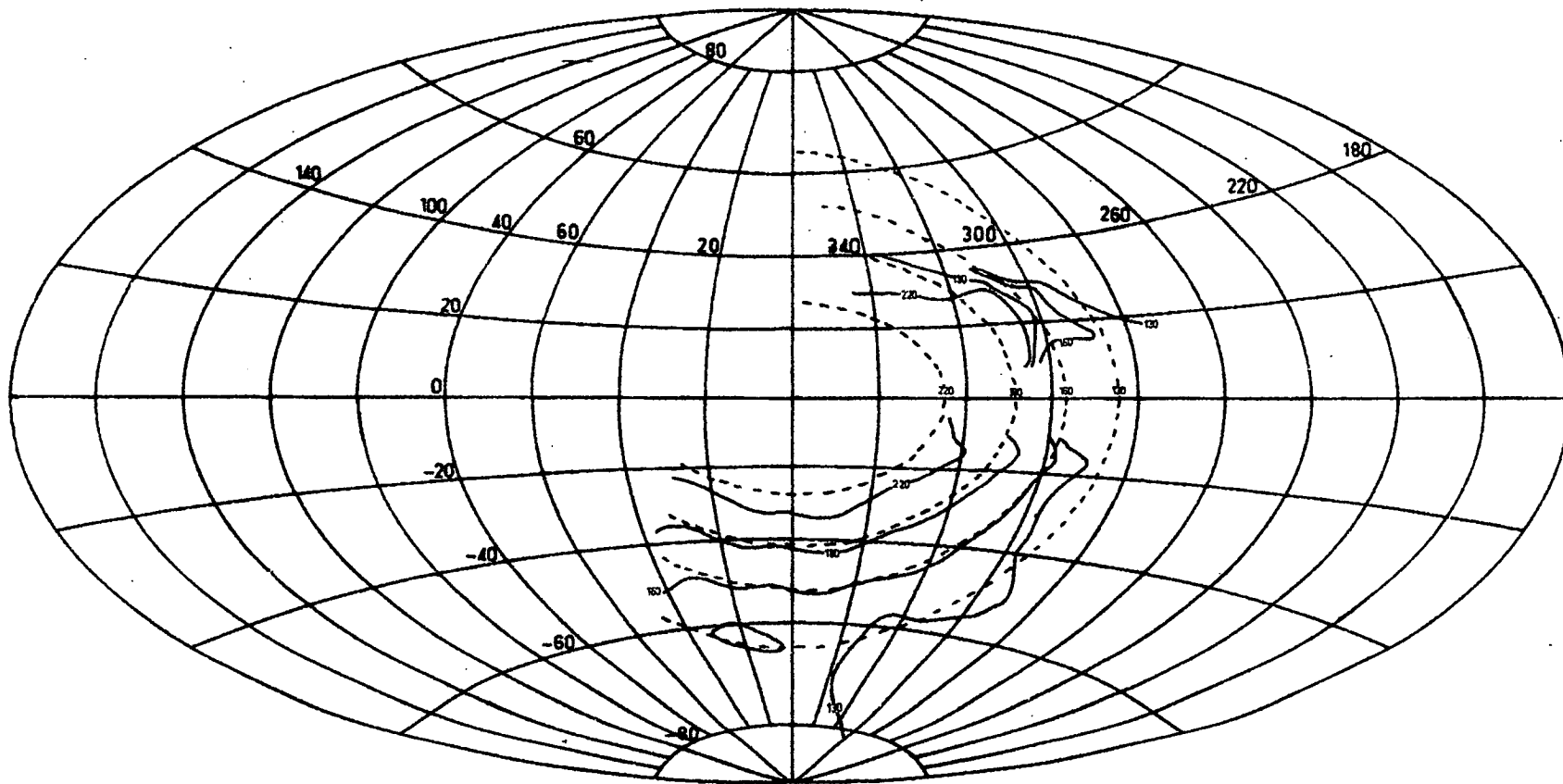
FIGURE 7.4: The Hamilton Halo. Emissivity measure, normalized to 100 in the South Galactic Pole direction.

of the ellipsoid are quite accurately defined by the data (allowing for a slight increase in emissivity towards the galactic centre); the absolute dimensions are defined by the solar distance, currently thought to be 10 kpc. Using this gives,

a major axis (in the galactic plane) of 29.2 kpc,

and minor axis (normal to the plane) of 26.6 kpc.

A solar distance of 8 kpc, as used by both Baldwin and Mills, decreases the size of the present model proportionally.

7.3.2 Synchrotron Emission

The measured diffuse radio emission is generally assumed to be of galactic origin, for reasons which include the measured anisotropy as above, calculations on possible cosmological models (Payne, 1969 and private communication) and a single direct measurement at 20 MHz limiting the extragalactic emission (Shain, 1959). All three methods arrive at an upper limit of about 10% for an extragalactic contribution. The shape of the spectrum above 100-200 MHz, as indicated in the northern halo data of figure (7.3) is further indirect evidence for a predominantly galactic origin. An extragalactic radio spectrum is assumed to arise from the superposition of spectra from unresolved point sources. Spectra of resolved extragalactic sources show no evidence for a uniform spectral bend necessary to explain a diffuse spectral discontinuity.

Galactic radio spectra are described in terms of synchrotron emission of relativistic electrons in a galactic magnetic field. A complete treatment of the synchrotron process is given by Westfold (1959) and more recently by Ginzburg and Syrovatskii (1964), who introduce a characteristic frequency

$$\nu_c \simeq 16.1 \; B_\perp \; E^2 \qquad MHz \qquad\qquad (7.9)$$

where   E is the electron energy, GeV

$B_\perp$ is the component of magnetic flux density

normal to the electron velocity, micro gauss.(μG).

The power radiated by a single electron is given by

$$P(\nu) = 2.34_{10} -29 \; B_\perp \; F(\nu/\nu_c)$$

where F is a modified Bessel function tabulated by Westfold.

For an electron spectrum of number density n(E)dE, in a randomly oriented field, the synchrotron emission will have no nett polarization (as observed) and will be isotropic. The synchrotron <u>emissivity</u> is given by

$$\varepsilon(\nu) \simeq 2.34_{10} -35 \; B_\perp \int n(E) \; F\left\{ \frac{\nu}{16.1 \; B_\perp \; E^2} \right\} dE$$

$$watts \quad m^{-3} Hz^{-1} \qquad (7.10)$$

For an electron spectrum, (see equation 7.3),

$$n(E)dE = N_0 E^{-m} \; dE \qquad\qquad (7.10a)$$

and assuming all the radiation occurs at the characteristic frequency ν_c , it can be shown (Mills, 1964) that

$$\varepsilon(\nu) \propto B_\perp^{\frac{1+m}{2}} \; \nu^{\frac{1-m}{2}}$$

or $\varepsilon(\nu) \propto \nu^{-\alpha} synchr$ where $\alpha_{synchr} = (m-1)/2$ (7.11)

This can be compared with equation (7.6) for the inverse Compton effect, and gives added significance to the correspondence between north and south radio and X-ray spectral indices.

The radio measurements give a total radiation, S(Watts $m^{-2} Hz^{-1} ster^{-1}$), in a given direction, which is related to the emissivity by

$$S(\nu) = \frac{1}{4\pi} \int_{o}^{L} \varepsilon(\nu) \, dl = \frac{\varepsilon L}{4\pi}$$ (7.12)

assuming uniform isotropic emissivity along the total path length L through the halo.

7.4   INTERSTELLAR MAGNETIC FIELDS

Direct information on interstellar magnetic fields comes from measurements on Zeeman splitting of the 21 cm hydrogen line and from Faraday rotation measures on extra-galactic and pulsar radio sources. Veerschuur (1969) obtains fields ranging from 0.55 μG to > 20 μG from Zeeman splitting measurements in various spiral arm directions. The strong fields are associated with "amplification" in dense interstellar clouds and excluding these, limits on field strengths much less than 10μG are established. Berge and Seielstad (1967) obtain Faraday rotation measures for extra-

galactic sources as a function of galactic latitude; an
interpretation of their results in terms of a field aligned
with the galactic disc gives

$$\int n_e B \, dr \simeq 20 \text{ cm}^{-3} \text{ } \mu G \text{ pc.}$$

for the direction of the galactic pole. Radhakrishnan (1969)
summarizes the Faraday rotation measures on pulsars, for
which the dispersion also gives $\int n_e \, dr$. Using a model for
the dispersing electrons given by Mills (1969) implies

$$\int n_e \, dr \simeq 10 \left| \cosec b \right| \text{ cm}^{-3} \text{pc.}$$

Thus in the direction of the poles, these two equations imply
a mean line-of-sight field in the disc, $B \sim 2\mu G$.

Two phenomena must be kept in mind, one is cloud
structure (which might amplify the field as suggested by
Veerschuur) and secondly (for the Faraday measurements) any
large scale field reversals will tend to cancel the rotation
measure. If we accept $2\mu G$ as a reasonable estimate of B in
the disc, a corresponding halo field might be expected to be
considerably less than $2\mu G$. Independent evidence for a
mean field strength (halo plus disc) with $B_\perp \sim 0.3 - 1\mu G$
in the direction of the north galactic pole is presented in
section 7.6. (For a randomly oriented field in the haloes
$\langle B_\perp^2 \rangle \simeq \frac{2}{3} B^2$).

7.5   INTERSTELLAR ELECTRON SPECTRA

Estimates of an interstellar electron spectrum hinge on measurements made close to earth in the range

$$2.5_{10} -4 < E < 500 \qquad \text{GeV.}$$

Ignoring various interpretative lines, the data are summarized in figure (7.5), adapted from Faneslow et al (1969). Recently published 1968 data between $3_{10} -2$ and 1 GeV, and > 100 GeV have been included, taken from a review by Pal (1969). In following general discussions, the review of Pal and others by Meyer (1969), Webber (1968) have been the principal sources of information.

Solar modulation obviously plays a big part in the $3_{10} -2$ to 1-2 GeV spectrum but apparently not outside these limits. The spectral flattening in this energy interval is very reminiscent of the behaviour of protons and He nuclei. Controversy on the demodulation procedure is normally restricted to the electron data < 2GeV, however even above this energy there are difficulties. For example Webber shows that to explain the radio emission from the galaxy using a demodulated electron spectrum requires line of sight averaged field strength $B_\perp = 7\mu$ G, significantly higher than that suggested in the previous section (unless there is a large scale field reversal.)
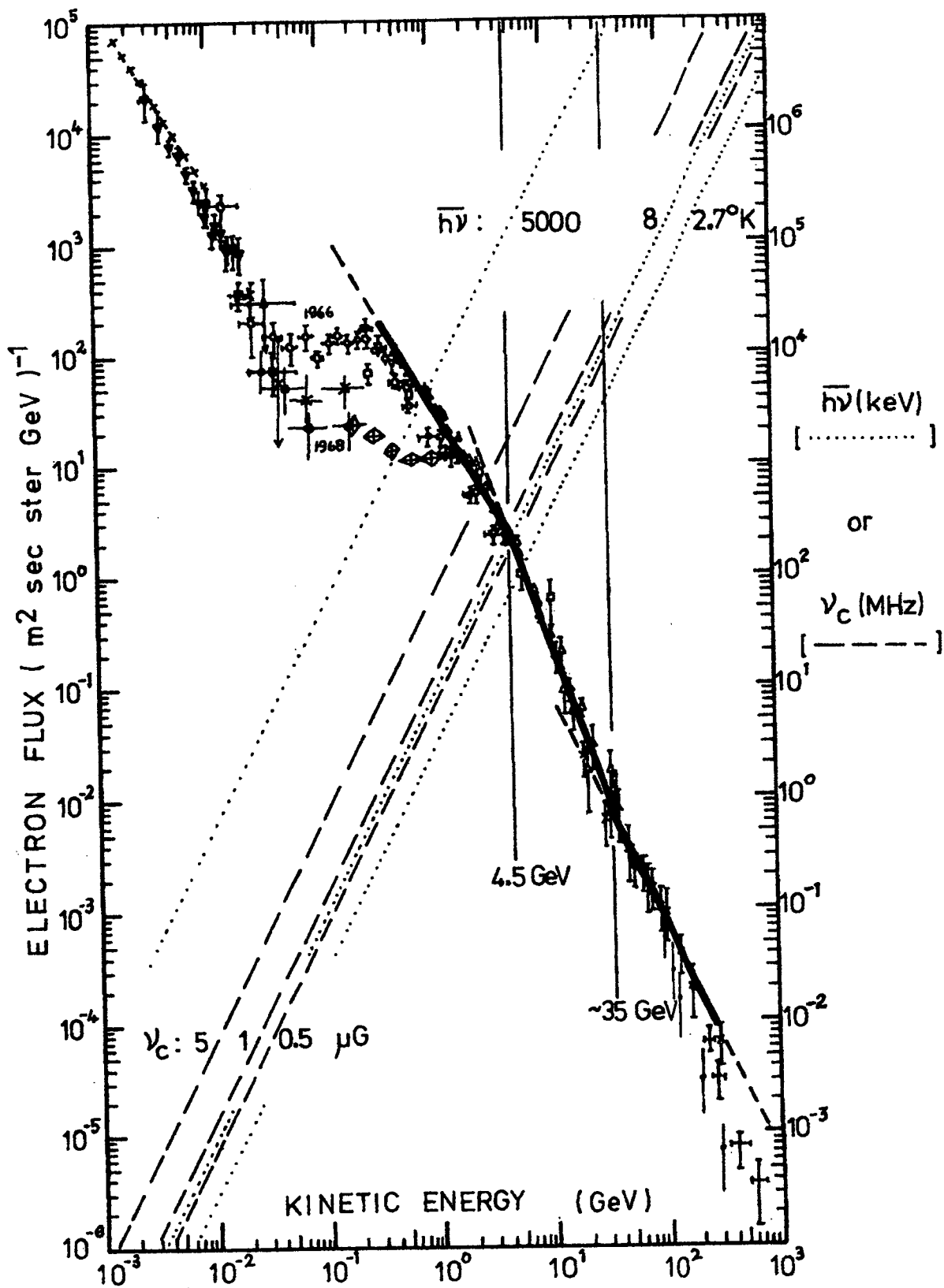
FIGURE 7.5: Summary of measurements of Electrons near earth. (Right hand scale and E⁻² lines allow prediction of mean Inverse Compton energy and/or characteristic synchrotron frequency.)

An alternative method of obtaining the interstellar electron spectrum starts with the observed galactic <u>radio</u> emission (e.g. Felten, 1965). Independent information on the relative values of the two unknowns, the electron density and magnetic field strength, is usually obtained by requiring a pressure equilibrium between the field and cosmic rays in the haloes (Shklovsky, 1960). That this leads to similar problems has long been recognized and for example Hamilton (1969) shows that the data from the southern halo require either an electron to proton ratio of $\sim$ 50% (c.f. $\leqslant$ 1% near earth), or again field strengths $(B_{\perp})$ of about $6\mu G$.

Because of such difficulties, the emphasis here is placed on the <u>shape</u> of the electron spectrum, and in particular on what Pal calls "the favourite occupation ......of kink hunting". The assumption is that discontinuities in the interstellar spectrum, whatever their cause, will be apparent also in radio and perhaps X-ray spectra. The data of figure (7.5) above 1-2 GeV are shown represented by the "best fit" power law. The choice of a basic power law shape is not required by any astrophysical argument except for a general tendency of cosmic ray observations to be described in this form. For example Anand et al (1968), fit a smoothly varying function to the data about 1-10 GeV. Also the quality of the data might not warrant such attention and for example it is normal practice to fit the data above 2-3 GeV

and below $\sim$ 100GeV by a single power law (Faneslow et al, 1969).

For the moment, accepting these "best" fit lines gives an

electron spectrum (see equation 7.3)

$$n(E) \; dE \;\; = \;\; n_0 \; E^{-m} \; dE \; (m^2 sec \; ster)^{-1}$$

where

$$
\begin{array}{llll}
n_0 \;\; = \;\; 33.7, & m \; = \; 1.74 & E \; < \; 4.5 \;\; GeV & \left.\vphantom{\begin{array}{c}1\\1\\1\end{array}}\right) \\[4pt]
n_0 \;\; = \;\; 190 \;, & m \; = \; 2.89 & 4.5 \; < \; E \; < \; 35 \; GeV & \left.\vphantom{\begin{array}{c}1\\1\\1\end{array}}\right) \quad (7.13) \\[4pt]
n_0 \;\; = \;\; 11.5, & m \; = \; 2.1 & 35 \; < \; E \; < \; 200 \; GeV & \left.\vphantom{\begin{array}{c}1\\1\\1\end{array}}\right)
\end{array}
$$

Possible causes of breaks in the electron spectrum are

discussed by Pal, Felten and Morrison (1966) and others. Of

particular importance here are energy losses from a galactic

electron spectrum due to synchrotron and/or inverse Compton

radiation. For an equilibrium situation, the electron storage

time (between source and observer) is given by

$$\tau \; = \; \frac{E}{dE/dt} \qquad \alpha \qquad \frac{1}{bE} \qquad ; \qquad\qquad (7.14)$$

b is proportional to the energy density of the background

radiation (ρ) in the case of Compton losses, or to the energy

density of the magnetic field ($B^2/8\pi$) for synchrotron losses.

For an injected power law electron spectrum of exponent m,

and for residence times exponentially distributed with mean

time τ, the spectrum steepens to m + 1 above an electron energy

$(b\tau)^{-1}$.

The charge composition of the electrons measured near

earth is considered significant to this problem. Measurements

in the energy range 0.5 - 10 GeV give a 10 fold negatron

excess, widely accepted as an indication that these electrons

are directly accelerated. An increasing positron ratio towards

lower energies is taken to represent an increasing

contribution of "secondary" electrons resulting from

interactions of the primary cosmic rays in the interstellar

medium (i.e. $\pi \rightarrow \mu \rightarrow e$ decay). A tentative result indicating

positron excess <u>above</u> 10GeV (Daniel and Stephens, 1966) is

interesting but requires further verification.

A break "upwards" in the electron spectrum as

indicated at $\sim$ 35GeV in figure (7.5) can only be the result

of an alternative production mechanism. In this respect the

inconclusive report of a high energy positron excess,

receives new significance. (If this particular kink is

ignored or attributed to experimental causes, the consequence

in the present context is to move the 4.5GeV break to slightly

lower energies).

7.6   COMPARISON OF DATA

The similarity of spectral indices in the 1-15 keV

X-ray and 10 - 100 MHz radio data has already been noted,

including corresponding differences between north and south

galactic halo spectra (equations 7.2, 7.8).

Equations (7.4), (7.9) can be used to estimate the
portions of the electron spectrum of interest for the cases of
inverse Compton X-rays and synchrotron radio waves
respectively. For convenience, these are included on figure
(7.5) by relabelling the right hand scale to read keV OR
MHz, depending on whether a mean Compton photon, $\overline{h\nu}$, OR the
characteristic synchrotron frequency, ν_c, is being discussed.
Dashes show ν_c for 0.5, 1.0, 5.0 μG fields.
Dots show $\overline{h\nu}$ for 2.7, 8, 5000 degK black-body fields.
The reason for including the 8 degK is discussed briefly at
the end of the section, the 5000 degK is taken to represent
starlight. For example 10 to 100 MHz radio waves are
obtained from a magnetic field with $B_\perp$ = 1μG from electrons
of ~ 0.8 < E < ~ 2.5 GeV. These electrons will produce
X-rays with 2 < $h\nu$ < 25 keV from a 2.7 degK blackbody
field or 5 < $h\nu$ < 40 MeV from starlight.

As a preliminary measure, the ν_c, $\overline{h\nu}$ corresponding to
electron energies at break positions can also be used to
estimate possible break positions in the radio and X-ray
spectra. The results are again striking, e.g. a 4.5GeV
electron gives a characteristic synchrotron frequency of
200 MHz for $B_\perp$ ~ 1μ G and a mean Compton energy ~ 60keV for
a 2.7 degK ambient field (c.f. figures 7.3, 7.1). In
addition the decrease in electron spectral index at 35GeV

implies a decrease in X-ray spectral index at $\sim 4_{,0}$ 3 keV and
is of the right magnitude to explain the 100 MeV data of
figure (7.1).

Because of the smeared and asymmetrical distribution of
the synchtrotron or inverse Compton radiation from a mono-
energetic electron spectrum it is not at all obvious that
the preliminary measure of predicting breaks is valid. For
this reason the electron spectrum represented by equation
(7.14), (extended down to 0.2GeV and up to 300GeV) has been
inserted into equation (7.10) and numerically integrated.
The integration is achieved using a series representation of
the tabulated Westfold values of the modified Bessel function
$F(\nu/\nu_c)$. An Algol program incorporating the method was
developed and tested by Dr. Hamilton and was kindly made
available for the present purpose. The resulting emissivities
are shown in figure (7.6), <u>normalized</u> to the northern radio
data at 20-30 MHz. Normalization factors relative to that
at $B_\perp$ = 1 μ G are

Field ($B_\perp$, μG)	Normalization Factor
0.5	0.38
1	1
2.5	3.6
5.0	9.7
10.0	26
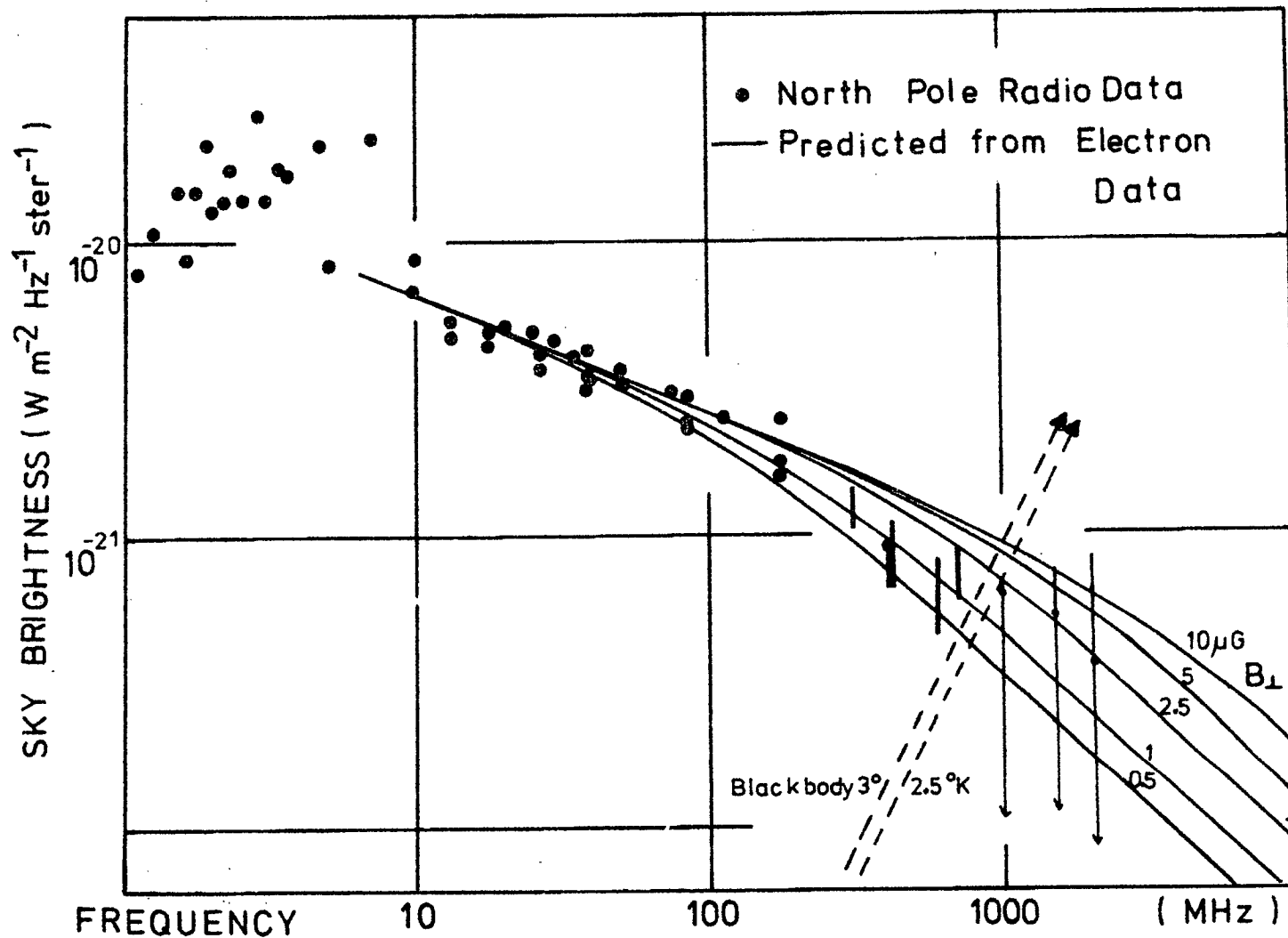
FIGURE 7.6: Synchrotron Spectra predicted from Observed Electron
Spectrum, normalized to North Galactic Pole Radio data.

For an observed brightness in the north pole direction,

figure (7.3), of

$$S(10 \text{ MHz})_N \ = \ 5.5_{10} -21 \quad Wm^{-2} Hz^{-1} ster^{-1}$$

and a total path length through the halo in the pole

direction similar to that observed in the south i.e.

$$L \ = \ 10 \text{ kpc} \ = \ 3.08 \ _{10}20 \text{ m.}$$

implies from equation (7.12), that

$$\epsilon(10 MHz)_N \ = \ 2.2_{10} -40 \quad Wm^{-3} Hz^{-1}.$$

The emissivity calculated above for a 1μ G field was

$$\epsilon'(10 MHz) \ = \ 4.5_{10} -41 \quad Wm^{-3} Hz^{-1}.$$

In other words to explain the intensity of the radio emission

implies ~ 5 times more electrons than observed near earth or

alternatively the same electron spectrum and a field with

$B_\perp \sim 3 \mu$ G. This field is not too unreasonable at first

sight and e.g. is similar to the value used by Sironi (1969)

from similar arguments, but not so well selected radio data.

Sironi goes on to claim support for this field on preliminary

evidence for a radio spectral steepening above 200 MHz and an

electron break at 3GeV. As can be seen from figure (7.6) a

break in the radio spectrum can only be interpreted in terms

of a value of B $<$ 2.5μ G with the present interpretation of

the electron spectrum. Remembering that the lower limits of

the bars representing data above 200 MHz are more likely to

be the correct values the northern halo field can be limited to

$$\sim 0.3 < B < 1 \mu G \qquad\qquad (7.15)$$

(If the electron spectrum break is shifted to lower energies, $B_\perp$ is increased, e.g. by comparison with the ν_c curve in figure (7.5) a 2GeV electron break requires $B_\perp \sim 5\mu G$).

As might be expected from (7.11), the agreement in slope between the observed electron spectrum and 10-100 MHz northern data is excellent. On the other hand it is very difficult to extract an electron slope matching the southern radio data. If an energy dependent solar modulation argument is employed to steepen the electron spectrum around 2GeV, then the agreement with the northern data is destroyed.

Electron spectra derived from the radio data can be used to predict the intensity of X-rays resulting from inverse Compton collisions with 2.7 degK blackbody radiation ($\rho = 0.24$ eV cm^{-3}). This is done in table (7.2) to allow comparison from north to south. In the pole directions the radio data and 2.7 degK field result in predicted X-ray fluxes up to about 6% of the observed flux. In directions away from the pole where R is large (e.g. R = 22 kpc, $l^{II} = 0$, $b^{II} = 30^\circ$) the contribution may be as much as 12%. Hamilton and Francey (1969) predicted X-ray fluxes as much as 30% of the observed. This resulted mainly from using a spectral index m = 2.32 for the south, obtained from the data by correcting for the influence of the galactic disc, and also using T = 3 degK, ($\rho = 0.4$ eV cm^{-3}). It is interesting that from the point of

TABLE 7.2

CALCULATED X-RAY INTENSITIES FROM RADIO

ELECTRONS AND 2.7 DEGK RADIATION IN HALOES

	North	South	Equation
Assumed Pole Dist. R (cm)	$3.08_{10}\ 20$	$3.08_{10}\ 20$	
Observed emissivity	$2.24_{10}\ -40$	$4.5_{10}\ -40$	7.12
α radio	0.4	0.6	
m	1.8	2.2	7.11
$B_\perp \int E^{-m}F\ dE$ at 10 MHz			7.10
$\qquad B_\perp = 0.7\mu G$	0.85	0.72	
$\qquad = 1.0\mu G$	1.40	1.27	
n_0 (el.cm^{-3} γ^{-1})			
$\qquad (0.7)$	$4.90_{10}\ -9$	$2.4_{10}\ -7$	7.10a
$\qquad (1.0)$	$3.0_{10}\ -9$	$9.36_{10}\ -7$	7.3
$I(3.6\ keV)$	$(630 n_0 R)$	$(30 n_0 R)$	
keV(keV cm^2 (0.7)	.10	.13	7.5
sec ster)$^{-1}$ (1.0)	.06	.23	
Observed I (3.6)	3.9 – 8.6	3.9–8.6	Table 7.1

view of X-ray isotropy, an increased electron flux indicated by the intensity of southern radio data is offset by the increased spectral index, in predicting X-ray intensities. The X-ray intensities of table (7.2) imply anisotropies at about the limit of present X-ray isotropy observations.

The submillimeter flux of $\sim 5_{10} -9$ Watts $cm^{-2} ster^{-1}$ is discussed in 1.6.4. If this is isotropic it implies an energy density ~ 12 eV cm^{-3} at a mean photon energy somewhere around $2_{10} -3$ eV (also the mean energy of an 8.3 degK blackbody). The electron fluxes used here then imply inverse Compton fluxes of the order of the observed flux.

7.7   CONCLUSIONS

This treatment is based principally on two pieces of evidence obtained from new high resolution and carefully selected low resolution radio data, and at variance with presently held views on galactic processes. These are

(1)   the existence of a radio galactic halo, at least in the south;

(2)   a marked difference in slope and intensity of the radio emission from the directions of the north and south galactic poles.

Also there is good evidence for a 200 MHz "break" in the northern radio spectrum, absent in the south, which gives

support to galactic origin or radio background. In a model of synchrotron emission from halo electrons and magnetic field, this puts limits on the halo field strength $(B_\perp)$. At this point in particular, there is conflict with the treatment of Daniel and Stephens (see Pal). They use the charge composition of the measured electron spectrum to construct an interstellar spectrum comprising primary (galactic accelerated) and secondary (nuclear collision) electrons. The resultant electron spectrum shape is slowly varying, producing a similar radio spectrum. The present radio data, particularly in a comparison from north to south, do not support this view. If it did a markedly different accelerated spectrum from the south would be required.

The value of $0.3 < B_\perp < 1\mu G$ is dependent on a break at 4.5GeV in the electron spectrum near earth being also present in the northern halo. The relatively low $B_\perp$ value is in line with recent estimates of low fields in the galactic disc.

In the present interpretation the difference in slope of radio data from north and south implies different electron spectra (possibly similar injection but different loss rates). An agreement in slope with the observed electron spectra near earth by only one of the two radio spectra then implies restricted access of halo electrons to the vicinity of the solar system (i.e. prior to solar modulation). The

discrepancy between the "radio electron" and observed electron

intensities, which exist for both halo and disc models of the

radio emission, is also removed if a halo model with

"restricted access" is adopted. No satisfactory mechanism

appears to exist to restrict electrons in this fashion.

From the point of view of both the magnitude and extent

of the halo field, and anisotropies from north to south, the

galactic field model of Piddington (1970), is attractive. In

this model the spiral motion of the galaxy "sweeps up" an

intergalactic field of $\sim 10^{-9}$ gauss and when the motion is at

an angle to the intergalactic field direction, haloes are

formed. These haloes are in a state of evolution, which also

relaxes some pressure equilibrium requirements.

The shape of the X-ray data, from north to south and with

the position of spectral breaks, is in excellent agreement with

inverse Compton radiation from a 2.7 degK field. On the other

hand predicted X-ray intensities using electron spectra derived

from the radio data amount to about 10% or less of that

measured. Also X-ray isotropy measurements appear to be an

obstacle to a predominantly galactic origin, though

anisotropies at the flux levels predicted here might become

observable with better X-ray observations in selected

directions (e.g. see figure 7.4).

The observed flux and spectral indices of X-rays can be

explained if the submillimeter radiation of Shivanandan et al

(1968) is of galactic extent, (in which case a break in the electron spectrum at 2GeV will produce a 40keV X-ray spectral break, if figure (7.5) can be validly used in this fashion). Again the isotropy measurements would appear to be restrictive.

The alternative to accepting a galactic explanation of the observed X-rays appears to be one of accepting widespread electron precipitation capable of contamination proportional counter X-ray observations. Careful observations of X-ray intensities in directions for which radio data are available (e.g. see figure 7.4), with particular attention to electron contamination, are required to resolve the question of halo X-ray anisotropies. Isotropy to within ∼1% in selected regions, for example representing large path length differences through the southern halo, will put severe restrictions on the interpretation of the radio data, or extent of photon fields in the galaxy.

CHAPTER EIGHT

THE EFFECT OF COSMIC X-RAYS ON THE IONOSPHERE

8.1   INTRODUCTION

An ionospheric effect due to cosmic X-rays has been reported by Edwards, Burtt and Knox (1969) who correlate a night-time phase advance of 20 kHz radio signals with the transit over the VLF propagation path (Boulder to Wellington) of the strong source Sco XR-1 during the period 1965 to 1968. Preliminary calculations, based on a measured spectrum for Sco XR-1 and another for the diffuse cosmic X-ray background indicate that these X-rays can be the dominant night-time ionizing radiation at about 80 km. Edwards (1969) also reports a small ionospheric effect due to Cen XR-2. The effect of Sco XR-1 on the field strength of 164 kHz VLF radio waves from Tashkent received at Ahmedabad between 1960 and 1963 is reported by Ananthakrishnan and Ramanathan (1969). Very recently, Burgess and Jones (1969) find no evidence for a celestial X-ray effect on 10.2 kHz waves between Trinidad and Ottawa, 1966 to 1968. However, they do find evidence for large semi-annual variations which "seem to originate from density changes in the 85-90 km level".

In the short history of X-ray astronomy Sco XR-1 has, except for two brief occasions, been the most dominant stellar source of X-rays, in the 1.5 - 15 keV energy range. Variations in its X-ray intensity with time scales ranging from minutes to many years have been reported. The possibility of studying the history of the source prior to its "discovery", already apparently realized by the data of Ananthakrishnan and Ramanathan, is of immense interest. Both Cen XR-2 (Apr67) and Cen XR-4 (Jul69) have had intensities comparable to Sco XR-1 for brief periods, and the possibility of monitoring such objects in the past, present and future by ground-based equipment is again very attractive.

On the other hand, if the cosmic X-rays provide a dominant and stable (or at least predictable) source of electron production at about 80 km, they may be a valuable tool in the study of the night-time ionospheric processes since the effective "loss rate" of electrons from the night-time atmosphere appears to vary from a near constant value of about $2_{10} -7$ $cm^3 sec^{-1}$ above 90 km to greater than $10^{-3} cm^3 sec^{-1}$ near 80 km (Mitra, 1968), and the night-time reflection height for VLF waves propagated over long distances is in this altitude range (Wait, 1963).

Calculations of the electron production rates in the lower ionosphere due to the diffuse X-ray background and galactic point sources with emphasis on possible variations in

the parameters describing the source spectra are carried out

in this chapter as a preliminary step in investigating the

application of this technique. These rates are compared with

electron production rates obtained from recent information on

galactic cosmic rays and night-time Lyman alpha. The content

of this chapter has been accepted for publication in J.G.R.,

September 1970.

8.2   CALCULATION OF ELECTRON PRODUCTION RATES

From figures (1.2a,b) the approximate levels in the

atmosphere where a vertically incident beam of X-rays (with

energy E keV) is attenuated to e^{-1} of the primary intensity

are as follows:

E (keV)	Altitude (km)
20	45
10	60
1	100
0.4	97
0.25	105

The altitude range of interest here lies between 60 and

100 km and more particularly between about 75 and 90 km. In

what follows, the small X-ray fluxes greater than 10keV will

not be considered. Between 10 and 1 keV the dominant

attentuation process is photoelectric absorption (see section

3.1.1). Between 1 and 0.4 keV (corresponding to the nitrogen

absorption edge), the X-rays are absorbed above the region of
interest. At energies just less than the nitrogen edge, photo-
electric absorption above 90 km still accounts for more than
90% of the incident X-rays and the contribution at these
energies will be mentioned only briefly.

Recall that the energy in a photon beam undergoing
photoelectric absorption is shared between ejected photoelectrons
and excitation of the residual atom, with subsequent emission
from the atom of characteristic X-rays or Auger electrons.
Nitrogen, oxygen and argon produce characteristic K X-rays at
energies 0.39, 0.53 and 3.2 keV with fluorescent yields of
.0015, .0022 and .13 respectively (Fink et al, 1966). For
example, 13% of only those photoelectric collisions between
argon atoms and X-rays with energies greater than the argon K
shell energy (and which produce a K shell vacancy) result in
the emission of 3.2keV X-rays. At densities representative of
80 km, a 3.2keV X-ray is "absorbed" in about 5 km, 0.39keV and
0.53keV X-rays, and the photo- and Auger electrons in less than
1 km. The energy lost from the beam is therefore effectively
spent in producing electrons in the region of the collisions.

The energy absorption per unit volume from a mono-
energetic beam of X-rays of intensity I (keV $cm^{-2} sec^{-1}$) in a
path dx (cm) of absorber is

$$dI/dx = \mu\rho I \qquad keV\ cm^{-3} sec^{-1}$$

where ρ is the density (g cm^{-3}) and μ the mass absorption

coefficient ($\simeq$ the photoelectric linear attentuation

coefficient/density, cm^2 g^{-1}), of the absorber. The electron

production rate in a volume element at altitude h km is then

$$q(h) = \mu\, \rho(h)\, I(h)/W \text{ electrons cm}^{-3}\text{sec}^{-1} \qquad (8.1)$$

where W = 0.035keV (Snell, 1962) is the average energy for the

production of an ion pair, and I(h) is related to the primary

source intensity I_{∞} and the mass of atmosphere between the

volume and the source (see section 1.3). This has been

described by

$$I(h) = I_{\infty} \exp\left[-\mu \int_h^{\infty} \frac{\rho(H)}{\cos z^*}\, dH \right]$$

A reasonable approximation to a curved atmosphere (for H > h

and zenith angle z < 90°) is obtained by using a "local"

zenith angle z^* at H, related to z at h by

$$\cos z^* = \left[1 - \left(\frac{R+h}{R+H} \sin z\right)^2 \right]^{\frac{1}{2}} \quad ,$$

R being the earth radius (= 6371 km).

For a continuous source spectrum of the form

$$J(E)\, dE = K\, f(E)\, dE \quad \text{keV cm}^{-2}\text{sec}^{-1},$$

the electron production rate at h due to X-rays between E1 and

E2 keV from a source at zenith angle z is, from equation 8.1,

$$q(h) \simeq \frac{\rho(h)K}{W} \int_{E1}^{E2} \mu(E)\, f(E)\, \exp\left\{ -\mu(E) \int_h^{h'} \rho(H). \right.$$

$$\left. \left[1 - \left(\frac{R+h}{R+H} \sin z\right)^2 \right]^{-\frac{1}{2}} dH \right\} dE \quad \text{electrons cm}^{-3}\text{sec}^{-1} \ (8.2)$$

(where in this chapter only, photon energy is given by E

rather than $h\nu$).

If we assume that the diffuse X-ray background is

isotropic and is described by

$$J(E)dE.d\Omega = K.f(E)dE.d\Omega \qquad \text{keV cm}^{-2}\text{ sec}^{-1}\text{ ster}^{-1}.$$

then q(h) is obtained by integrating the contribution per

element of solid angle $d\Omega$ over the zenith angles z and

azimuths $\theta = 0$ to 2π. Since $d\Omega = \sin z.d\theta.dz$, then

$$q(h) \simeq \frac{2\pi\rho(h)K}{W} \int_{E1}^{E2} \mu(E)f(E) \int_{0}^{\frac{\pi}{2}} \sin z \, \exp\left\{ -\mu(E) \int_{h}^{h'} \rho(H). \right.$$

$$\left[1 - \left(\frac{R+h}{R+H} \sin z \right)^2 \right]^{-\frac{1}{2}} dH \left. \right\} dE \quad \text{electrons cm}^{-3}\text{sec}^{-1} \quad (8.3)$$

Excellent fits of a continuous function to standard atmospheric

densities (including selected perturbations) over the range 60

to 250 km (h') are obtained in the form

$$\ln\rho = \sum_{i=0}^{m} a_i h^i, \quad \text{for } m \simeq 10$$

The photoelectric mass absorption coefficient for air can be

adequately represented over restricted energy ranges by curves

of the form

$$\mu(E) = AE^{-B}$$

See figure 1.2(b).

Equations (8.2) and (8.3) were numerically integrated to

obtain the results reported in the following sections.

8.3   VARIATIONS IN ELECTRON PRODUCTION

The three sources of ionization considered here are the cosmic X-rays, the galactic cosmic rays and hydrogen Lyman radiation (solar and galactic). In a selected region of the atmosphere, perturbations in the night-time electron production rate will depend on the following:

(1)   Time variations, in the source, of intensity and/or energy dependence of the ionizing radiation. Point X-ray sources are in this category; Lyman alpha and beta, scattering from the geocorona would be expected to vary with sunspot activity.

(2)   Variations, due to the earth's rotation, in the positions of point or anisotropic galactic sources relative to the selected region of the atmosphere. Point X-ray sources are included along with possible anisotropic galactic diffuse X-ray and ultra violet emissions. Scattered solar Lyman radiation will depend on the anti-solar direction.

(3)   Modulation of the source flux in interplanetary space; this results in the 11-year cycle in galactic cosmic ray intensity.

(4)   Variations in the earth's magnetosphere. The low energy galactic cosmic rays are preferentially screened by the magnetic field introducing latitude and solar activity effects. Also variations in the hydrogen content in a geocorona will modulate the scattered Lyman radiation.

Each of these variations is discussed in more detail

under the relevant headings in following sections. A final

source of variation to be discussed here is

(5)   the variation in time and with altitude of the density

of the absorbing constituent of the earth's atmosphere.

All three sources ionize at a rate $q(h)$ in a form

similar to equation (8.1), where μ/W is independent of the

physical state of the absorber. For the X-rays we have

seen that a photon is completely absorbed to produce ions,

so that J is dependent on the mass of atmosphere already

traversed above h, i.e. while absorption of the primary beam

is small

$$q(h) \; \propto \; \rho(h)$$

and at lower altitudes where absorption becomes appreciable,

$q(h)$ varies approximately as

$$q(h) \; \propto \; \rho(h) \; \exp\{-\rho(h)\}$$

However, for the corpuscular radiation, J is effectively

independent of h, since only a small fraction of the particle

energy is lost in ionization, i.e.

$$q(h) \; \propto \; \rho(h)$$

The effect of density variations on $q(h)$ due to the

representative diffuse X-ray spectrum of Gorenstein, Kellog

and Gursky (1969) are illustrated in figure (8.1). The result

for the mean CIRA (1965) density curve is compared to those

for the extreme curves (see section 1.3). The dotted curve

is the result for the U.S. Standard Atmosphere (1962). The

relative invariance of q(h) with density between 80 and 90

km for this type of radiation is a most interesting feature.

For example, unless extremely localized, the semi annual

density variations suggested by Burgess and Jones (1969)

will produce a marked effect only when X-rays are not the

principal ionizing agent. Further indication of the

variations due to density in q(h) for the Lyman radiation

and cosmic rays is included in the relevant sections. (In

the case of Lyman alpha, whereas O_2 is the main absorber,

only trace concentrations of nitric oxide are believed to be

ionized, i.e. $q(h) \propto \rho(NO).\exp\{-\rho(O_2)\}$, and above 80 km,

$\rho(NO)$ is a critical factor.) All other X-ray results

reported here will use the mean CIRA (1965) atmosphere.

8.4   X-RAY SOURCES

8.4.1   The Diffuse Flux

Even with the possibility of galactic contributions

to the diffuse X-ray background discussed in the previous

chapter, the general tendency to isotropy already

established plus the extreme improbability of temporal

variations above the atmosphere make this the most constant

source of D-region ionization.

The 2-10 keV data are adequately described by a simple
power law,

$$J(E) \quad = \quad KE^{-k} \quad keV.keV^{-1} \ cm^{-2} \ sec^{-1} \ ster^{-1}$$

(see 1.6.4). The data of Henry et al (1968), (K ≃ 12.5,
k ≃ 0.4) and Seward et al (1967), (K ≃ 9.5, k ≃ 0.7) are
taken to represent the range of the various observations.
The electron production rates calculated from equation (8.3),
assuming isotropy and with $f(E) = E^{-k}$, are shown in figure
(8.2). As an illustration of the energy dependence, the
contributions of photons in the energy ranges 1-2 keV,
2-5 keV and 5-10 keV (dashed lines) are compared to the
total 1-10 keV effect of the Seward et al spectrum.

At energies less than 1keV, instrumental difficulties
and uncertainties in background and absorption corrections
increase and this is probably reflected in the order of
magnitude differences in present estimates of the flux at
0.27keV. The data of Henry et al (1968), obtained on the
same rocket flight as above, represents an upper limit of
such measurements. Arbitrarily assuming a sharp break in
spectral index at 1.5keV, so that the background energy
spectrum passes through their point at 0.27keV, the D-region
ionization due to photoelectric absorption of this spectrum
(between 0.25 and 0.4 keV) is shown as a dotted line in
figure (8.2).

8.4.2   Sco XR-1

Sco XR-1, because of its consistent brightness, is the
most intensely studied of the X-ray sources.   Its
identification, spectrum and possible nature have been
discussed in section 1.6. Chodil et al (1968a) and Mark et
al (1969a) have conducted a series of four simultaneous
optical and X-ray observations of Sco XR-1 in which the
measured X-ray intensity and the optical brightness (as
indicated by the B magnitude) varied proportionally.
Harries (private communication) has (4.3 day averaged)
X-ray count rate data on Sco XR-1 from late May to mid
August and around September 28, 1967, from an IMP satellite.
Despite poor statistics, there is evidence for a significant
flux increase ($\leqslant 4.3$ days duration) around June 10, and a
general overall increase in flux over the $2\frac{1}{2}$ months
continuous data.   The latter result is in agreement with
data above 20keV obtained from three balloon flights by
Overbeck and Tananbaum (1968) in which the June 26-27 flux
was approximately twice that observed on May 16 and May 25,
1967.   A short-term flare of only 20 mins duration has been
reported at "balloon" energies by Lewin et al (1968a) and a
similar activity by Agrawal et al (1969).   Finally Rao et al
(1969b) point out that the rocket observations over the
period 1965 to 1968 indicate a gradual overall decrease in
intensity of Sco XR-1.

All of the available proportional counter data have,
where possible, been represented in the form

$$J(E) \;=\; K \exp - (E/k) \qquad keV.keV^{-1} \, cm^{-2} \, sec^{-1}$$

(see section 1.6.2, equation 1.5). The majority of data are
accurately described by this equation over the range of
observations. Energy fluxes in the ranges 2-5 keV and 5-10
keV (i.e. $\int_{2}^{5} J(E)dE$ and $\int_{5}^{10} J(E)dE$) are plotted in figure
(8.3a) as a function of time. The author has taken the
liberty to "normalize" the 2.7-5.9 keV and 6-8.6 keV count
rate data of Harries by replotting his curves, to pass
through the 2-5 keV and 5-10 keV data points of Rappaport
et al (1969a) obtained on July 7, 1967. As a rough rule
in interpreting figure (8.3a), more weight has been given
to more recent observations, and in comparing data from
different flights more emphasis has been placed on data
from the same group of experimenters.

The data of the Livermore Research Laboratories (LRL)
group (solid circles) give a good example of the overall
"decay" of Sco XR-1, and include the lowest observed plasma
temperature on September 29, 1967. The highest plasma
temperature was measured by the American Science and
Engineering (ASE) group on March 8, 1966. Figure (8.3b)
shows q(h) for these cases and a 0° zenith. The effect
with zenith angle is shown for the May 18, 1967, LRL
spectrum, in Figure (8.3c).

8.4.3 Cen XR-2 (Apr.67)

Figure (8.4a) summarizes the history of the proportional

counter observations of Cen XR-2 (see also table 6.1). The

2-5 keV energy fluxes $\int_{2}^{5} KE^{-k} dE$ are plotted. The data of

Rao et al (1969a) reporting a "reappearance" of low energy

X-rays from this region of the sky, are included.

The electron production rates corresponding to the

measured spectra on April 4, 20, and May 18, 1967, and

November 3, 1968, are shown in figure (8.4b). Because of

the high declination of Cen XR-2 (-64°), the results are

shown for a 40° zenith (the 80 km production rate must be

increased by approximately 13% for 0° zenith). If the

intensity measurement of Cooke et al (1967) represents the

peak intensity of Cen XR-2, then the maximum ionospheric

effect is approximately that shown for April 4. However,

uncertainties in the observations do not preclude a

steadily decreasing intensity through the April data points.

By _quite_ arbitrarily assigning some features of the

source Cen XR-4 to Cen XR-2 (namely the steadily increasing

spectral index through peak intensity and a 5-day increase

to a peak approximately twice Sco XR-1, see figure 6.3) a

possible sequence for ionospheric effects of such sources

can be described. Thus, the plausible effects at peak

intensity (March 22) and half peak intensity (March 19) are

included as dotted lines on figure (8.4b). The effect of
decreasing spectral "hardness" is most noticeable; and
would complicate any direct interpretation from ionospheric
records.

8.4.4   Crab Nebula, Galactic Centre

Tau XR-1, at approximately 1/8 the 2-10 keV Sco XR-1
intensity, represents the second most intense of the "long
term" galactic sources. Its spectrum has been measured by
Chodil et al (1967b), Gorenstein et al (1969) and Boldt et
al (1969a). These data span 15 months and are in good
agreement. The last of these spectra, in the form

$$J(E) \; = \; 8.6E^{-0.93} \qquad keV.keV^{-1} \; cm^{-2} \; sec^{-1}$$

is used here.

About a dozen sources lie close to the galactic plane
($\pm \; 3^{\circ}$) and within about $\pm \; 15^{\circ}$ of the galactic centre (see
figure 5.1). Individual spectra measured by Gursky et al
(1967) and Rappaport et al (1969) show examples of both
power law and exponential spectra similar to, or softer than
the "mean" Sco XR-1 spectrum (k = 5keV); there is a general
tendency for a depletion of photons less than 3keV, presumably
due to interstellar or "self" absorption. Thus an
integrated spectrum of exponential form and with a temperature
of 6.5keV ("harder" than Sco XR-1) is used here. (This
value is compatible with flight I and II data for an

integrated response from the region.) The number and 2-5 keV fluxes of sources is obtained from Gorenstein et al (1967). Electron production rates for these sources, and for Tau XR-1, all at 0° zenith, are plotted in figure (8.5).

8.5   GALACTIC COSMIC RAYS

The D-region ionization due to galactic cosmic rays has been investigated by Webber (1962), and in more detail by Velinov (1968). The data of Velinov are used in figure (8.6) to illustrate the variation in q(h) with geomagnetic latitude (λ_m), solar activity and season. At these altitudes the air density is greater in summer than in winter and the seasonal effect is much more pronounced at high latitudes. Also the effect with solar activity is small at the equator and more pronounced at higher latitudes. The largest effect over the earth's surface is the variation of q(h) with geomagnetic latitude, an effect normally described in terms of a "cut-off rigidity", R_c (momentum per unit charge). Particles with rigidities less than R_c are deflected by the geomegnetic field and do not reach the atmosphere. R_c varies approximately as $\cos^4 \lambda_m$, and because of the steep spectrum and greater ionizing capability of the low energy cosmic rays, q(h) varies very approximately as $(\cos^4 \lambda_m)^{-1}$.

8.6   HYDROGEN LYMAN RADIATION

Prediction of night-time D-region ionization rates due to Lyman radiation is extremely difficult owing to lack of data on fluxes and atmospheric composition at these altitudes. At the same time, rough calculations included below indicate that a thorough understanding of this aspect will be necessary preparatory to using this region of the ionosphere for the study of X-ray sources, or alternatively using the effect of X-ray sources to study the ionosphere.

The origin of a night-time flux of Lyman alpha $(L\alpha)$, measured on a number of occasions by rocket has caused considerable controversy. Tinsley (1969) discusses the controversies and interprets measured flux contours in terms of solar $L\alpha$ multiply scattered from a geocorona, with the isophotes centred about a minimum near the antisolar direction. Departures from contours predicted for pure geocoronal scattering are ascribed to emission from gaseous nebula associated with the Milky Way. The flux of φ_0 of $L\alpha$ will be considered for the cases

$$\varphi_0 \cong (1-1.5)_{10}-3 \, \text{ergs cm}^{-2}\text{sec}^{-1}\text{ster}^{-1}$$ geocoronal scattering at solar minimum, and also of the order of a Milky Way component,

and $\varphi_0 \cong (3-5)_{10}-3 \, \text{ergs cm}^{-2}\text{sec}^{-1}\text{ster}^{-1}$ geocoronal scattering at solar maximum,

with the lower number in each case referring to the antisolar

direction. These figures are consistent with the observations

discussed by Tinsley.

The Lα incident on the atmosphere is absorbed by O_2

with an absorption cross-section of 10^{-20} cm^{-2} in the narrow

"window" at 1216$\overset{o}{A}$ (Watanabe, 1958). The low energy per

photon of the Lα prevents ionization of the more common

atmospheric species and it is thought that nitric oxide is

the main source of electrons. The photoionization cross-

section of NO at 1216$\overset{o}{A}$ is $2_{,0}-18$ cm² (Watanabe, 1954).

Mitra (1968) discusses the conflicting evidence on the

concentration of nitric oxide in the D-layer, and arrives

at an expression for the number density,

$$n(NO) = 0.4 \ \exp(-\frac{3700}{T}) \ n(O_2) + (5_{,0}-7) \ n(0) \qquad (8.4)$$

which is in agreement with data from ionospheric and photo-

chemical methods but in considerable disagreement with a

direct observation of NO airglow on a number of rocket

flights by Barth (1966). Mitra points to a strong

temperature dependence in (8.4) and to the fact that one of

Barth's flights corresponded to a day of abnormal D-region

warming. However, Pearce (1969) on a rocket flight in which

simultaneous measurements of temperature were obtained, found

nitrogen oxide concentrations exceeding those of Barth, and

accompanied by temperatures much less than the CIRA extreme.

The rocket measurements were obtained in twilight, and Pearce

suggests that the reaction $NO + O_3 \rightarrow NO_2 + O_2$, with a time constant of 3-5 hours (using night-time ozone densities predicted by Hunt, 1966) will result in the removal of NO during the night. Popoff and Whitten (1969) rule out the possibility of an observable cosmic X-ray effect on the ionosphere on the basis of the direct measurements of NO, in conflict with the data of Edwards and Ananthakrishnan et al. They do not consider the possibility of variation in NO concentration after sunset.

Figure (8.7) shows the electron production rates for isotropic fluxes of $\varphi_0 = 1_{,0}-3$ and $5_{,0}-3$ ergs $cm^{-2} sec^{-1} ster^{-1}$ on the CIRA mean atmosphere using NO concentrations given by (8.4). The dashed curves are for the CIRA extreme atmospheres (maximum positive deviations of density {applied to both $n(O_2)$ and $n(O)$} corresponding to maximum negative deviation in temperature, and vice versa), and with $\varphi_0 = 1_{,0}-3$. Above about 70-75 km, the $q(h)$ profile corresponds to the NO profile, below 70-75 km absorption by O_2 dominates. In the "mean" curves and the maximum positive density deviation curve above 90 km, the profile is determined by $n(O)$, while for the negative deviation curve, the temperature term of (4) dominates.

Figure (8.7) also shows $q(h)$ for the twilight nitric oxide concentration given by Pearce (1969) again for $\varphi_0 = 1_{,0}-3$.

The first night-time observation of Lyman beta $(L\beta)$
has been made by Young et al (1968) who observed an emission
rate of 5-10 rayleighs above 215 km. The ionization due to
this flux is shown for the CIRA mean and extreme atmospheres
in figure (8.7), as dotted lines. The Lyman beta is absorbed
in O_2 with a cross-section of $1.52_{10}-18$ cm^{-2}, and ionizes O_2
with an efficiency of 0.64 (Samson and Cairns, 1964). The
$L\beta$ profile will also be subject to a solar cycle variation
of about a factor of 2 (Meier, 1969).

8.7   VLF TECHNIQUES

An increase in electron production rate implies an
increased electron population (dependent on the effective
recombination rate) and also some fluorescence of the
atmosphere as a result of recombination processes. Ground
based detection of optical or infra-red fluorescence in the
D-region is in general hampered by large amounts of similar
fluorescence from higher in the ionosphere, but within the
line of sight of the detector. VLF radio waves transmitted
from the surface of the earth, however are reflected at the
relatively rapid changes in electron density in the D-region,
which at night occur about the height of the X-ray
perturbations predicted in the previous subsections. Edwards
(1969) and Ananthakrishnan and Ramanathan (1969) both use

VLF waves propagated over long distances to observe the
effect of Sco XR-1, the former employing measurements of
the phase change in the signal the latter changes in the
field strength.

Wait and Walters (1963a,b,c) have studied the
reflection of vertically polarized VLF waves at high oblique
incidence, off horizontally stratified layers of an
inhomogeneous isotropic medium whose effective conductivity
varies smoothly with height. The undisturbed conductivity
profile is given in terms of the conductivity parameter
$1/L(Z)$ where

$$1/L(Z) \quad = \quad \exp (\beta Z)/L \qquad\qquad (8.5)$$

β is a gradient parameter, Z the height above a reference
level $Z = 0$ and L is a constant which for VLF is given by

$$L \quad \simeq \quad \frac{\omega \nu}{\omega_0{}^2}$$

Here ω is the angular frequency, ω_0 the plasma frequency
and ν the collision frequency.

In general

$$1/L(Z) \; \alpha \; N(Z)/\nu(Z) \qquad\qquad (8.6)$$

where the electron density at altitude $h = (\text{ref.level} + Z)$,
for an electron production rate q and loss rate ψ is

$$N(h) \quad = \quad \{q(h)/\psi\}^{\frac{1}{2}} \qquad\qquad (8.7)$$

Wait and Walters (1963b) have introduced a Gaussian
perturbation in electron density,

$$\Delta N(Z) \quad = \quad \Delta N_0 \exp \left\{-\left(\frac{Z-F}{D}\right)^2\right\}$$

and assuming a collision frequency profile of the form

$$\nu(Z) = \nu_0 \exp\left(-\beta Z/2\right) \tag{8.8}$$

obtain a conductivity profile

$$\frac{1}{L(Z)} = \frac{1}{L(0)} \left\{ \exp(\beta Z) + \frac{\Delta N_0}{N_0} \exp\left[\frac{\beta Z}{2} - \left(\frac{Z-F}{D}\right)^2\right] \right\}.$$

This is used to calculate and plot the reflection coefficient and phase angle for the case of 20kHz waves {implying $L(0) = 0.5$, $\beta = 0.3 \text{km}^{-1}$} with a range of values for the spread D, and height F of the perturbation. The reflection coefficient depends on the angle of incidence onto the reflecting layer and values around 80° are included, appropriate to propagation of VLF over long distances. The results apply to daytime conditions, but at night (8.8) decreases much more rapidly with height (Mitra, 1968). General features of the results applicable at night, and also in the case of a hyperbolic perturbation (Wait and Walters, 1963c), are

(1)   the magnitude of the reflection coefficient may either increase or decrease within the expected ranges of the parameters

(2)   the phase angle is only affected in a manner corresponding to a lowering of the reflection height. Measurements of phase angle therefore provide a more satisfactory means of detecting a disturbance, particularly if superposition of records is necessary.

Even in the absence of the sharp night time recombination profile the exponential perturbation is

generally applicable because of interstellar absorption.

In view of the night time recombination, a narrow disturbance

(D = 2 km) is used here in applying Wait and Walters results

to obtain a rough estimate of the magnitude of the expected

VLF effect.   In the absence of Lyman alpha effects, (figure

8.7) and for reflection near the equator (figure 8.6) Sco X-1

would have produced a $\Delta N_0/N_0$ = 2 in 1965 (figures 8.1, 8.3b).

The phase then increases about 50° from the undisturbed wave.

This corresponds to approximately 7 μsec in a 20kHz wave

compared to a typical diurnal phase variation of around

100 μsec amplitude.

Records of the phase and field strength of VLF signals

received at Melbourne from NLK/NPG(18.6kHz), Washington DC,

were kindly provided by the Defence Standards Laboratories,

Victoria, for the period July-August, 1969.   These were

inspected for an effect due to Cen XR-4.   Unfortunately the

transit times of the source over the propagation path

correspond to the "sunset phase" of the records (when Lyman

alpha is expected to dominate a cosmic X-ray effect in the

D-region).   The records are distrubed about the dates and

times of Cen XR-4 birth and transit.   The absence of a "quiet

time curve" and of a familiarity with the types of

disturbance (including instrumental) frequently seen on the

records precludes any definite statement on a cosmic X-ray

effect at this time.

8.8   CONCLUSIONS

(1)   The diffuse X-ray background is an extremely constant

source of ionization between 80 and 90 km. The source will

be stable in time but may contain some small anisotropies

over the galaxy. There is no interplanetary modulation and

the electron production profile is practically independent

of atmospheric density variations in this altitude range

(assuming that the density at, e.g. 80 km, varies in the same

fashion as the integrated densities immediately above 80 km).

The contribution to the total electron population in this

altitude range is nearly a factor of 4 greater than that

due to galactic cosmic rays near the equator, and, depending

on season and solar activity, becomes equal to the cosmic ray

contribution at geomagnetic latitudes between 35 and 45°.

(2)   The strong source Sco XR-1 produces electrons at a

peak rate which has exceeded that due to the diffuse flux

since 1965, for source zenith angles less than about 20-40°.

The X-ray flux has exhibited a steady over-all decline in

intensity so that at the present time the ionospheric effect

of Sco XR-1 at zenith and the diffuse X-ray flux should be

very similar. An ionospheric effect due to Sco XR-1 was

apparently observed in 1960 (Ananthakrishnan and Ramanathan,

1969) prior to its discovery by rocket. If the source

continued to increase in intensity going back in time, the

effect should be even more pronounced, and (subject to factors discussed below) early ionospheric records may even contain a nova-like appearance of X-rays. Short term "flares" have apparently been observed, superimposed upon the overall decline. Such "flares" appear to be associated with changes in spectral "hardness" of the source with a corresponding change in height of the peak electron production.

(3)   On two occasions since 1967, X-ray sources have "flared" to brightnesses greater than or equal to that of Sco XR-1. A characteristic sudden appearance of such sources plus gradual decline should facilitate ionospheric detection, however direct interpretation from such records will be hampered by variations with time of the source spectral "hardness".

(4)   All other recorded cosmic X-ray sources give ionospheric effects small compared with the diffuse X-ray background plus cosmic rays.

(5)   The Lyman alpha production is critically dependent on the atmospheric nitric oxide profile and its variations. At concentrations of NO obtained from direct observations at twilight, the reaction

$$L\alpha \; + \; NO \; \rightarrow \; NO^+ \; + \; e^-$$
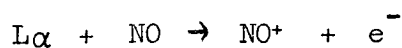
will dominate electron production above 70 km and will exceed the night time X-ray contributions between 80 and

90 km by more than an order of magnitude. The observation
of ionospheric effects due to X-ray sources implies that
the night time NO concentration is very much smaller than
the measured values, at least during portion of most nights.
If a nitric oxide concentration similar to that given by
Mitra, 1968, applied during portion of the night, AND a
major part of the Lyman alpha is of solar origin, then
winter temperatures at solar maximum will result in electron
production rates at 85 km exceeding that due to the diffuse
background by as much as a factor of 5, while the production
in the "mean" atmosphere never exceeds that due to the
diffuse flux at this altitude.

(6)   Electron production due to Lyman beta has little
effect below 90 km but is quite important above this
altitude.

(7)   Obviously, the observations and interpretation of
night time ionospheric effects associated with the altitudes
80 to 90 km must be made with due consideration to a large
number of factors, e.g.

latitude (low cosmic ray fluxes and small seasonal density
    variations are associated with low latitudes);

galactic co-ordinates of the zenith (associated with galactic
    sources of X-rays and Lyman radiation);

local time (small Lyman fluxes are associated with the anti-

  solar direction, small nitric oxide concentrations are

  apparently associated with the late hours of night, and

  there will be diurnal variations in other constituents,

  including hydrogen in the geocorona, Anderson and Francis,

  1966);

season (affecting the atmospheric densities and temperature,

  particularly at high latitudes);

solar activity (sunspot maximum is associated with large

  Lyman fluxes and small cosmic ray fluxes and vice versa,

  and there will be some variation in atmospheric densities -

  including hydrogen).

315.

FIGURE CAPTIONS

FIGURE 8.1 The electron production rate q(h), as a
function of altitude for the diffuse X-ray
spectrum of Gorenstein et al (1969),
showing the effects of density variations
in the atmosphere.

FIGURE 8.2 The q(h) profile for different measurements
of the diffuse X-ray spectrum. The separate
contributions to the Seward et al (1967)
spectrum of photons between 1-2 keV, 2-5 keV
and 5-10 keV are shown by dashed lines. The
dotted line shows an upper limit to the
contribution of 0.25-0.4 keV photons.

FIGURE 8.3(a) A summary of rocket observations of Sco XR-1.
An estimate of the energy fluxes in the
ranges 2-5 keV and 5-10 keV have been
plotted as a function of time. Points
obtained from the same experimental group
have the same symbol. The references to
these observations are as follows: 12Jun.65,
Chodil et al (1965): 26Jul.65, Hayakawa et
al (1965): 30Sept.65, Fisher et al (1968):
28Oct.65, Grader et al (1966): 8Mar.66 and
11Oct.66, Gorenstein et al (1968): 28Jul.66,
Chodil et al (1967a): 6Feb.67, Matsuoka et
al (1969): 4Apr.67 and 20Apr.67, Francey et
al 1967: 10Apr.67, Cooke et al (1967):
18May.67 and 29Sept.67, Chodil et al (1968a):
Late May to mid August, and Sept.28,1967,
Harries (private communication): 7Jul.67
Rappaport et al (1969): 7Sept.67, Meekins
et al (1969): 2Oct.67, Hill et al (1968):
9May.68 and 19May.68 Mark et al (1969a):
Rao et al (1969b).

FIGURE 8.3(b)   The q(h) profiles for Sco XR-1 at 0°
zenith using data of Chodil et al, and
Mark et al, (LRL) and Gorenstein et al (ASE)
from Figure 8.3(a). The solid lines are
taken to represent a steady decline in
Sco XR-1 intensity over 4 years, the dash
and dot lines unusual spectra or flares.

FIGURE 8.3(c)   The q(h) profiles for the 18May.67, LRL
Sco XR-1 spectrum are shown as a function
of source zenith angle.

FIGURE 8.4(a)   A summary of rocket observations of Cen XR-2.
The superposed lines represent an arbitrary
history used to show certain ionospheric
effects. The references to the observations
are as follows: 28Oct.65, Grader et al (1966):
4Apr.67 and 20Apr.67, Francey et al (1967):
10Apr.67, Cooke et al (1967): 18May.67 and
28Sept.67, Chodil et al (1968): 1Dec.67,
Barnden and Francey (unpublished): 12Jul.68,
Pounds et al (1969): 3Nov.68 and 7Nov.68,
Rao et al (1969a).

FIGURE 8.4(b)   The q(h) profiles for the observation of
Cen XR-2 (solid lines) and for an arbitrary
peak intensity (22 March 1967) and half peak
intensity during increase (19 March 1967),
(dashed lines). Zenith angle is 40°.

FIGURE 8.5   The q(h) profiles for Tau XR-1 and the
Galactic centre group of X-ray sources, for
a 0° zenith.

FIGURE 8.6   The q(h) profiles for galactic cosmic rays
shown as a function of geomagnetic
latitude (λ_m) and season (Velinov, 1968).

FIGURE 8.7   Estimates of q(h) due to Lyman alpha and
beta in the night time sky. The solid
curves represent Lα estimates at solar
maximum, and solar minimum (possibly
similar to an anisotropic galactic
contribution), using the nitric oxide
intensity profile of Mitra (1968). The
dashed curves correspond to this solar
minimum profile for the CIRA extreme
atmospheres. The dot-dash curve corresponds
to solar minimum, with a nitric oxide
concentration measured at twilight by
Pearce (1969). The dotted curves are q(h)
profiles for a Lβ flux, as measured by
Young et al (1968), on the CIRA mean and
extreme atmospheres.

FIGURE 8.1   DIFFUSE X RAYS
(DENSITY DEVIATIONS)

Altitude km.

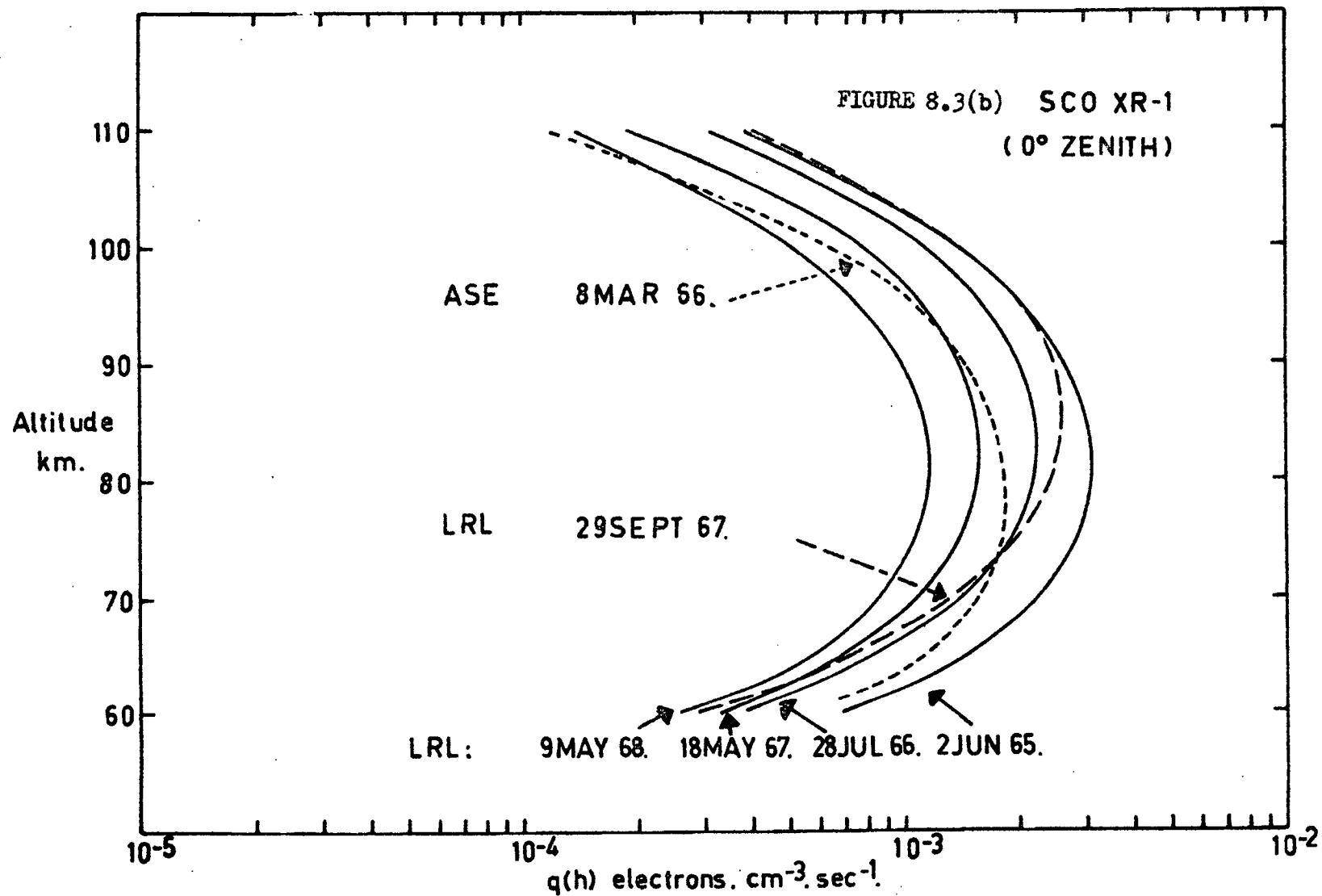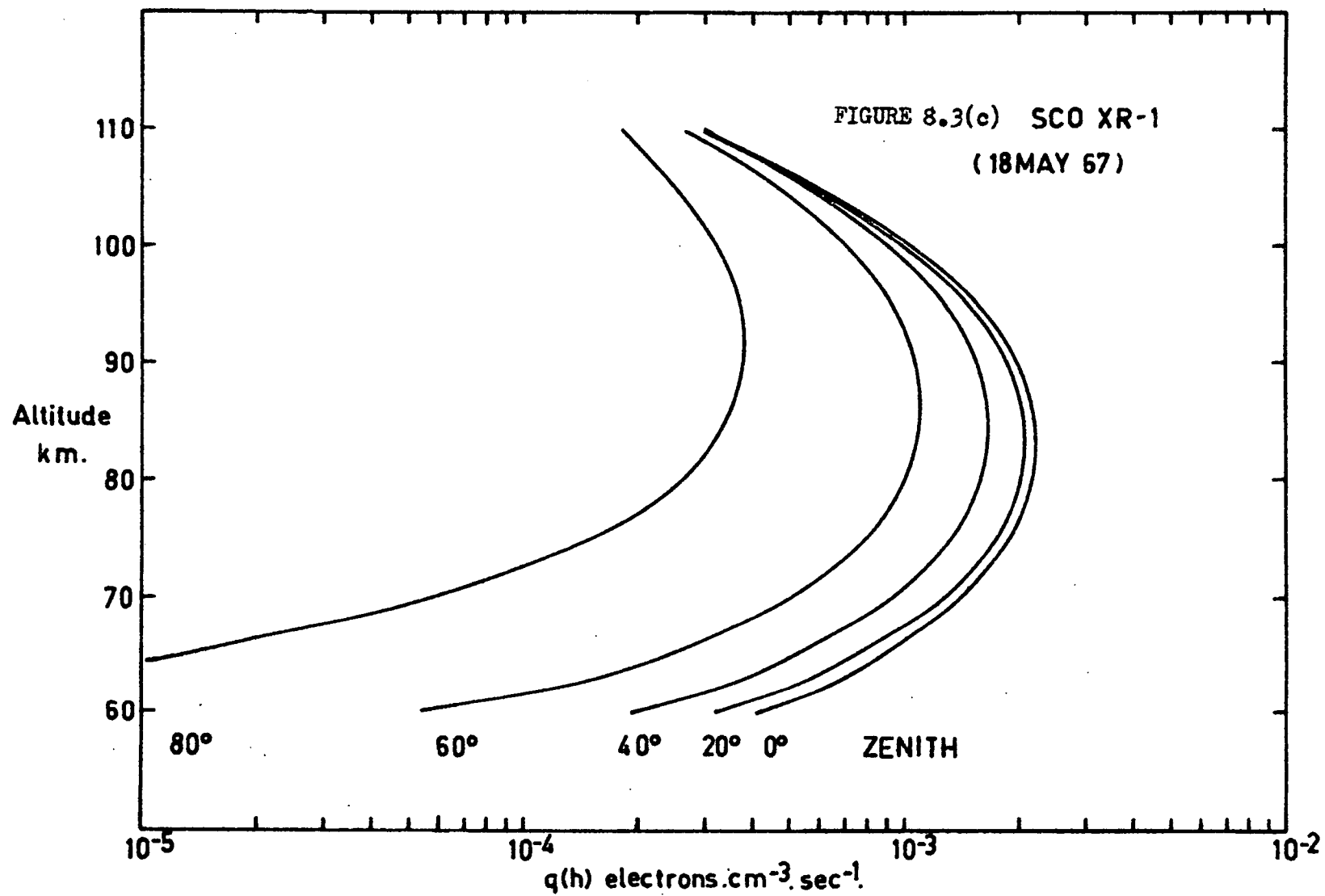CIRA max-ve   US standard   CIRA mean   CIRA max +ve

$q(h)$ electrons.cm^{-3}.sec^{-1}.
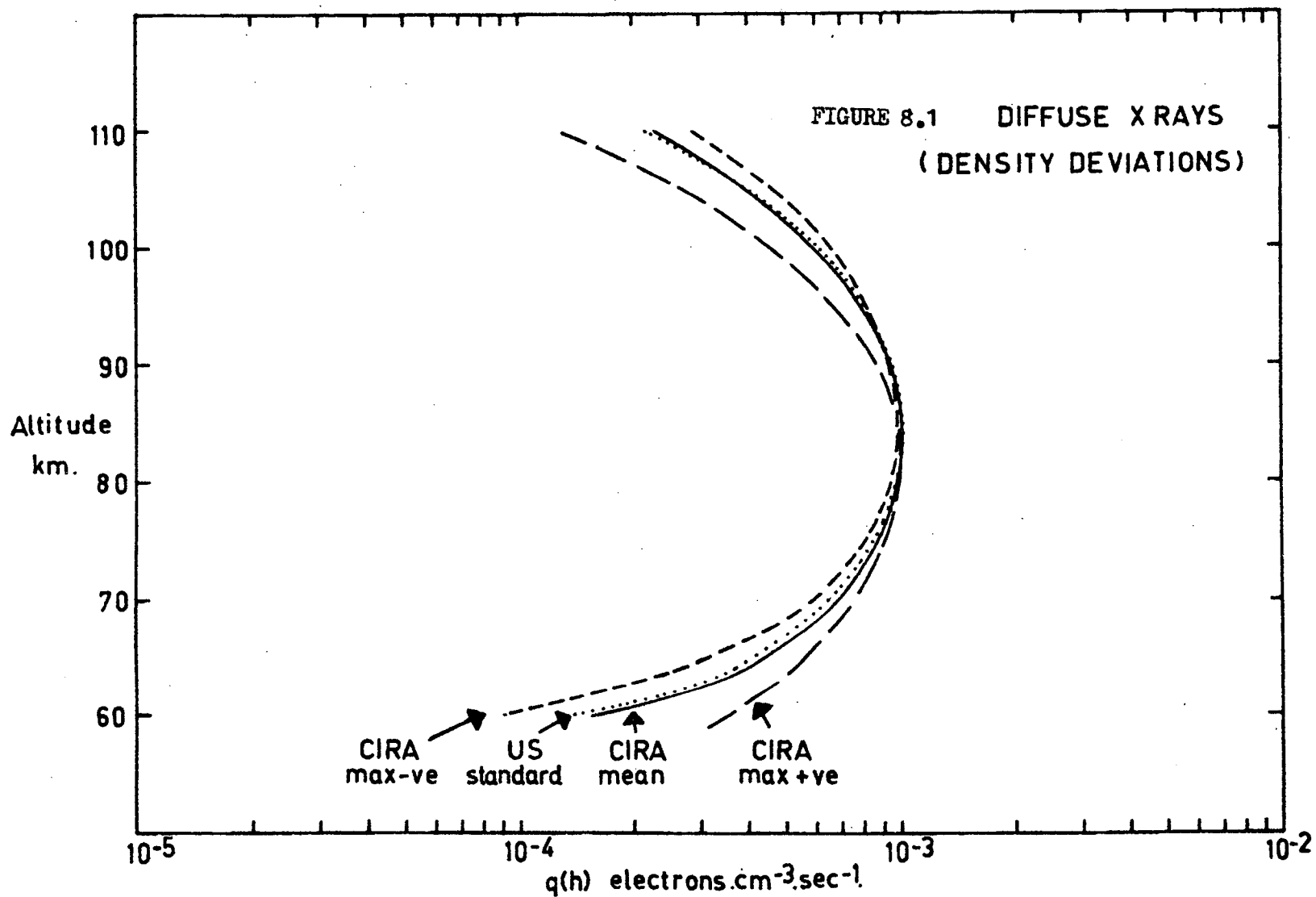
FIGURE 8.2 DIFFUSE XRAYS

FIGURE 8.3(a)

FIGURE 8.3(b)   SCO XR-1
(0° ZENITH)

ASE   8 MAR 66.

LRL   29 SEPT 67.

LRL: 9 MAY 68.   18 MAY 67.   28 JUL 66.   2 JUN 65.

Altitude km.

q(h) electrons. cm^{-3}. sec^{-1}.

FIGURE 8.3(c) SCO XR-1 (18MAY 67)

CEN XR-2
(2-5 kev)

FIGURE 8.4(a)

FIGURE 8.4(b) CEN XR-2
(40° ZENITH)
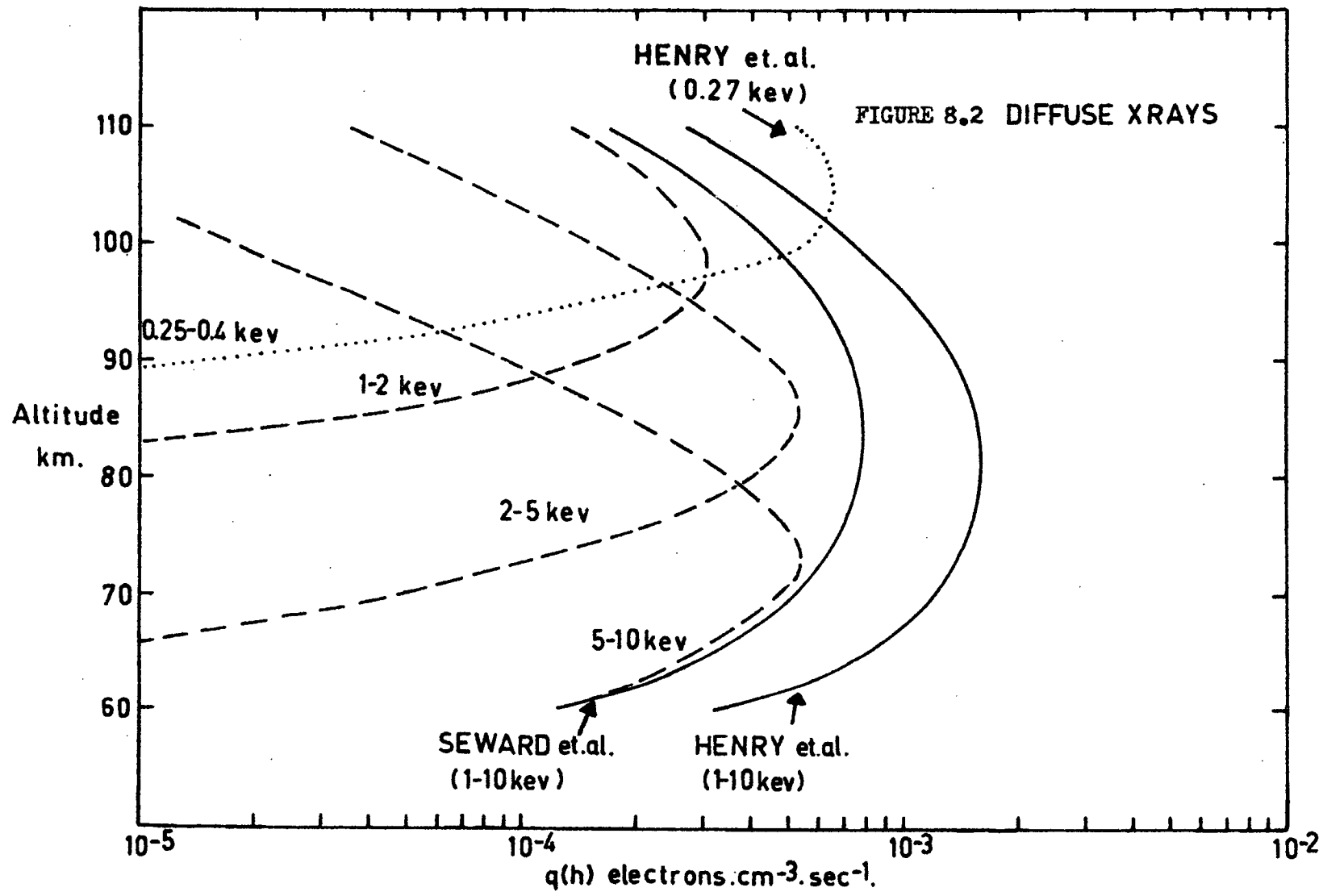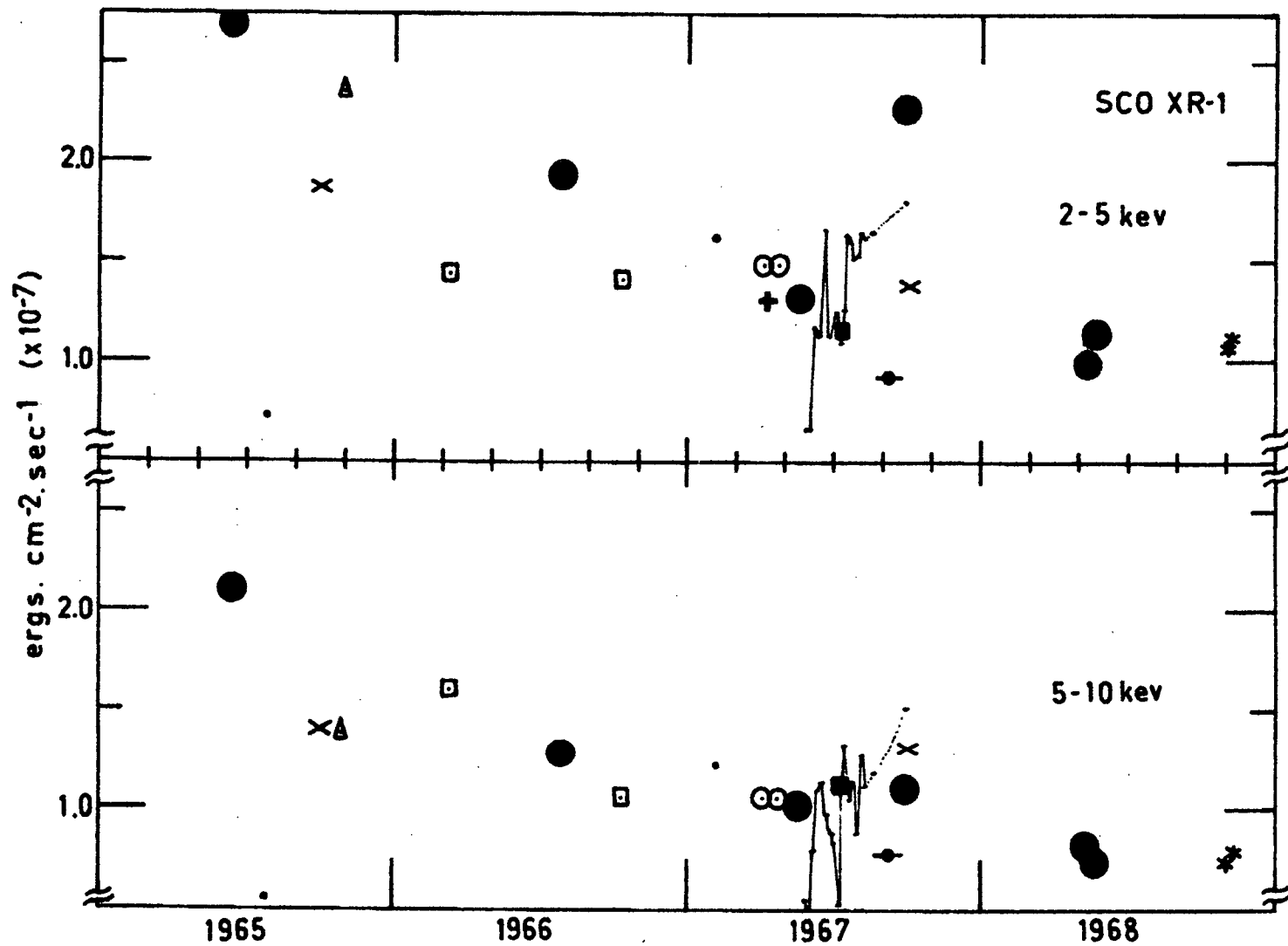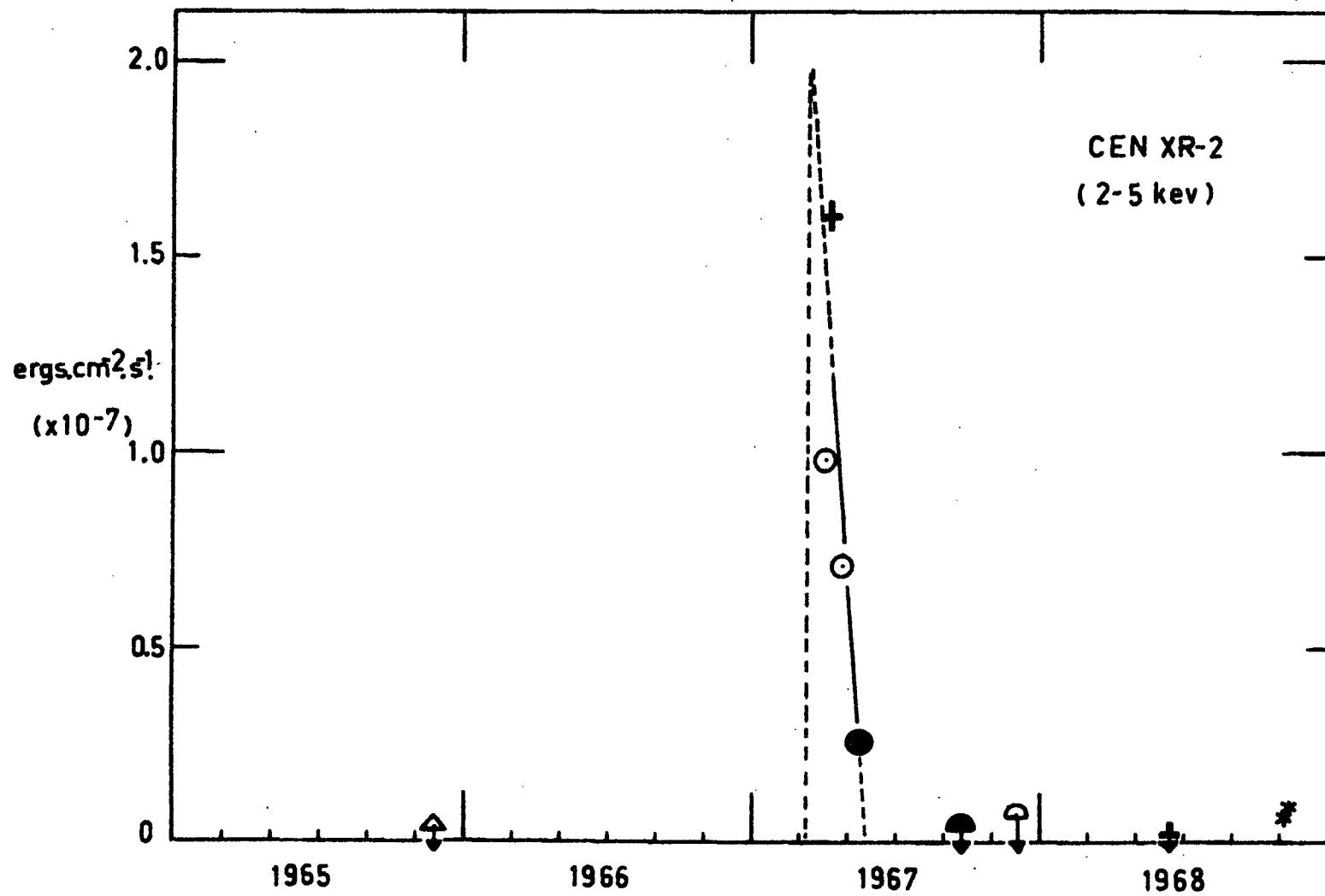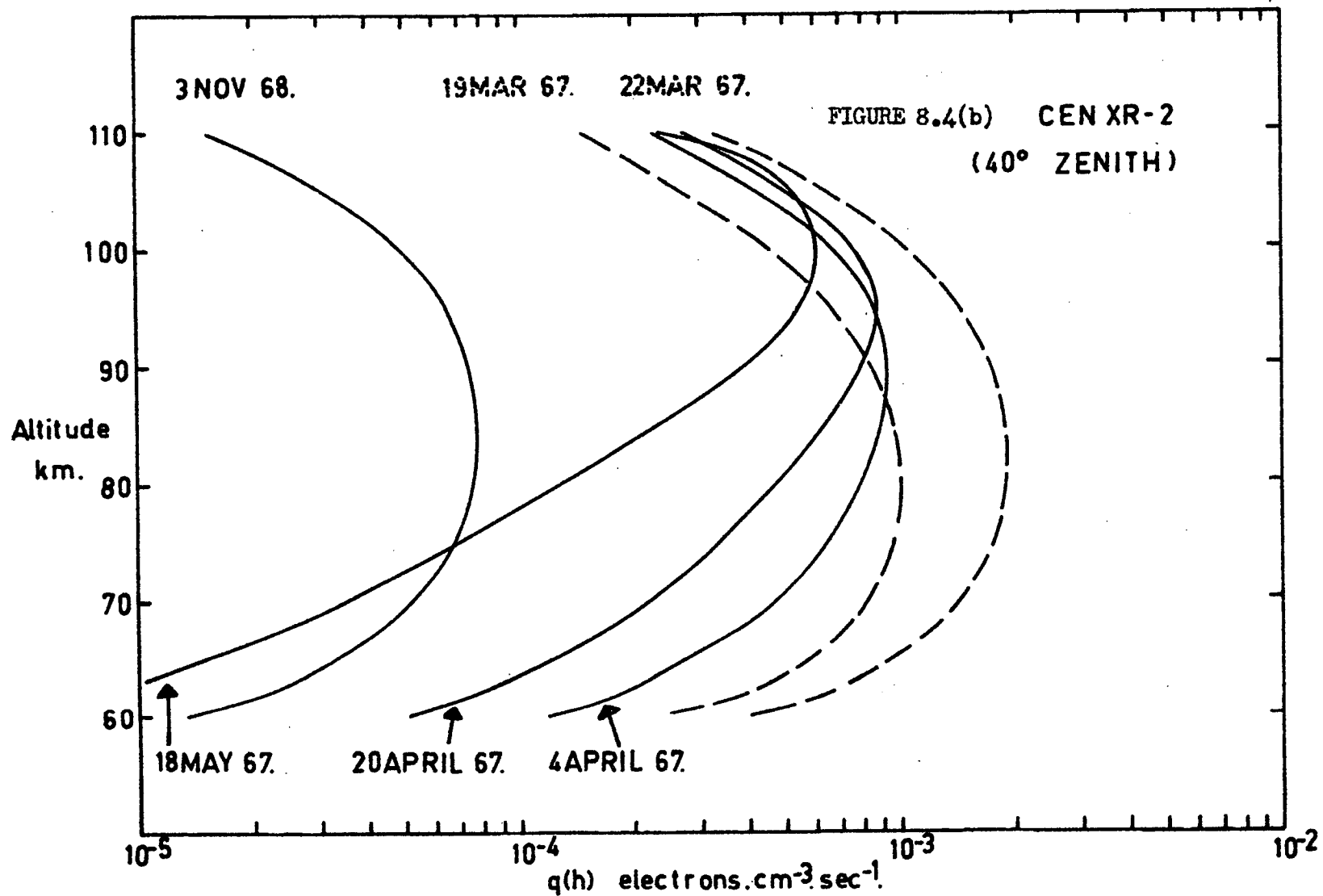
FIGURE 8.5   TAU XR-1 , GALACTIC CENTRE .
(0° ZENITH)

FIGURE 8.6   GALACTIC COSMIC RAYS

(Velinov, 1968)
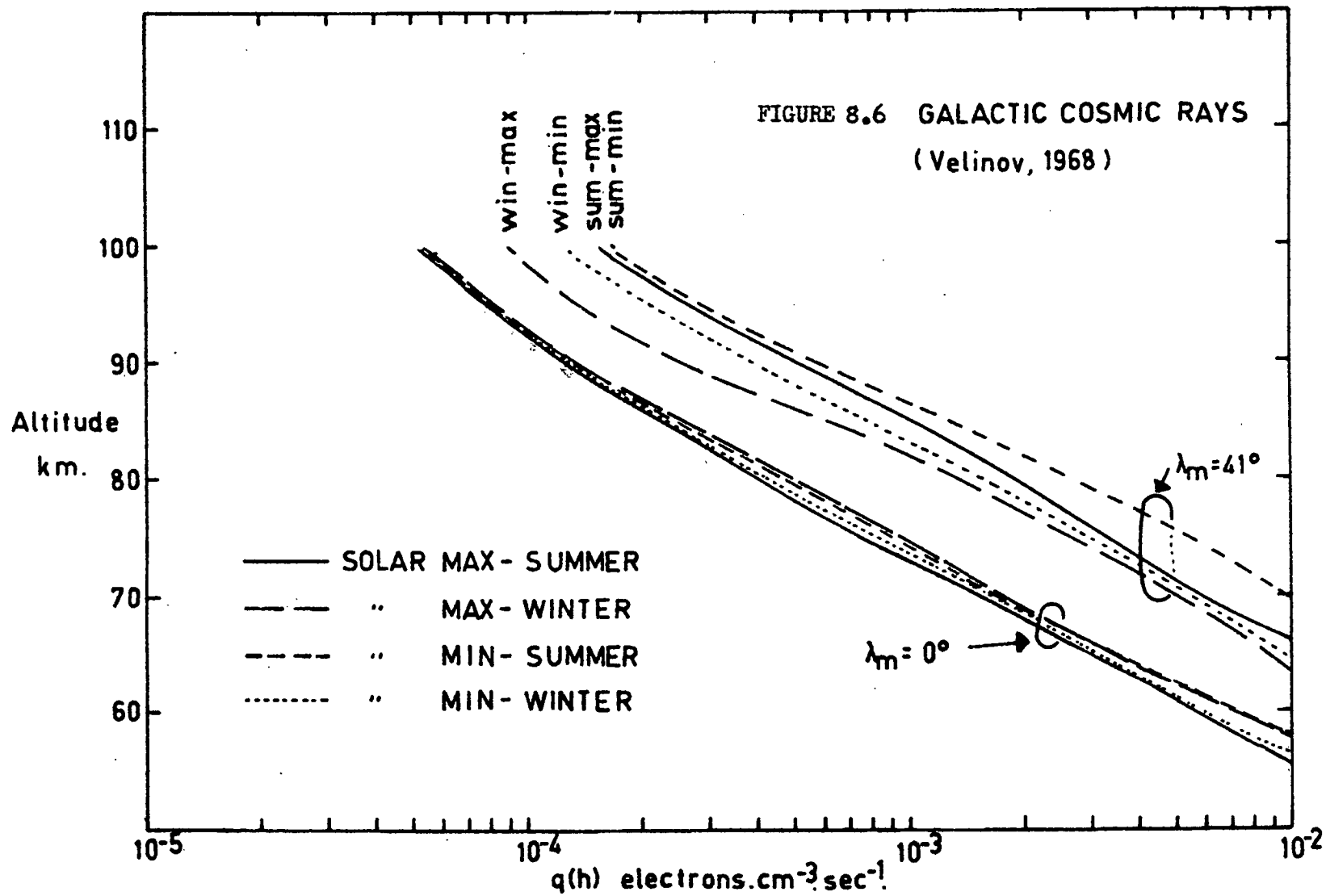
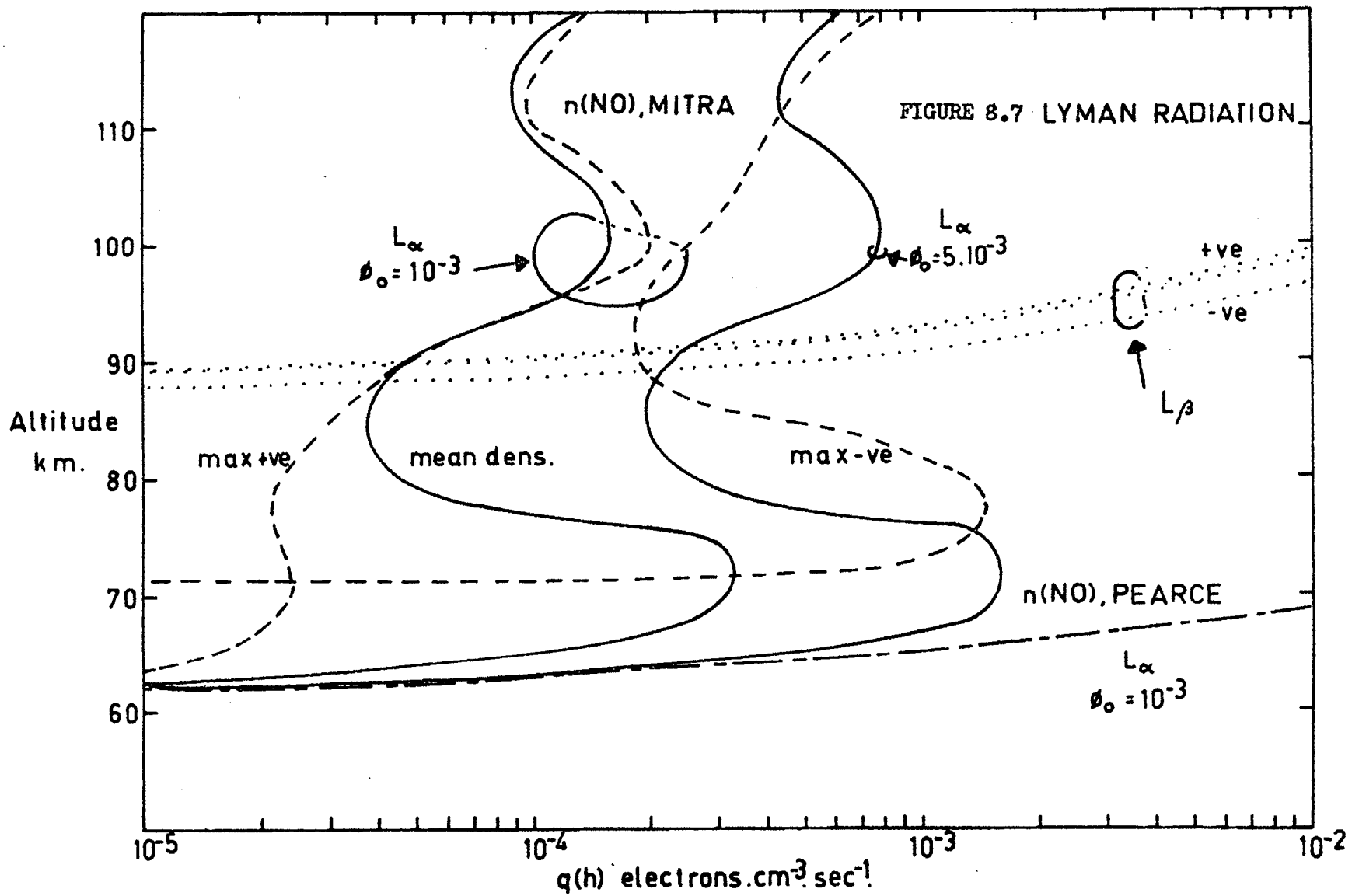FIGURE 8.7 LYMAN RADIATION
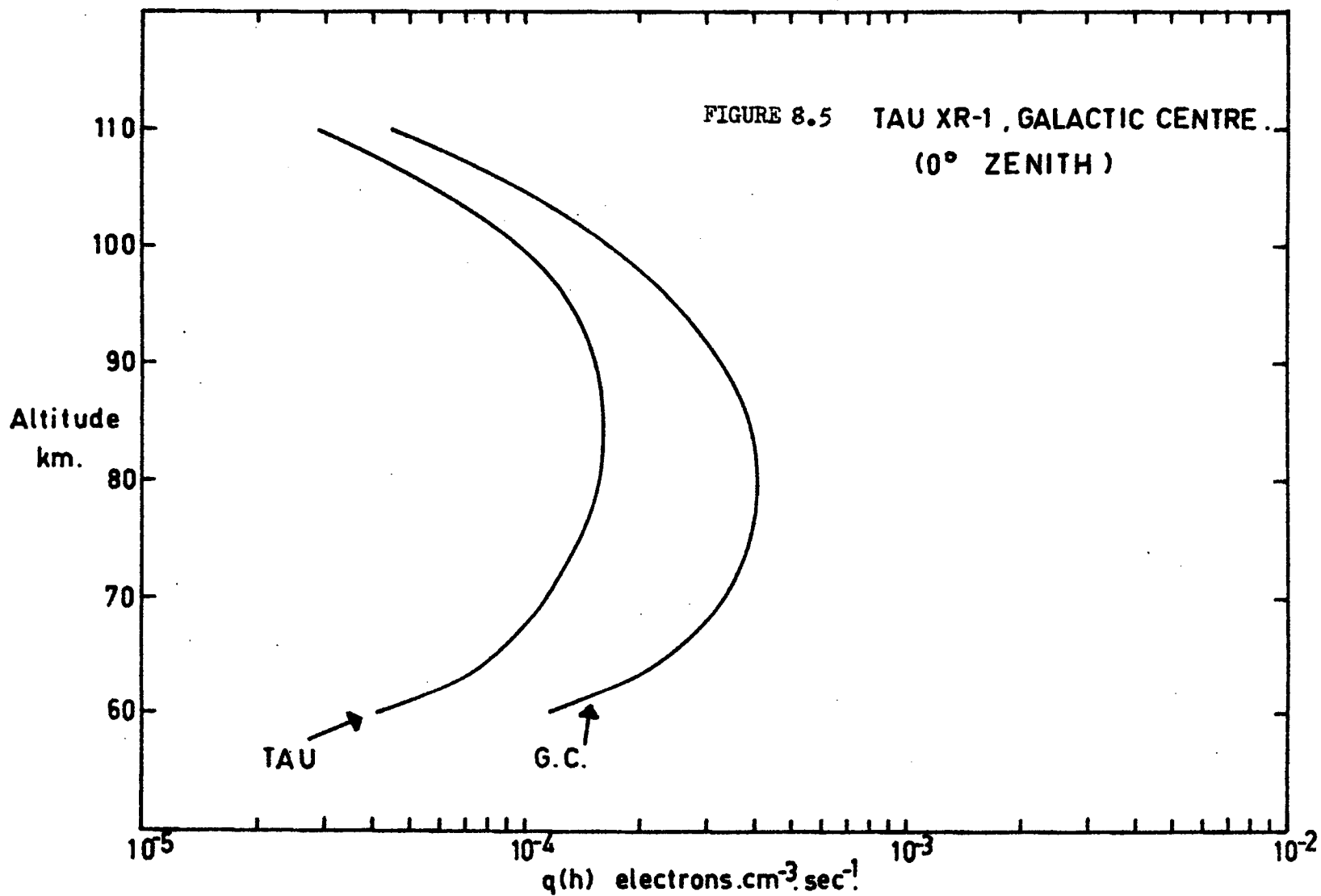
PUBLICATIONS

1. A Strong X-ray Source in the Vicinity of the Constellation Crux, J.R. Harries, K.G. McCracken, R.J. Francey and A.G. Fenton, Nature, 215, 38, 1967.

2. Variability of Centaurus XR-2, R.J. Francey, A.G. Fenton, J.R. Harries and K.G. McCracken, Nature, 216, 773, 1967.

3. The Variability of Centaurus XR-2, R.J. Francey, A.G. Fenton, J.R. Harries and K.G. McCracken, Proc.A.S.A., 1, 108, 1968.

4. The X-ray Albedo from the Earth, J.R. Harries and R.J. Francey, Proc.A.S.A., 1, 111, 1968.

5. Observations of Cen XR-2, Sco XR-1, and Terrestrial X-ray, J.R. Harries and R.J. Francey, Aust.J.Phys., 21, 715, 1968.

6. A New X-ray Object at High Galactic Latitude, L.R. Barnden and R.J. Francey, Proc.A.S.A., 1, 236, 1969.

7. The Development of UAT Rocket Instrumentation for X-ray Astronomy, R.J. Francey, A.G. Fenton, K.B. Fenton, D.J. Cooke, L.R. Barnden, L.E. Doherty, A.G. Gregory, K.G. McCracken and I.R. Tuohy, Proc.A.S.A., 1, 240, 1969.

8. Synchrotron Emission from the Galaxy and the Diffuse X-ray Background, P.A. Hamilton and R.J. Francey, Nature, 224, 1090, 1969.

9. Electron Production in the Ionospheric D Region by Cosmic X-rays, R.J. Francey, J.G.R., September 1, 1970.

REFERENCES

Aarons J., and McCray, R.   1969, Ap.J. (Letters), 158, L91

Ables, J.G.   1969, Proc.A.S.A., 1, 237

Agrawal, P.C., Biswas, S., Gokhale, G.S., Iyengar, V.S.,
    Kunte, P.K., Manchanda, R.K., and Sreekantan, B.V.   1969,
    Nature, 224, 51.

Agrawal, P.C., Biswas, S., Gokhale, G.S., Iyengar, V.S.,
    Kunte, P.K., Manchanda, R.K., and Sreekantan, B.V.   1969a,
    I.A.V. Symposium No.37, Rome, May 8-10.

Aitken, D.W.   1968, I.E.E.E. Trans.Nucl.Sci., NS10, 10.

Alkhazov, G.D., Komar, A.P., and Vorob'ev, A.A.   1967,
    Nucl.Instrum.Meth., 48, 1.

Allen, S.J.M., taken from CRC Handbook of Chemistry and Physics,
    46th Edition 1965-66, The Chemical Rubber Co.

Aller, L.H.   1961, Abundance of the Elements, p 179,
    Interscience, New York.

Anand, K.C., Daniel, R.R., and Stephens, S.A.   1968,
    Phys.Rev.Letters, 20, 764.

Ananthakrishnan, S., and Ramanathan, K.R.   1969, Nature, 223, 488.

Anderson, R.C., and Fike, R.M.   1969, J.Spacecraft and Rockets,
    6, 214.

Anderson, A.D., and Francis, W.E.   1966, J.Atmosph.Sci., 23, 110.

Andrew, B.H., and Purton, C.R.   1968, Nature, 218, 855.

Angel, J.R.P.   1969, Nature 224, 160.

Baldwin, J.E.   1955, M.N.R.A.S., 115, 684.

Barkas, W.H., and Berger, M.J.   1964, Nat.Acad.Sci - Nat.Res.
    Council publication 1133, Washington D.C.

Barth, C.A.   1966, Ann.Geophys., 22, 198.

Baxter, A.J., Wilson, B.G., and Green, D.W. 1969, Ap.J.(Letters), 155, L145.

Bearden, A.J. 1966, J.Appl.Phys., 37, 1681.

Bell, K.L., and Kingston, A.E. 1967, M.N.R.A.S., 136, 241.

Bergamini, R., Londrillo, P., and Setti, G. 1968, Il.Nuov.Cim, L111B, 518.

Berger, M.J., and Seltzer, S.M. 1964, Nat.Acad.Sci. - Nat.Res. Council publication 1133, Washington,D.C.

Berge, G.L., and Seielstad, G.A. 1967, Ap.J., 148, 367.

Benjamin, P.W., Kemshall, C.D., and Redfearn, J. 1968, Nucl.Instrum.Meth., 59, 77.

Bingham, R.G., and Clark, C.D. 1969, Ap.J., 158, 207.

Blanco, V., Kunkel, W., Hiltner, W.A., Chodil, G., Mark, M., Rodrigues, R., Seward, F., and Swift, C.D. 1968, Ap.J.(Letters), 152, L135.

Bleeker, J.A.M., and Deerenberg, A.J.M. 1970, Ap.J., 159, 215.

Boggende, den A.J.F., Brinkman, A.C., and Graff, de W. 1969, J.Sci.Instrum., 2, 2, 701.

Boldt, E.A., Desai, U.D., and Holt, S.S. 1969a, I.A.U. Symposium No. 37, Rome, May 8-10.

Boldt, E.A., Desai, U.D., and Holt, S.S. 1969b, Ap.J., 156,427

Boldt, E.A., and Serlemitsos, P. 1969, Ap.J., 157, 557.

Bortner, T.E., Hurst, G.S., and Stone, W.G. 1957, Rev.Sci. Instrum., 28, 103.

Bortolot, J.V., Clauser, J.F., and Thaddeus, P. 1969, Phys.Rev.Letters, 22, 307.

Bowyer, C.S., Byram, E.T., Chubb, T.A., Friedman, H. 1964, Science, 146, 912.

Bowyer, C.S., Field, G.B., and Mack, J.E. 1968, Nature, 217, 32.

Bowyer, C.S., and Field, G.B. 1969, Nature, 223, 573. (225, 362 (1970)).

Boynton, P.E., Stokes, R.A., and Wilkinson, D.T. 1968, Phys.Rev. Letters, 21, 462.

Bradt, H., Mayer, W., Naranan, S., Rappaport, S., and Spada, G. 1967, Ap.J. (Letters), 150, L199.

Bradt, H., Naranan, S., Rappaport, S., and Spada, G. 1968, Ap.J., 152, 1005.

Bradt, H., Rappaport, S., Mayer, W., Nather, R.E., Warner, B., MacFarlane, M., and Kristian, J. 1969, Nature, 222, 728.

Brecher, K., and Morrison, P. 1967, Ap.J.(Letters), 150, L61.

Brecher, K., and Silk, J. 1969, Ap.J., 158, 91.

Brown, R.L., and Gould, R.J. 1969, Preprint.

Bunner, A.N., Coleman, P.C., Kraushaar, W.L., McCammon, D., Palmieri, T.M., Shilepsky, A., and Ulmer, M. 1969, Nature, 223, 1222.

Bunner, A.N., and Palmieri, T.M. 1969, Ap.J.(Letters), 158, L35.

Burgess, B., and Jones, T.B. 1969, Nature 224, 680.

Buselli, G. 1968, Proc.A.S.A., 1, 168.

Byram, E.T., Chubb, T.A., and Friedman, H. 1966, Science, 152, 66.

Byrne, J. 1962, quoted from Charles and Cooke (1969).

Byrne, J. 1969, Nucl.Instrum.Meth., 74, 291.

Cameron, A.G.W. 1969, Astrophys. Letters, 3, 171.

Campbell, A.J. 1967, Norelco Reporter, 24, 103.

Campbell, J.L., and Ledingham, K.W.D. 1966, Brit.J.Appl.Phys., 17, 769.

Carver, J.H., and Mitchell, P. 1967, Nucl.Instrum.Meth., 52, 130.

Charakhch'yan, A.N., and Charakhch'yan, T.N. 1967, Geomag. and Aeronomy, 6, 791.

Charles, M.W., and Cooke, B.A. 1968, Nucl.Instrum.Meth., 61, 31.

Charpak, G., Boucher, R., Bressani, T., Favier, J., and
    Zupancic, C. 1968, Nucl.Instrum.Meth., 62, 262.

Chodil, G., Jopson, R.C., Mark, H., Seward, F., and Swift, C.D.
    1965, Phys.Rev.Letters, 15, 605.

Chodil, G., Mark, H., Rodrigues, R., Seward, F.D., and Swift,
    C.D. 1967a, Ap.J., 150, 57.

Chodil, G., Mark, H., Rodrigues, R., Seward, F.D., Swift, C.D.,
    Hiltner, W.A., Wallerstein, G., and Mannery, J. 1967b,
    Phys.Rev.Letters, 19, 681.

Chodil, G., Mark, H., Rodrigues, R., Seward, F.D., Swift, C.D.,
    Turiel, I., Hiltner, W.A., Wallerstein, G., and Mannery, J.
    1968a, Ap.J., 154, 645.

Chodil, G., Mark, H., Rodrigues, R., and Swift, C.D. 1968b,
    Ap.J. (Letters), 152, L45.

Chodil, G., Mark, H., Rodrigues, R., and Swift, C.D. 1968c,
    Ap.J. (Letters), 151, L1.

Cladis, J.B., Chase, L.F.Jr., Imhof, W.L., and Knecht, D.J.
    1961, J.G.R., 66, 2297.

Clark, B.C., and Gross, W. 1969, Rev.Sci.Instrum., 40, 504.

Clark, G.W., Garmire, G.P., and Kraushaar, W.L. 1968,
    Ap.J. (Letters), 153, L203.

Cocke, W.J., Disney, M.J., and Taylor, D.J. 1969, Nature,
    221, 525.

Cockroft, A.L., and Curran, S.C. 1951, Rev.Sci.Instrum., 22,37.

Conner, J.P., Evans, W.D., and Belian, R.D. 1969, Ap.J.(Letters),
    157, L157.

Cooke, B.A., Pounds, K.A., Stewardson, E.A., and Adams, D.J.
    1967, Ap.J.(Letters), 150, L189.

Cooke, B.A., Griffiths, R.E., and Pounds, K.A. 1969, Nature,
    224, 134.

Cookson, A.H., and Lewis, T.J. 1966, Brit.J.Appl.Phys., 17,1473.

Cornell, C.M., Grader, R.J., Harri, J.H., Hill, R.W., Rumble,R.P., and Salmi, D.S. 1968, Rev.Sci.Instrum., 39, 951.

Cospar International Reference Atmosphere, 1965, North Holland, Amsterdam, 1965.

Cowsik, R., and Pal, Y. 1969, 10th I.C.C.R., Budapest.

Culhane, J.L., Herring, J., Sanford, P.W., O'Shea, G., and Phillips, R.D. 1966, J.Sci.Instrum., 43, 908.

Curran, S.C., and Craggs, J.D. 1949. Counting Tubes - Theory and Application, Butterworths Sci.Publ., London.

Curran, S.C., Angus, J., and Cockroft, A.L. 1949, Phil.Mag. 40, 929.

Daniel, R.R., and Stephens, S.A. 1966, Proc.Ind.Acad.Sci., 65, 319.

Diethorn, W. 1956, quoted from Williams and Sara (1962).

Ducros, G., Ducros, R., Rocchia, R., and Tarrius, A. 1969, quoted from Bleeker and Deerenberg (1970).

Edwards, P.J. 1968, Nature, 217, 43.

Edwards, P.J. 1969, Proc.A.S.A., 1, 290.

Edwards, P.J., Burtt, G.J., and Knox, F. 1969, Nature, 222, 1053.

Eggen, O.J., Freeman, K.C., and Sandage, A. 1968, Ap.J.(Letters), 15, L27.

English, W.N., and Hanna, G.C. 1953, Canad.J.Phys., 31, 768.

Evans, R.D. 1955, The Atomic Nucleus, McGraw Hill, 1967.

Evans, W.D., Belian, R.D., and Conner, J.P. 1970, Ap.J.(Letters), 159, L57.

Faneslow, J.L., Hartman, R.C., Hildebrand, R.H., and Meyer, P. 1969, Preprint, E.F.I. 69-22, Uni. of Chicago.

Fano, U. 1947, Phys.Rev., 72, 26.

Fazio, G.G., and Stecker, F.W. 1970, Nature, 226, 135.

Feast, M.W. 1967, Nature, 216, 775.

Felten, J.E. 1966, Ap.J. 145, 589.

Felten, J.E., and Gould, R. 1966, Phys.Rev.Letters, 17, 401.

Felten, J.E., and Morrison, P. 1966, Ap.J., 146, 686.

Felten, J.E., and Rees, M.J. 1969, Nature, 221, 924.

Fenton, K.B. 1969, Proc.A.S.A., 1, 269.

Fink, R.W., Jopson, R.C., Mark, H., and Swift, C.D. 1966,
    Rev.Mod.Phys. 38, 513.

Fisher, P.C., and Meyerott, A.J. 1966, I.E.E.E. Trans.Nucl.
    Sci., NS-13, 580.

Fisher, P.C., Jordan, W.C., Meyerott, A.J., Acton, L.W., and
    Roethig, D.T. 1968, Ap.J., 151, 1.

Franzen, W., and Cochran, L.W. 1962, Nuclear Instruments and
    Their Uses (ed. A.H. Snell), 1, 3. John Wiley and Sons Inc.

Freeman, K.C., Rodgers, A.W., and Lyngå, G. 1968, Nature,
    219, 251.

Friedman, H., and Byram, E.T. 1967, Science, 158, 257.

Friedman, H., Byram, E.T., and Chubb, T.A. 1967, Science,
    156, 374.

Fritz, G., Henry, R.C., Meekins, J.F., Chubb, T.A. and
    Friedman, H. 1969, I.A.U. Circular No. 2141.

Giacconi, R., Gursky, H., Paolini, F.R., and Rossi, B.B. 1962.
    Phys.Rev.Letters, 9, 439.

Giacconi, R., Gorenstein, P., Gursky, H., and Waters, J.R. 1967,
    Ap.J.(Letters), 148, L119.

Giacconi, R., Reidy, W.P., Vaiana, G.S., Van Speybroeck, L.P.,
    and Zehnpfennig, T.F. 1969, Space Sci.Rev., 2, 3.

Gold, R., and Bennett, E.F. 1966, Phys.Rev., 147, 201.

Gorenstein, P., Giacconi, R., and Gursky, H. 1967, Ap.J.
    (Letters), 150, L85.

Gorenstein, P., and Mickiewicz, S. 1968, Rev.Sci.Instrum,
    39, 816.

Gorenstein, P., Gursky, H., and Garmire, G. 1968, Ap.J.,153,885.

Gorenstein, P., Kellog, E.M., and Gursky, H. 1969, Ap.J.,
    156, 315.

Goss, W.M., and Shaver, P.A. 1968, Ap.J.(Letters), 154, L75.

Gould, R.J., and Burbidge, G.R. 1963, Ap.J., 138, 969.

Gould, R.J. 1967, Amer.J.Phys., 35, 376.

Grader, R.J., Hill, R.W., Seward, F.D., and Toor, A. 1966,
    Science, 152, 1499.

Grader, R.J., Hill, R.W., and Seward, F.D. 1969, Sky and
    Telescope, 37, 79.

Grader, R.J., Hill, R.W., Seward, F.D., and Hiltner, W.A. 1970,
    Ap.J., 159, 201.

Green, D., Skirrow, J., and Wilson, B.G. 1968, Canad.J.Phys.,
    46, 5470.

Grodstein, G.W. 1957, Nat.Bur.Stand., Circular 583.

Gursky, H., Giacconi, R., Paolini, F.R., and Rossi, B.B. 1963,
    Phys.Rev.Letters 11, 530.

Gursky, H., Gorenstein, P., and Giacconi, R. 1967, Ap.J.
    (Letters), 150, L75.

Hamilton, P.A. 1969, unpublished thesis, University of Tasmania.

Hamilton, P.A., and Haynes, R.F. 1968, Aust.J.Phys., 21, 895.

Hanna, G.C., Kirkwood, D.H.W., and Pontevorvo, B. 1949,
    Phys.Rev., 75, 985.

Harries, J.R. 1968, unpublished thesis, University of Adelaide.

Hayakawa, S., Matsuoka, M., and Yamashita, K. 1965, Proc.
    9th I.C.C.R., London, 1, 119.

Hayakawa, S., Matsuoka, M., and Yamashita, K. 1966,
    Rep.Ionos.Sp.Sci.(Japan), 20, 480.

336.

Henke, B.L., Elgin, R.L., Lent, R.E., and Ledingham, R.B. 1967, Norelco Reporter, 14, 112.

Henry, R.C., Fritz, G., Meekins, J.F., Friedman, H., and Byram, E.T. 1968, Ap.J.(Letters), 153, L11

Hendrick, R.W. 1957, J.Opt.Soc.Amer., 47, 165.

Hendricks, R.W. 1969, Rev. Sci. Instrum., 40, 1216.

Herbert, P.J. 1967, "Determination of the Attitude of the Skylark Rocket in Free Space", presented to the A.I.A.A. Sounding Rocket Vehicle Technology Specialist Conference, Williamsburg, Virginia, U.S.A.

Hill, R.W., Grader, R.J., and Seward, F.W. 1968, Ap.J., 154, 655.

Holt, S.S., Boldt, E.A., and Serlemitsos, P. 1969, Ap.J. (Letters), 158, L155.

Howell, T.F., and Shakeshaft, J.R. 1967, Nature, 216, 753.

Hoyle, F. 1963, Ap.J., 137, 993.

Hoyle, F. 1965, Phys.Rev.Letters, 15, 131.

Houck, J.R., and Harwit, M. 1969, Ap.J.(Letters), 157, L45.

Hudson, H.S., Peterson, L.E., and Schwartz, D.A. 1970, Ap.J.(Letters), 159, L51.

Hunt, B.G. 1966, J.G.R., 71, 1385.

Jesse, W.P., and Sadauskis, J. 1955, Phys.Rev., 97, 1668.

Jones, F. 1967, preprint X-641-66-379, Goddard Sp.Fl.Center.

Karzas, W.J., and Latter, R. 1961, Ap.J.Suppl.Ser., 6, 167.

Kennel, C.F., and Petscheck, H.E. 1966, J.G.R., 71, 1.

Kocharov, G.E., and Naidenov, V.O. 1964, presented at 14th All Union Conf. on Nucl. Spectroscopy, Tbilisi.

Kitamura, T., Matsuoka, M., Miyamoto, S., Nakagawa, M., Oda, M., Ogawara, Y., and Takagishi, K. 1969, Nature, 224, 784.

Legler, W. 1967, Brit.J.Appl.Phys., 18, 1275.

Lewin, W.H.G., Clark, G.W., and Smith, W.B. 1968a, Ap.J. (Letters), 152, L55.

Lewin, W.H.G., Clark, G.W., and Smith, W.B. 1968b, Nature, 219, 1235.

Manley, O.P. 1966, Ap.J., 144, 1253.

Manley, O.P. 1967, Phys.Rev.Letters, 19, 1144.

Manley, O.P. 1968, Nature, 219, 1237.

Manley, O.P. and Olbert, S. 1969, Ap.J., 157, 223.

Maraschi, L., Perola, G.C., and Schwarz, S. 1968, Il Nuov.Cim., 53B, 443.

Mark, H., Price, R.E., Rodrigues, R., Seward, F.D., Swift, C.D., and Hiltner, W.A. 1969a, Ap.J.(Letters), 156, L67.

Mark, H., Price, R.E., Rodrigues, R., Seward, F.D., Swift, C.D. 1969b, Ap.J. (Letters), 155, L143.

Mathieson, E., and Charles, M.W. 1969a, Nucl.Instrum.Meth., 72, 155.

Mathieson, E., and Charles, M.W. 1969b, Nucl.Instrum.Meth., 72, 355.

Mathieson, E., and Sanford, P.W. 1963, Proc.Int.Symp.Nucl. Electronics, p 65, Paris.

Matsuoka, M., Oda, M., Ogawara, Y., Hayakawa, S., and Kato, T. 1969, Astrophys. and Sp.Sci., 4, 44.

Mayer, W., Bradt, H.V., and Rappaport, S., preprint, submitted to Ap.J. Dec. 1969.

McDonald, F.B., and Webber, W.R. 1961, Proc. 7th I.C.C.R., II, 14, Kyoto.

Meekins, J.F., Henry, R.C., Fritz, G., Friedman, H., and Byram, E.T. 1969, Ap.J. 157, 197.

Meier, R.R. 1969, J.G.R., 74, 3561.

Melton, C.E., Hurst, G.S., and Hortner, T.E. 1954, Phys.Rev., 96, 643.

Metzger, A.E., Anderson, E.C., and Dilla, M.A.van 1964, Nature, 204, 766.

Meyer, P. 1969, Ann.Rev.Astron.Astrophys., 7.

Mills, B.Y. 1959, Publ.Astron.Soc.Pacif., 71, 267.

Mills, B.Y. 1969, Proc.A.S.A., 1, 176.

Milne, D.K. 1970, Proc.A.S.A., 1, 333.

Mitra, A.P. 1968, J.Atmos.Terr.Phys., 30, 1065.

Morrison, P. 1967, Ann.Rev.Astron.Astrophys., 5, 325.

Mulvey, T., and Campbell, A.J. 1958, Brit.J.Appl.Phys., 9, 406.

Neugebauer, G., Becklin, E.E., Kristian, J., Leighton, R.B., Snellen, G., and Westphal, J.A. 1969a, Ap.J. (Letters), 156, L115.

Neugebauer, G., Oke, J.B., Becklin, E., and Garmire, G. 1969b, Ap.J., 155, 1.

O'Brien, B.J., Allum, F.R., and Goldwire, H.C. 1965, J.G.R., 70, 161.

O'Connell, R.F., and Verma, S.D. 1969, Phys.Rev.Letters, 22, 1443.

Oda, M., Bradt, H., Garmire, G., Spada, G., Sreekantan, B., Gursky, H., Giacconi, R., Gorenstein, P., and Waters, J. 1967, Ap.J. (Letters), 148, L5.

Overbeck, J.W., and Tananbaum, H.D. 1968, Ap.J., 153, 899.

Pal, Y. 1969, Rapporteur Papers p.240, 11th ICCR, Budapest.

Payne, A.D. 1969, Aust.J.Phys., 22, 521.

Pauliny-Toth, I.I.K., and Shakeshaft, J.R. 1962, M.N.R.A.S., 124, 61.

Pearce, J.B. 1969, J.G.R., 74, 853.

Pelyuskenko, S.A., and Stankevich, K.S. 1969, Sov. Astron.AJ., 13, 223.

Penzias, A.A., and Wilson, R.W. 1965, Ap.J., 142, 419.

Peterson, L.E. 1969, I.A.U. Symposium No.37, Rome, May 8-10.

Piddington, J.H. 1970, preprint submitted to Aust.J.Phys.

Popoff, I.G., and Whitten, R.C. 1969, Nature, 224, 1187.

Pottasch, S.R. 1966, Bull.Astr.Inst.Netherlands, 18, 156.

Poveda, A., and Woltjer, L. 1968, Astron.J., 73,65.

Prendergast, K.H., and Burbidge, G.R. 1968, Ap.J.(Letters),
    151, L83.

Price, R.M. 1969, Aust. J. Phys., 22, 641.
**
Rao, U.R., Chitnis, E.V., Prakasarao, A.S., and Jayanthi, U.B.
    1969a, Ap.J. (Letters), 157, L127.

Rao, U.R., Jayanthi, U.B., and Prakasarao, A.S. 1969b,
    Ap.J. (Letters), 157, L133.

Rappaport, S., Bradt, H.V., Naranan, S., and Spada, G. 1969a,
    Nature, 221, 428.

Rappaport, S., Bradt, H.V., and Mayer, W. 1969b, Ap.J.(Letters),
    157, L21.

Reiser, L.M. 1957, J.Opt.Soc.Amer., 47, 987.

Ricker, G.R.Jr., and Gomes, J.J. 1969, Rev.Sci.Instrum., 40,
    227.

Rocchia, R., Rothenflug, R., Boclet, D., Ducros, G., and
    Labeyrie, J. 1966, 7th Int.Sp.Sci.Symposium, Vienna, May 11-17.

Rohan, P., and Soden, L.B. 1970, Aust.J.Phys., 23,223.

Rose, M.E., and Korff, S.S. 1941, Phys.Rev., 59, 850.

Rossi, B.B. 1965, Space Res V, North Holland, Amsterdam.

Rossi, B.B. 1968, Int.Symposium on Contemp.Phys., Trieste.

Samson, J.A.R., and Cairns, R.B. 1964, J.G.R., 69, 4583.

Sandage, A.R., Osmer, P., Giacconi, R., Gorenstein, P., Gursky,
    H., Waters, J., Bradt, H., Garmire, G., Sreekantan, B.V.,
    Oda, M., Osawa, K., and Jugaku, J. 1966, Ap.J., 146, 316.

Sartori, L., and Morrison, P. 1967, Ap.J., 150, 385.

Schwartz, D.A. 1969, unpublished thesis, University of California, San Diego.

Seward, F., Chodil, G., Mark, H., Swift, C., and Toor, A, 1967, Ap.J., 150, 845.

Shain, C.A. 1959, Paris Symp. on Radio Astron., ed. R.N. Bracewell (Stanford Uni. Press, Stanford).

Shivanandan, K., Houck, J.R., and Harwit, M.O. 1968, Phys.Rev.Letters, 21, 1460.

Shklovsky, I.S. 1960, Cosmic Radio Waves (Harvard Uni. Press).

Silk, J. 1968, Ap.J. (Letters), 151, L19.

Silk, J. 1969, Nature, 221, 347.

Silk, J., and McCray, R. 1969, Astrophys.Letters, 3, 59.

Sironi, G. 1969, Planet.Space Sci., 17, 1.

Snell, A.H. 1962, Nuclear Instruments and Their Uses, Volume 1, John Wiley and Sons Inc.

Spielberg, N., Rev. Sci. Instrum., 38, 291.

Staelin, D.H., and Reufenstein, E.C. III 1968, Science, 162, 1481.

Stecker, F.W. 1969, Ap.J. 157, 507.

Stecker, F.W., Tsuruta, S., and Fazio, G.G. 1968, Ap.J., 151, 881.

Stern, D. 1960, Suppl. 2, Il Nuov. Cim., 16, 153.

Symon, K.R. 1960, Mechanics, Addison-Wesley, Massachusetts.

Tarter, B.C., Tucker, W.H., and Salpeter, E.E. 1969, Ap.J. 156, 943.

Thomas, R.M., Buselli, G., Clancy, M.C., and Davison, P.J.N. 1969, preprint submitted to Ap.J.(Letters), Oct.1969.

Tinsley, B.A. 1969, J.G.R., 74, 2327.

Toor, A., Seward, F.D., Cathey, L.R., and Kunkel, W.E.   1970,
    Ap.J., 160, 209.

Trombka, J.I.   1970, Nature, 226, 827.

Tucker, W.H., and Gould, R.J.   1966, Ap.J., 144, 244.

Tucker, W.H.   1967, Ap.J., 148, 745.

Tucker, W.H.   1969, Nature, 223, 1250.

U.S. Standard Atmosphere 1962, Handbook of Geophysics and Space
    Environment, McGraw Hill Book Co. Inc., 1965.

Valentine, J.M., and Curran, S.C.   1958, Rep. on Prog. Phys.,
    21, 1.

Veerschuur, G.L.   1969, Ap.J. (Letters), 155, L155.

Velinov, P.   1968, J. Atmos. Terrestr. Phys., 30, 1891.

Verma, S.D.   1968, Ap.J., 152, 537.

Vette, J.I., Matteson, J.L., Gruber, D., and Peterson, L.E.
    1969, I.A.U. Symposium No. 37, Rome.

Victoreen, J.A.   1949, J.Appl. Phys., 20, 1141.

Wait, J.R.   1963, J.G.R., 68, 338.

Wait, J.R., and Walters, L.C.   1963a, J.Res.Nat.Bur.Stand.,
    67D, 361.

Wait, J.R., and Walters, L.C.   1963b, J.Res.Nat.Bur.Stand.,
    67D, 519.

Wait, J.R., and Walters, L.C.   1963c, J.Res.Nat.Bur.Stand.,
    67D, 747.

Wall, J.V., Chu, T.Y., and Yen, J.L.   1970, Aust.J.Phys.,
    23, 45.

Watanabe, K.   1954, J.Chem.Phys., 22, 1564.

Watanabe, K.   1958, Adv. in Geophys., 5, 153 (Academic Press).

Watt, D.E.   1967, Nucl. Instrum. Meth., 50, 353.

Webber, W. 1962, J.G.R., $\underline{67}$, 5091.

Webber, W. 1968, Aust. J. Phys., $\underline{21}$, 845.

West, D. 1953, Prog. Nucl. Phys., $\underline{3}$, 18 (ed. O.R. Frisch, Permagon Press).

Westfold, K.C. 1959, Ap.J., $\underline{130}$, 241.

Wilkes, M.V. 1954, Proc. Phys. Soc. (London), $\underline{B67}$, 304.

Wilkinson, D. 1950, Ionization Chambers and Counters, Cambridge Uni. Press.

Williams, A., and Sara, R.I. 1962, Int.J.Appl.Rad. and Isotopes, $\underline{13}$, 229.

Wilson, B.G., Baxter, A.J., and Green, D.W. 1969, Canad.J.Phys., $\underline{47}$, 2429.

Wolf, R.A. 1966, Ap.J., $\underline{145}$, 834.

Zastawny, A. 1966, J.Sci.Instrum., $\underline{43}$, 179.

Zastawny, A. 1967, J.Sci.Instrum., $\underline{44}$, 395.

Zel'dovich, Y.B., and Shakura, N.I. 1969, Sov.Astron. AJ., $\underline{13}$, 175.

Young, J.M., Carruthers, G.R., Holmes, H.C., Johnson, Y.C., and Patterson, N.P. 1968, Science, $\underline{160}$, 990.

* Ginzburg, V.L., and Syrovatskii, S.I. 1964, The Origin of Cosmic Rays, (Pergamon Press).

** Radhakrishnan, V. 1969, Proc.A.S.A., $\underline{1}$, 254.